UNIVERSIDADE FEDERAL DE SANTA CATARINA
PROGRAMA DE PÓS-GRADUAÇÃO EM ENGENHARIA MECÂNICA

Felipe Gesser Battisti

METODOLOGIA DE OTIMIZAÇÃO DE CICLOS DE POTÊNCIA UTILIZANDO CO_2 SUPERCRÍTICO

Florianópolis
2015

Felipe Gesser Battisti

METODOLOGIA DE OTIMIZAÇÃO DE CICLOS DE POTÊNCIA UTILIZANDO CO_2 SUPERCRÍTICO

Dissertação submetido(a) ao Programa de Pós-graduação em Engenharia Mecânica da Universidade Federal de Santa Catarina para a obtenção do Grau de Mestre em Engenharia Mecânica.
Orientador: Prof. Alexandre Kupka da Silva, Ph.D.

Florianópolis
2015

Ficha de identificação da obra elaborada pelo autor,
através do Programa de Geração Automática da Biblioteca Universitária da UFSC.

Battisti, Felipe Gesser
Metodologia de otimização de ciclos de potência utilizando CO2 supercrítico / Felipe Gesser Battisti ; orientador, Alexandre Kupka da Silva - Florianópolis, SC, 2015.
129 p.

Dissertação (mestrado) - Universidade Federal de Santa Catarina, Centro Tecnológico. Programa de Pós-Graduação em Engenharia Mecânica.

Inclui referências

1. Engenharia Mecânica. 2. Dióxido de carbono. 3. Ciclos de potência. 4. Otimização. 5. Condutância dos trocadores de calor. I. Silva, Alexandre Kupka da. II. Universidade Federal de Santa Catarina. Programa de Pós-Graduação em Engenharia Mecânica. III. Título.

Felipe Gesser Battisti

METODOLOGIA DE OTIMIZAÇÃO DE CICLOS DE POTÊNCIA UTILIZANDO CO_2 SUPERCRÍTICO

Esta dissertação foi julgada adequada para a obtenção do título de **Mestre em Engenharia Mecânica**, especialidade Engenharia e Ciencias Térmicas, e aprovada em sua forma final pelo Programa de Pós-Graduação em Engenharia Mecânica da Universiadde Federal de Santa Catarina..

Florianópolis, 23 de fevereiro de 2015

Prof. Armando Albertazzi Gonçalves Junior, Dr.Eng.
Coordenador do Programa de Pós-Graduação em Engenharia Mecânica

Banca examinadora:

Prof. Alexandre Kupka da Silva, Ph.D.
Presidente – Orientador
UFSC

Prof. Marcia Barbosa Henriques Mantelli, Ph.D.
UFSC

Prof. José Miguel Cardemil Iglesias, Dr.Eng.
UDP/Chile

Prof. Edson Bazzo, Dr.Eng.
UFSC

Aos meus pais, Sirlei e Gilson,
pelos apoio e incentivo incessantes.

A todos os que de alguma forma
contribiuíram com este trabalho.

AGRADECIMENTOS

Agradeço à minha família. De forma bastante especial, agradeço aos meus pais Gilson Aristides Battisti e Sirlei Lorena Gesser Battisti, à minha irmã Helena Gesser Battisti, à minha avó Lorena Maria Salm Gesser e a minha tia avó Lurdete Maria Salm por me darem condições de seguir minha formação acadêmica, sempre confiando em mim e me apoiando incondicionalmente.

Ao Prof. Ph.D. Alexandre Kupka da Silva, meu orientador, pelas confiança e atenção, pelos apoio e conhecimentos, por ter me dado esta oportunidade singular de crescer academicamente além do que eu poderia sequer imaginar.

Ao Prof. Dr.Eng. José Miguel Cardemil Iglesias pelos conselhos e indispensável apoio no desenvolvimento desta trabalho, pelas ajuda e correções.

Ao LEPTEN, ao Prof. D.Sc. Sergio Colle e à Prof. Ph.D. Marcia Barbosa Henriques Mantelli pelo apoio e pela infraestrutura.

À família LEPTEN pelas colaboração e amizade, em especial, aos M.Eng. Allan Ricardo Starke, M.Eng. Carlos Javier Noriega Sánchez, M.Eng. Julio Nelson Scussel, M.Eng. Luigi Antonio de Araujo Passos, M.Sc. Rubinei Dorneles Machado, M.Eng. Juan Pablo Florez Mera, M.Eng. Luis Hernán Rodríguez Cisterna, M.Eng. Nelson Yurako Londoño Pabón, M.Eng. Luis Alonso Betancur Arboleda, M.Eng. João Carlos Pozzobon, M.Eng. Alexandre Bittencourt de Sá, M.Eng. Estevan Grosch Tavares, M.Eng. Marcus Vinicius Volponi Mortean, à Eng. Franciene Izis Pacheco de Sá, aos Eng. Thiago Brand Taranto, Eng. Andrés Paul Sarmiento Cajamarca, Eng. Tiago Ramos de Alvarenga, ao Gustavo Marques Hobold e ao Arthur Pandolfo da Veiga entre outros antes meus colegas de trabalho, hoje meus amigos.

À Rosângela Avi de Sousa, Carolina Maria Coelho e Luiza de Leon Nóbrega Reses por toda ajuda, pelos conselhos.

À PETROBRAS e ao CNPq pelo apoio durante o curso.

À UFSC e ao POSMEC pela oportunidade ímpar de cursar esta pós-graduação

Aos meus amigos De Sempre pela amizade de tantos anos.

Enfim, a todos que contribuíram de quaisquer formas para a concretização deste trabalho.

"Chop your own wood and it will warm you twice".
(Henry Ford)

RESUMO

Este estudo considera análises e otimizações termodinâmicas multivariáveis da performance de ciclos Rankine transcríticos e um ciclo Brayton supercrítico que utilizam CO_2 (dióxido de carbono) como fluido de trabalho. Três variáveis dependentes foram usadas como figuras de mérito: a potência líquida produzida pelos ciclos e suas eficiências de primeira e segunda leis, todas calculadas em valores absolutos, bem como normalizadas por unidade de condutância global total, a qual é definida como a soma das condutâncias globais de todos os trocadores de calor usados no ciclo. As análises dos ciclos Rankine foram conduzidas em relação a duas variáveis independentes, a pressão máxima do CO_2 no ciclo e a temperatura da fonte de calor, junto às seguintes configurações de ciclo: (i) um ciclo de potência básico, (ii) um ciclo com um recuperador, (iii) um ciclo com reaquecimento e (iv) um ciclo com um recuperador e reaquecimento, denominado ciclo combinado. O processo de otimização se baseou em rotinas de otimização e considerou fontes de calor latente e sensível. As análises do ciclo Brayton foram conduzidas com respeito a seis parâmetros independentes, a temperatura máxima e as pressões máxima e mínima do CO_2, a temperatura e a vazão mássica da fonte de calor e a fração mássica no aquecedor, junto à configuração de ciclo combinado. Foi dada especial importância à otimização da eficiência de segunda lei normalizada e apenas fontes de calor sensíveis foram consideradas. Os resultados obtidos foram capazes de mostrar que, enquanto as figuras de mérito em termos absolutos apresentaram tendências praticamente estabelecidas, as figuras de mérito normalizadas são altamente dependentes dos parâmetros considerados e claramente apresentam a existência de valores ótimos – os quais dependem da configuração do ciclo, das figuras de mérito consideradas, dos parâmetros de operação –, os quais podem ser associados ao dimensionamento ótimo de plantas de potência.

Palavras-chaves: dióxido de carbono, ciclos de potência, otimização, condutância dos trocadores de calor.

PUBLICAÇÃO

Alguns dos resultados e das discussões obtidas durante o desenvolvimento desta dissertação são apresentados no seguinte artigo:

- BATTISTI, F. G.; CARDEMIL, J. M.; MILLER, F. M.; DA SILVA, A. K. Normalized performance optimization of supercritical, CO_2-based power cycles. *Energy*, v. 82, p. 108–118, 2015.

OPTIMIZATION METHODOLOGY FOR SUPERCRITICAL CO_2 POWER CYCLES

ABSTRACT

This study considers multivariable thermodynamic performance analyzes and optimizations of four CO_2 (carbon dioxide) transcritical Rankine cycles and one CO_2 supercritical Brayton cycle. Three dependent variables were used as figures of merit: the net power produced by the cycles and their 1^{st} and 2^{nd} Law efficiencies, all calculated in absolute terms, as well as normalized per unit of total global conductance, which is defined as the sum of the global conductances of all heat exchangers used in the cycle. The analyzes of the Rankine cycles were performed with respect to two independent variables, the high pressure of CO_2 within the cycle and the temperature of the heat source, along with the following cycle configurations: (i) a basic power cycle, (ii) a cycle with a recuperator, (iii) a cycle with re-heating and (iv) a cycle with a recuperator and re-heating, namely, combined cycle. The optimization process relied on optimization routines and considered latent and sensible heat sources. The analyzes of the Brayton cycle were carried out with respect to six independent variables, the maximal temperature and the high and low pressures of CO_2, the temperature and mass flow rate of the heat source and the heater mass fraction, along with only the combined cycle configuration. The optimization was focused on the normalized 2^{nd} Law efficiency and only sensible heat sources were considered. The results obtained were able to show that while the individually defined figures of merit mostly presented established trends, the normalized ones are highly dependent on the parameters considered and clearly show the existence of optimum values – which are a function of the configuration of the cycle, figures of merit considered, operation parameters – that may be associated to optimally sizing power plants.

Keywords: carbon dioxide, power cycles, optimization, heat exchanger conductance.

PUBLICATION

Some of the results and discussions obtained during the development of this thesis are presented in the following paper:

- BATTISTI, F. G.; CARDEMIL, J. M.; MILLER, F. M.; DA SILVA, A. K. Normalized performance optimization of supercritical, CO_2-based power cycles. *Energy*, v. 82, p. 108–118, 2015.

LIST OF FIGURES

LIST OF TABLES

NOMENCLATURE

Acronyms

GWP	Global warming potential	[-]
IML	Innermost layer	
LMTD	Logarithmic mean temperature difference	
ODP	Ozone depletion potential	[-]

Greek alphabet

(ΔT)	Temperature difference or increment	[K]
ϵ	Effectiveness	[-]
η	Efficiency	[-]
λ	Condenser mass fraction	[-]
Φ	Heater mass fraction	[-]

Latin alphabet

$\dot{m}$	Mass flow rate	[kg/s]
$\dot{E}$	Exergy rate	[kW]
$\dot{W}$	Power produced	[kW]
$\dot{Q}$	Thermal power transferred	[kW]
(UA)	Global conductance	[kW/K]
A	Area	[m^2]
c	Specific heat	[kJ/(kg·K)]
e	Specific exergy	[kJ/kg]
h	Specific enthalpy	[kJ/kg]
I	Exergy destruction	[kW]
N	Number of re-heating stages	[-]
P	Pressure	[MPa]

s	Specific entropy	[kJ/(kg·K)]
T	Temperature	[K]
U	Global heat transfer coefficient	[kW/(m^2.K)]
w	Specific work produced	[kJ/kg]
x	Fluid quality	[-]

Subscripts

0	Refers to the dead state
1,2,...	Cycle location index
C	Compressor
CO2	Carbon dioxide
Cold	Cold
Cond	Condenser
Cool	Cooler
Crit	Critical
Heat	Heater
High	High
Hot	Hot
HSi	Heat sink
HSo	Heat source
HX	Heat exchanger
I	Refers to 1st law
II	Refers to 2nd law
In	Inlet
Inter	Intermediate
Iso	Refers to a isentropic process
LM	Logarithmic mean temperature difference
Low	Low

Max	Maximum
Min	Minimum
Net	Net
Opt	Optimum
Out	Outlet
P	Refers to an isobaric process
r	Refers to a reduced property with respect to the critical point
Rec	Recuperator
Reh	Re-heater
T	Turbine
Total	Total

CONTENTS

1 INTRODUCTION

The imbalance between power generation capacity - closely connected to economic development - and the necessary global energy increases with the growth of the world's population and the energy expenditure per capita. Figure 1 indicates the world's growth of total primary energy supply by source from 1971 to 2012. As can be seen, in 41 years, the energy supply has more than doubled while the main sources remain predominantly non-renewable.

Furthermore, environmental concerns are becoming more relevant as the obvious consequences caused by the ever-increasing emissions of pollutants, as known as greenhouse gases, such as carbon dioxide (i.e., CO_2), are becoming more apparent. Figure 2 indicates the world's growth of CO_2 emissions by source from 1971 to 2012.

Figure 1 – World's growth of total primary energy supply by source from 1971 to 2012 by source [Mtoe]

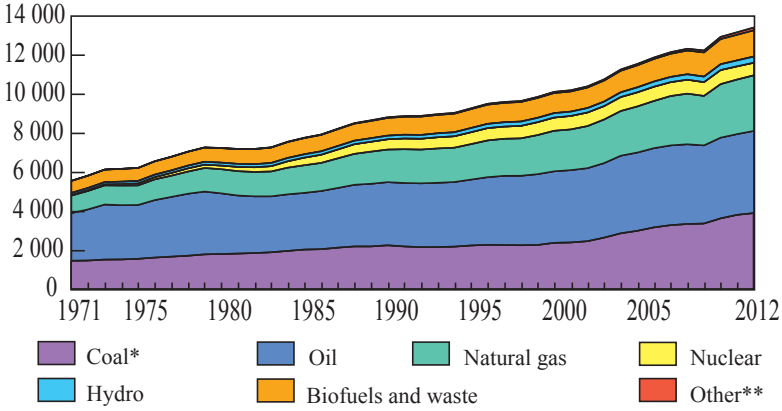

Source: Adapted from Reference [1]

Note: *Calculated using the IEA's energy balances and the Revised 1996 IPCC Guidelines. CO_2 emissions are from fuel combustion only **Peat and oil shale are aggregated with coal

Figure 2 – World's growth of CO_2 emissions from 1971 to 2012 by fuel [Mt]

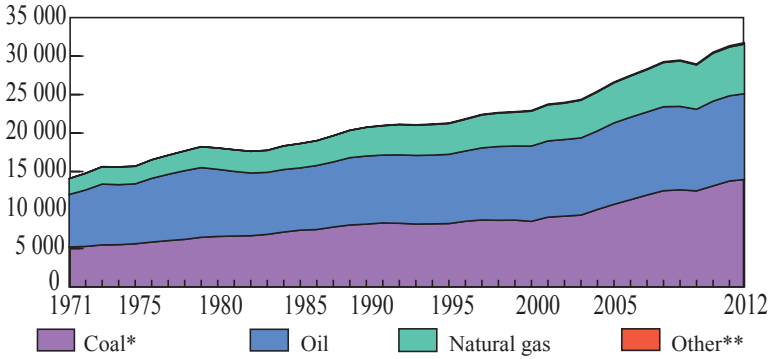

Source: Adapted from Reference [1]

Note: *Peat and oil shale are aggregated with coal **Includes industrial waste and non-renewable municipal waste

With this in mind, the importance of studying and optimizing energy production processes, such as thermal power cycles, becomes obvious. Consequently, CO_2 appears not only as a known greenhouse gas villain, but also as a possible ally, since it might be used as a primary working fluid in power and refrigeration cycles. For instance, if focusing specifically in the use of supercritical CO_2 in power cycles, which often are referred to as transcritical Rankine and supercritical Brayton power cycles, e.g., References [2–5], at least two of its thermodynamic aspects can be emphasized. First, is the low environmental impact, which is comparable to fluids like water and significantly lower than plausible competitors such as ethane (e.g., CO_2 can be considered to have low GWP[1] and ODP[2] values if compared with other working fluids [6]). Second, the strong variation of key thermodynamic properties such as the specific heat and thermal conductivity, while having a low critical

[1] The measure of how much heat a mass of a chemical compound traps in the atmosphere relative the same mass of carbon dioxide, whose GWP is standardized to 1.0. GWP is calculated over a specific time interval, commonly 20, 100 or 500 years.

[2] The measure of the degradation to the ozone layer that a chemical compound can cause relative to the trichlorofluoromethane (R-11), whose ODP is standardized to 1.0.

temperature of approximately 31 °C and a moderate critical pressure of approximately 7.4 MPa, as often discussed in the literature, e.g., References [6–9]. Among the several benefits derived from the features described above, CO_2 power cycles can reach very high specific power levels (i.e., high compactness levels) [10–12].

Despite the above-mentioned advantages associated with the use of CO_2 in power cycles, and the fact that studies concerning the thermal performance of CO_2 in power cycles are not new – take, for instance, the classic studies of Angelino's (References [13, 14]) and Feher's (Reference [15]) published in the late 1960s – a limited number of studies have dealt with the optimization of such systems. Good examples are the studies provided by Sarkar [5, 16], which optimized operational parameters of re-compression cycles. Also, Baik [17] optimized and compared the net power produced between cycles operating with CO_2 and R125. In a recently published study, a combination of technical and economical aspects was considered in the optimization as reported in Reference [18]. An exergetic optimization analysis assisted by a multivariable optimization routine was reported in Reference [19]. Furthermore, by extending the discussion to other working fluids, an even larger body of work can be mentioned, e.g., References [20, 21]. Finally, it is important to emphasize that, generally speaking, these have considered traditionally defined figures of merit, such as the net power produced and the exergetic efficiency, for example.

Additionally, arguably even fewer studies propose a direct comparison between different working fluids and CO_2 operating within a wide range of generic yet, plausible operational conditions, without overlooking, at least initially, a specific heat source or application, such that the upper performance limits for these cycles can be determined. In fact, a large number of studies analyze a given configuration, to which is given some flexibility with respect to the design of the plant, while considering a specific heat source. While this type of study is indeed appropriate for well-known working fluids such as water in power cycles and R134a in refrigeration cycles, e.g., References [22–25], other less considered fluids could potentially benefit from a broader perspective.

Certainly, CO_2 can be placed under such category, especially if considering its use in power cycles, since the available literature for refrigeration applications is well developed, e.g., References [26–28].

Aware of the potential benefits associated with the use of CO_2, the present study aims to specifically determine the trend-wise optimal scale for CO_2 transcritical Rankine and supercritical Brayton cycles for a wide range of conditions and several configurations, while considering newly defined figures of merit. In total, four different cycle configurations were simulated, along with up to six independent variables:the maximal temperature and the high and low pressures of CO_2 within the cycle, the temperature and the mass flow rate of the heat source and the heater mass fraction. However, differently from existing optimization thermodynamic studies, this analysis focuses on determining optimal values for three well-known figures of merit, the net power produced and the 1^{st} and 2^{nd} Law efficiencies, all per unit of overall global conductance $(UA)_{Total}$ of the cycle. In other words, the study maximizes the performance of the cycle, which is normalized by its total global conductance. As will be detailed along the thesis, the definition of these ratios allows for the appearance of well-defined optimal values, which can be related to the scale (i.e., size) of the power plant.

1.1 OBJECTIVES OF THE PRESENT WORK

1.1.1 Global objective

This thesis aims to study, simulate, analyze and optimize the performance of CO_2 transcritical Rankine and supercritical Brayton cycles with respect to three main figures of merit, i.e., net power produced and 1^{st} and 2^{nd} Law efficiencies. A new performance optimization methodology of power cycles is proposed through the utilization of figures of merit normalized per unit of total global conductance $(UA)_{Total}$ – the (UA) value needed for operating the cycle –, which is taken as indicator of the size/scale of the power plant.

1.1.2 Specific objectives

In order to accomplish the main objective of this work, some specific objectives, listed below, were adopted:

- Review the available literature on thermal cycles
- Simulate different configurations of CO_2 transcritical Rankine and supercritical Brayton cycles
- Analyze the effect of operational parameters on the figures of merit adopted
- Introduce the utilization of total global conductance normalized figures of merit in thermodynamic analyzes of cycles
- Optimize the operational parameters of the cycles selected

1.2 STRUCTURE OF THE THESIS

The structure of the thesis was conceived in seven Chapters and two appendixes. Apart from this introduction, the six remaining Chapters are individually commented below.

Chapter 2 is dedicated to the literature review. First, historical aspects regarding working fluids used in thermal cycles, with particular interest in CO_2, are presented. Then, concepts and definitions used throughout the thesis are presented and discussed. Finally, a review of selected works used as base to the development of the present work is presented.

The methodology employed in this study and the results obtained are presented in two separate blocks: one dedicated to Rankine (Chapters 3 and 4) and one dedicated to Brayton (5 and 6) cycles. Chapter 3 presents the model developed and its validation with respect to published results, along with the parameters and equations used, as well as a step-by-step illustrative calculation procedure. Chapter 4 presents the results obtained and discussions. Chapters 5 and 6 are equivalent

to Chapters 3 and 4, respectively, but are dedicated to Brayton cycle analysis.

Finally, Chapter 7 is dedicated to conclusions and suggestions of future works.

2 LITERATURE REVIEW

This Chapter is dedicated to the literature review. First, historical aspects about working fluids for thermal cycles, with particular interest in CO_2, are presented. Then, concepts and definitions used throughout the thesis are presented and discussed. Finally, a review of selected works used as base for the development of the present work is detailed.

2.1 HISTORICAL ASPECTS ABOUT THE UTILIZATION OF CO_2 IN THERMAL CYCLES

Initially, fluids used in refrigeration systems were inorganic, natural, toxic and flammable compounds, being ether the first to be used in a refrigeration cycle. By 1920s, the most common refrigerants were ammonia, methyl chloride and sulfur dioxide. In the 1930s, some of the previously used fluids were gradually replaced by halogenated hydrocarbons and these by hydrofluorocarbons with the Montreal Protocol, in 1974. In the last decades, researchers returned to uphold the introduction of natural working fluids [29].

2.1.1 Refrigeration cycles

By the end of the nineteenth century, CO_2 was used in refrigeration systems at supermarkets and restaurants, in air conditioning systems on ships, theaters, hospitals, and applications where toxic fluids were not acceptable [28]. CO_2 facilities had low capacity, reduced efficiency at high ambient temperatures, they were susceptible to frequent leaks due to the high pressures and the poor sealing technology, which required specialized compressors (a great disadvantage compared to other refrigerants) [27]. In the early twentieth century, CO_2 was gradually replaced, first by ammonia and subsequently by halogenated fluids [29].

In the 1990s, with the worsening of environmental concerns, the interest on CO_2 was renovated [30] and since then, CO_2 has been used, for example, in food and beverage commercial refrigeration systems and heat pumps.

2.1.2 Power cycles

Research on CO_2 power cycles was first proposed by Sulzer Bros in 1948, then studies were carried out in countries like the former Soviet Union, Italy, United States [31]. After the intense interest on such cycles during the 1960s, there was a decline in the number of studies concerning these cycles until the 1990s, mainly due to heat source limitations and lacking of components for such cycles [10]. Nevertheless, many researchers have focused on supercritical Brayton cycles using high temperature heat sources (above 800 °C) and high pressures for nuclear reactor applications [32]. Currently, however, it can be observed an increasing interest in studies using low temperature heat sources (under 300 °C), particularly for transcritical Rankine cycles, utilizing waste heat, solar and geothermal heat sources.

2.2 THERMODYNAMIC CONCEPTS

Concepts, definitions, discussions and the relevant equations necessary to the proper understanding of this thesis are briefly presented in this Section.

2.2.1 Critical phenomena and supercritical state

Charles Cagniard de la Tour, in 1822, conducted a series of experiments dealing with the discontinuity of the splashing sound of a ball in a rolling pressurized Papin's digester[1] partially filled with a fluid (e.g. References [33, 34]) – as the solid ball penetrated the liquid-vapor interface. At sufficiently high temperatures, no splashing sound

[1] A high-pressure steam cooker invented by French physicist Denis Papin, in 1679, which is the forerunner of the autoclave and the domestic pressure cooker.

was generated since the fluid have become supercritical [35]. The term "critical point" was coined by Andrews in 1869 [36].

The liquid-vapor critical point of a pure fluid is defined as the point where the saturated liquid and the saturated vapor states are identical, wherein the P-s-T manifold presents $\left.\frac{\partial T}{\partial s}\right|_P = \left.\frac{\partial^2 T}{\partial s^2}\right|_P = 0$ [37]. The temperature and pressure at the critical point are called critical; a fluid is called supercritical if its temperature and pressure are above its critical values.

In the supercritical state there is no clear phase transition between liquid and gas leading to coinciding (homogeneous) thermophysical properties. Supercritical fluids can permeate solids as gases and dissolved materials as liquids [35]. According to References [38] and [39], the physical understanding of critical phenomena, and therefore supercritical state, continues to be lacking, even though, there are various applications for substances at such thermodynamic conditions such as cooling, power generation, dry washing, extraction of substances, solvents.

2.2.2 Net power produced, 1st and 2nd Law efficiencies: definition and discussion

Some of the most commonly used performance indicators in thermodynamic analysis are the net power produced and the 1st and 2nd Law efficiencies. While the net power produced ($\dot{W}_{Net}$) is traditionally defined as the difference between the power produced through the turbines and the power spent with pumps (or compressors), and the 1st Law efficiency (η_I) is defined by the ratio between ($\dot{W}_{Net}$) and the total thermal power added to the cycle ($\dot{Q}_{In}$), it is important to explicitly define the 2nd Law efficiency (η_{II}), as several formulations are available. Therefore, the 2nd Law efficiency is defined in this thesis as the ratio between the net power produced and the total incoming exergy available within the heat source ($\dot{E}_{HSo,In}$). Equations 2.1, 2.2 and 2.3 explicitly show the definitions just introduced above.

$$\dot{W}_{Net} = \sum \dot{W}_{Produced} - \sum \dot{W}_{Spent} \tag{2.1}$$

$$\eta_{\mathrm{I}} = \frac{\dot{\mathrm{W}}_{\mathrm{Net}}}{\dot{\mathrm{Q}}_{\mathrm{In}}} \tag{2.2}$$

$$\eta_{\mathrm{II}} = \frac{\dot{\mathrm{W}}_{\mathrm{Net}}}{\dot{\mathrm{E}}_{\mathrm{HSo,In}}} \tag{2.3}$$

The net power produced is used to quantify the cycle power output, i.e., the amount of power that will be actually available to be used/sold. The 1st Law efficiency is usually understood as a measurement of how good a given cycle is to transform thermal power in net power. The 2nd Law efficiency, as already said, has been differently defined by many authors, but in this study it will be understood as a measurement of how good a given cycle is at utilizing the total available exergy within the hot source. The definition of the latter figure of merit was chosen to fairly evaluate different configurations of cycles.

2.2.3 Power cycles

Power cycles are thermodynamic apparatuses conceived to transform heat from a hot source into net power (i.e., generally mechanical power), rejecting part of the received heat to a cold source. A first classification of these cycles is relative to the existence or not of, at least, one state in which the working fluid is liquid, i.e. steam cycle (Rankine) or gas cycle (Brayton), respectively. A second classification is relative to the renewal of the working fluid: if the fluid at the end of the cycle returns to the initial state or if it leaves the cycle and is replaced, i.e. closed cycle or open cycle, respectively. A third classification is relative to the heat source used: if heat is externally added to the working fluid or if it is obtained inside the cycle itself [40]. Another possible classification of power cycles is relative to the existence of supercritical states. If there are no supercritical states, the cycle is called subcritical; if there are only supercritical states, the cycle is called supercritical; if there are both subcritical and supercritical states, the cycle is called transcritical.

There are several strategies to improve the performance of thermal cycles. Some of the most common are relative to the optimization of operational parameters and configuration of the cycle. On the optimization of operational parameters, one of the most obvious ways to increase the efficiency of the cycle is to increase the highest and/or decrease the lowest temperatures of the working fluid within the cycle as stated by Equation 2.4, which is the maximal theoretical efficiency achievable, as known as the Carnot's efficiency.

$$\eta_{\mathrm{I}} = 1 - \frac{\mathrm{T_{Cold}}}{\mathrm{T_{Hot}}} \tag{2.4}$$

Nevertheless there are numerous limitations on implementing this strategy. The temperature of the cold source usually is limited by the temperature of the environment, as well as low temperatures are usually associated with low pressures, which could lead to the occurrence of condensate within the turbines. On the other hand, high temperatures are limited by materials employed to build the power plants as well as economical constraints. A similar effect is observed with the increase of the high and the decrease of the low pressures of the working fluid within the cycle.

On the optimization of the configuration of the cycle, the use of split expansion with intermediate re-heating increases the power produced by turbines, as well as the split compression with intermediate cooling decreases the power spent by pumps and compressors – one should note that it is possible of optimize these intermediate pressures to increase the performance.

The use of recuperators is very beneficial when the working fluid exits the turbines with high temperature and pressure levels that are not thermodynamically profitable anymore. Therefore, part of the remain thermal energy of the expanded working fluid can be used to preheat the compressed working fluid before it is effectively heated by the hot source, which decreases the amount of heat added to the cycle, increasing its 1^{st} Law efficiency.

Re-compression may be seen as a way to overcome limitations on

the use of recuperators for working fluids presenting strong thermophysical proprieties variations. As pinch-point[2] problems are mainly caused by the difference in the fluid capacity rates between the high and low pressure streams – as a result of specific heat at constant pressure (c_P) variations –, the re-compression cycle reduces the difference in fluid capacitances rates by decreasing the mass flow rate of the high pressure stream relative to the low pressure stream – a single recuperator can be split into a high and a low temperature recuperators [41]. After the fluid goes through the low pressure side of both recuperators, it is split and a fraction is cooled, compressed and goes through the high pressure side of the low temperature recuperator; the remaining flow rate is simply compressed. Both streams are mixed (at the same pressure) before entering the high pressure side of the high temperature recuperator. By doing that, 2nd Law violations in the recuperator may be prevented.

Regeneration is another option in which a fraction of the flow of the working fluid with high temperature is extracted from the turbine at an intermediate pressure to preheat the working fluid before it is effectively heated by the hot source. If done properly, even with the loss of power production caused by the extraction of working fluid before the end of the expansion, the effect of raising the mean temperature of the cycle may increase its 1st Law efficiency.

Cogeneration is not always a viable alternative since it depends on other processes/demands, but is also an important mechanism to be kept in mind. The working fluid is utilized not only to produce power but also to provide heat to another process, i.e., a fraction of the thermal power rejection of the cycle may be reused.

Of course the above presented configuration alternatives generally imply in higher costs of implementation, mainly due to the addition of components and to the increase in the complexity of the cycle. Therefore any modification must be clearly analyzed with respect to the objective of the power plant.

---

[2] The location in a heat exchanger where the temperature difference between the hot and the cold flows is minimal.

2.2.4 Pinch point analysis and discussion

The location in a heat exchanger where the temperature difference between the hot and the cold flows is minimal is called pinch point, which represents a fundamental parameter for designing thermal power and refrigeration cycles [42]. Figure 3 shows a generic representation of a pinch point in a discretized heat exchanger. The temperatures of the hot and the cold flows (T_{Hot} and T_{Cold}, respectively) are represented in the left y-axis; the temperature difference between both flows in a section ($\Delta T = T_{Hot} - T_{Cold}$) is represented in the right y-axis.

Figure 3 – Generic representation of a pinch point in a discretized heat exchanger

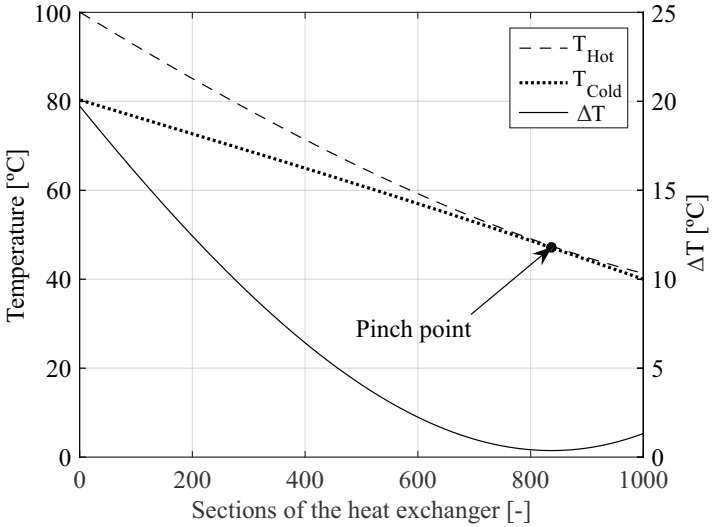

A small ΔT_{Min} makes the heat transfer difficult and, therefore, a bigger heat transfer area or global conductance (UA) is needed; in the limit of $\Delta T_{Min} \rightarrow 0$, an infinite heat transfer area or (UA) would be required. On the other hand, a high ΔT_{Min} corresponds to a smaller, less expensive, but also less effective heat exchanger. So pinch point analysis represents a very important parameter when designing thermal cycles from thermodynamic, economic and sizing standpoints.

As heat spontaneously flows from higher to lower temperatures, in any simulation, the pinch point temperature difference must always be positive ($\Delta T>0$), in order to not violate the 2nd Law, i.e., to ensure that within the entire heat exchanger, $T_{Hot}>T_{Cold}$. Even though the pinch point temperature difference is always positive in a real heat exchanger, in simulations, depending on the calculation procedure, this may not always be the case, which is addressed as a pinch point problem. Figure 4 shows a generic representation of a simulation with a 2nd Law violation in a discretized heat exchanger. The two areas colored in gray make evident the problematic region.

Figure 4 – Generic representation of 2nd Law violation in a discretized heat exchanger

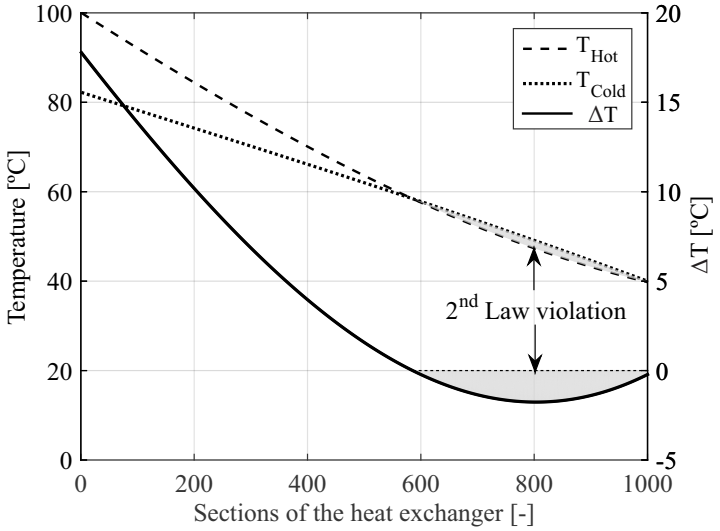

2.2.5 Heat exchanger discretization

Heat exchangers are devices conceived to transfer heat from a hot to a cold fluid through a solid wall. Some possible classifications to these devices are related to the configuration of the flows, e.g. parallel,

counter current, cross, and type of construction, e.g. tube in tube, shell and tube.

An essential step, and often the most inaccurate in any heat exchanger analysis, is the determination of the overall heat transfer coefficient U [43]. Usually this step is accomplished through a complete thermohydraulic project of the heat exchanger [44], but an alternative procedure is to calculate the inverse of the total thermal resistance of a heat exchanger, which is commonly referred to as the heat exchanger conductance (UA) [45].

One of the most typically used methods to determine (UA) is the logarithmic mean temperature difference (LMTD) method which is subjected to some considerations: (a) the heat exchanger is thermally isolated from its neighborhood, i.e., the only heat transfer occurs from the hot to the cold fluid; (b) axial heat conduction, kinetic and gravitational energy variations, pressure drop are negligible; (c) the specific heats of both fluids are constant; (d) the global heat transfer coefficient is constant. The expression to calculate the heat exchanged is indicated by Equation 2.5 [43].

$$\dot{Q} = (UA)\Delta T_{LM} \tag{2.5}$$

In Equation 2.5, ΔT_{LM} is the logarithm mean temperature which is defined by Equations 2.6 and 2.7 for parallel and counter current heat exchangers, respectively [43].

$$\Delta T_{LM} = \frac{(T_{Hot,In} - T_{Cold,In}) - (T_{Hot,Out} - T_{Cold,Out})}{\log\left(\frac{T_{Hot,In} - T_{Cold,In}}{T_{Hot,Out} - T_{Cold,Out}}\right)} \tag{2.6}$$

$$\Delta T_{LM} = \frac{(T_{Hot,In} - T_{Cold,Out}) - (T_{Hot,Out} - T_{Cold,In})}{\log\left(\frac{T_{Hot,In} - T_{Cold,Out}}{T_{Hot,Out} - T_{Cold,In}}\right)} \tag{2.7}$$

Unfortunately, some of the simplifications described above (e.g., “c” and “d”) may not be applied to a large set of applications such as those in which thermophysical property variations are significant.

Therefore, an alternative method to obtain a numerical solution of heat exchanger problems is presented by Reference [45], which is based on slicing the device in n sub-heat exchangers, so assumptions “a”-“d” may be consider valid locally, even though not to the entire assembly.

For this heat exchanger slicing methodology, several quantities may be discretized such as the heat transferred, length, area, (UA). One of the most simple procedures is shown in Figure 5 for a counter current heat exchanger, which consists in the discretization of the total heat transferred $\dot{Q}$ in such way that at each sub-heat exchanger the amount of heat transferred is considered the same, i.e., a $\dot{Q}/n$ constant fraction of the total given heat to be exchanged – the heat transfer area of each sub-heat exchanger is considered variable. As the pressure drop is considered negligible (i.e. heat transfer at constant pressure) for both flows, the heat transferred is due to discrete enthalpy changes. With the inlet conditions of both streams (i.e., hot and cold), it is possible to determine the temperature profiles of both fluids and, therefore, ΔT_{LM} for all slices of the heat exchanger. Then, applying Equation 2.5, the determination of (UA) is possible for all the sub-heat exchangers and the overall global conductance (UA) of the heat exchanger is simply the sum of the (UA) of all sub-heat exchangers.

2.2.6 Equations for energy-exergy analysis

The equations used in this thesis are based on traditional formulations presented by many authors of thermodynamic works, e.g., References [40, 46] – hydrodynamic and heat losses were neglected in all models used. The proper definition of any state within the cycle was done with respect to two thermodynamic properties. In the follow equations, the subscript “Iso” denotes that the property is evaluated with respect to a given outlet parameter and to the inlet specific entropy, i.e., as the process was isentropic.

The specific enthalpy used to determine the outlet state of a turbine is given by Equation 2.8, and it is based on its isentropic

Figure 5 – Schematic of the discretization of a counter current heat exchanger

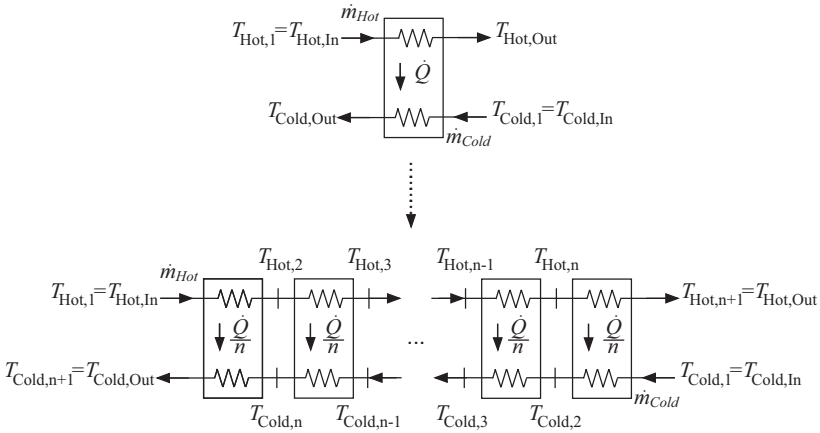

Source: Adapted from Reference [45]

efficiency (η_{T}).

$$\mathrm{h_{Out}} = \mathrm{h_{In}} - \eta_{\mathrm{T}} \left(\mathrm{h_{In}} - \mathrm{h_{Out,Iso}}\right) \tag{2.8}$$

In a similar manner, the specific enthalpy used to determine the outlet state of a pump (or a compressors) is given by Equation 2.9, and it is based on its isentropic efficiency (η_{P} for pump or η_{C} for compressor).

$$\mathrm{h_{Out}} = \mathrm{h_{In}} + \left(\frac{\mathrm{h_{Out,Iso}} - \mathrm{h_{In}}}{\eta_{\mathrm{P}}}\right) \tag{2.9}$$

The sensible thermal power transferred in a heat exchanger is given by Equation 2.10 and depends on its effectiveness (ϵ) and on the maximal exchangeable thermal power $\dot{\mathrm{Q}}_{\mathrm{Max}}$.

$$\dot{\mathrm{Q}} = \epsilon\, \dot{\mathrm{Q}}_{\mathrm{Max}} \tag{2.10}$$

In Equation 2.10, $\dot{\mathrm{Q}}_{\mathrm{Max}}$ is given by Equation 2.11 based on the

inlet parameters of both streams.

$$\dot{Q}_{Max} = \min \begin{cases} \dot{Q}_{Hot,Max} = \dot{m}_{Hot} \left(h_{Hot,In} - h_{Hot} \left(P_{Hot}, T_{Cold,In} \right) \right) \\ \dot{Q}_{Cold,Max} = \dot{m}_{Cold} \left(h_{Cold} \left(P_{Cold}, T_{Hot,In} \right) - h_{Cold,In} \right) \end{cases} \tag{2.11}$$

Another set of equations used in this thesis is referent to the calculation of the exergy destruction (or entropy generation) ($\dot{I}$) of each component of the cycle. Given that the parameters of the dead state (or reference state) are referred to as P_0 and T_0, the specific exergy of each state is given by Equation 2.12.

$$e = [h - h(P_0, T_0)] - T_0 [s - s(P_0, T_0)] \tag{2.12}$$

The exergy destroyed in turbines, pumps (or compressors) and heat exchangers, as well as the total exergy destroyed are given by Equations 2.13, 2.14, 2.15 and 2.16, respectively.

$$\dot{I}_T = \dot{m} T_0 \left(s_{Out} - s_{In} \right) \tag{2.13}$$

$$\dot{I}_P = \dot{m} T_0 \left(s_{Out} - s_{In} \right) \tag{2.14}$$

$$\dot{I}_{HX} = [\dot{m}_{Hot} \left(e_{Hot,In} - e_{Hot,Out} \right)] - [\dot{m}_{Cold} \left(e_{Cold,Out} - e_{Cold,In} \right)] \tag{2.15}$$

$$\dot{I}_{Total} = \sum \dot{I} \tag{2.16}$$

Other equations used in this thesis were basic mass and energy balances.

2.3 CARBON DIOXIDE AS WORKING FLUID

CO_2 shows several advantages when compared with other working fluids: it is non-expensive, abundant, non-toxic, non-explosive, non-corrosive, more chemically stable and reliable, it has a considerably low

critical temperature and a moderate critical pressure, its thermophysical properties are sufficiently known, it is environment friendly as well as studies suggest that CO_2 cycles achieve high compactness levels [19, 28, 47, 48].

In the vicinity of the critical point, thermophysical properties of CO_2 are strongly affected by variations of temperature and pressure. There are several studies dealing with properties variations of supercritical fluids, such as References [49, 50], and particularly focused on CO_2 as reported in References [51–54].

To illustrate the thermodynamic behavior of CO_2, its specific heat at constant pressure (c_P), specific volume (v), thermal conductivity (k) and dynamic viscosity (μ) are shown in Figures 6 and 7 for reduced pressures P_r=P/P_{Crit}=1.05 and P_r=1.25, respectively, as a function of the reduced temperature T_r=T/T_{Crit}.

Figure 6 – Selected CO_2 properties at P_r=1.25 as a function of T_r

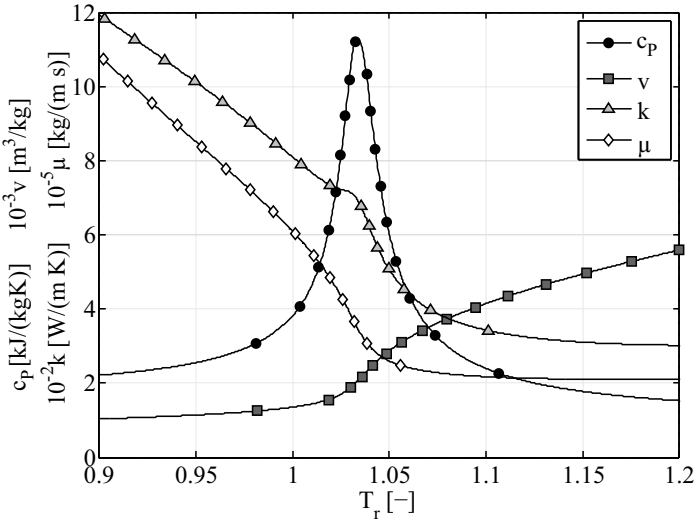

From Figures 6 and 7, it is clear that as $T_r \to 1$ and $P_r \to 1$ the properties variations become stronger. Noteworthy is the peak presented by c_P, which arguably is the main parameter influencing the temperature profiles in heat exchangers.

Figure 7 – Selected CO_2 properties at P_r=1.05 as a function of T_r

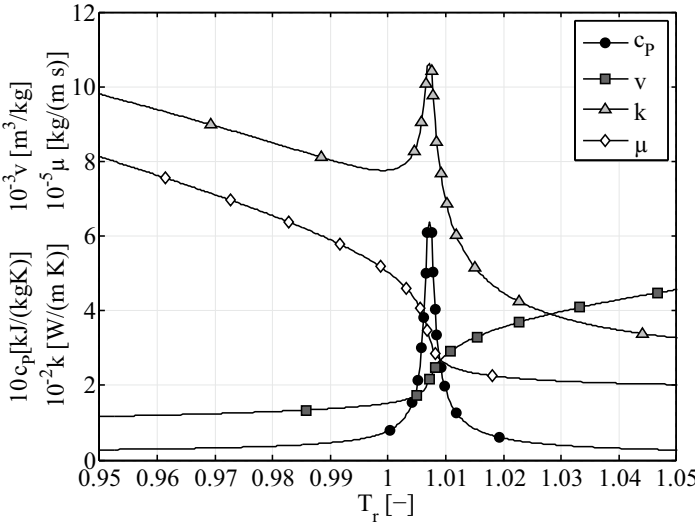

Even though the physical understanding of these properties variations is lacking, as presented in Subsection 2.2.1, they may be exploited to increase the performance of cycles and thermal devices in general. As an example, the size of heat exchangers is significantly affected by sharp variations of the thermophysical properties of CO_2 near to the critical point. Therefore, the performance of such devices should be evaluated and further optimized by taking these effects into account [48].

Another advantage of supercritical CO_2 is clearly shown by Figure 8. From the three options analyzed (a pure organic fluid, a binary mixture and a supercritical fluid) the best fit between temperature profile and sensible heat source is achieved by the supercritical fluid.

It is important to mention that supercritical CO_2 also presents some disadvantages, such as limitations in heat exchangers due to the easy occurrence of pinch point problems [48, 55], the difficult heat rejection to the ambient due to the low critical temperature, the common high temperatures at turbine outlets, and the lacking of properly designed devices to cycles.

Figure 8 – Temperature profile fits between a sensible heat source and (i) a pure organic fluid, (ii) a binary mixture and (iii) a supercritical fluid

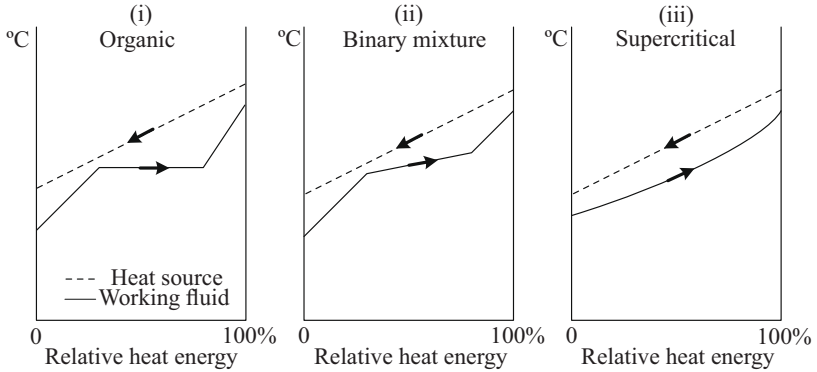

Source: Adapted from Reference [47]

2.4 REVIEW OF SELECTED WORKS

Several selected works are presented next in order to give a comprehensive idea of what has already been developed on CO_2 power cycles. The works were divided in two groups according with the range of the temperature of the heat source used – cycles using low and high temperature sources, respectively – being followed by a summary table. It must be noted that different 2nd Law efficiency definitions were used in this works.

2.4.1 Low temperature sources

Yamaguchi et al. [11] used solar energy collected through evacuated tubes to supply heat to a CO_2 transcritical Rankine cycle. The goal was to provide electricity and heat. Due to the lack of a turbine that could operate with the supercritical fluid, a throttle valve was used as a substitute, therefore, the prototype could not actually generate electricity, which was then thermodynamically estimated.

Zhang et al. [2, 56] investigated theoretically and then experi-

mentally a CO_2 transcritical Rankine cycle powered by solar energy also collected by evacuated tubes, aiming to supply heat and generate electricity. In the theoretical study, an average temperature of 180 °C was adopted and a throttle valve with 90% efficiency was used instead of a turbine. In the experimental prototype, the same cycle configuration was used (same components) reaching a maximal temperature of 187 °C and 70% collector efficiency. Furthermore, through the theoretical study, the annual efficiency of electricity generation and heat supply reached 11.4% and 36.2%, respectively, and it was pointed out that, when compared to other working fluids, CO_2 presented the best performance. In the experimental study, the efficiency of power generation ranged from 8.78% to 9.45% (with the theoretical maximum of 10.7% to 11.6%).

Cayer et al. [47] studied the use of CO_2 in transcritical Rankine cycles with and without a recuperator, using a low temperature waste heat source. The study involved energy and exergy analyzes, finite size thermodynamics and calculation of the surface area of the heat exchangers. The simulations were performed with the Engineering Equation Solver (EES) considering a modified LMTD method and heat transfer correlations. Results show the existence of optimal high pressures that maximize the efficiencies of the cycles or minimize the surface area or (UA) expenditure with the heat exchangers.

Wang et al. [19] optimized the parameters of a CO_2 transcritical Rankine power cycle with a low temperature heat source (60 °C–90 °C) using genetic algorithm and artificial neural networks. The 2nd Law efficiency was used as the objective function for the optimization process. The proposed cycle was composed by a pump with isentropic efficiency of 70%, a turbine with isentropic efficiency of 75%, a heat exchanger to heat the CO_2 using a mixture of 70% steam and 30% air with mass flow rate of 210 kg/s having variable temperature and pressure, and a heat exchanger to cool down the CO_2 using water at 15 °C and with a mass flow rate of 200 kg/s. The influence of parameters such as the high temperature and pressure (from 8 MPa to 11 MPa) of CO_2 over the 2nd Law efficiency was analyzed. A study was also conducted to evaluate the exergy destruction on each component of the cycle as a function of the

above-mentioned parameters relatively to the ambient temperature. The 2nd Law efficiency ranged from about 18% to about 31% and 1st Law efficiency from about 2.5% to about 4.8%. The artificial neural network was shown to be capable of quickly finding the optimal parameters for the cycle and the deviations obtained between the genetic algorithm and by artificial neural network were less than 0.1%. The authors concluded that the operational parameters used to heat the CO_2, the ambient conditions and the parameters at the inlet of the turbine have significant effects on the 2nd Law efficiency.

Cayer et al. [4] conducted a parametric optimization study of a CO_2 transcritical Rankine power cycle based on six performance indicators: 1st and 2nd Law efficiencies, specific net power produced, $(UA)_{Total}$, surface area of heat exchange and relative cost of system. The maximal temperature and pressure as well as the net power produced were used as independent parameters. For a low temperature source, the study revealed the existence of two main net power produced values: the maximal value and the value that minimizes the specific production cost. Also, a comparison of optimized results was conducted between CO_2, ethane and R125. The results show that each fluid has better performance with respect to some particular indicator, as well as that a simple analysis according to the 1st Law is not sufficient to optimally select a working fluid. The authors concluded that there is no way to simultaneously optimize all performance indicators, suggesting the necessity of a compromise solution among the combinations of optimized performance indicators.

Baik et al. [17] theoretically compared the performances of CO_2 and R125 in a transcritical Rankine cycle using the net work produced as the objective function. The cycle consisted of a turbine, a pump and two countercurrent tube-in-tube heat exchangers, which could be easily discretized in the simulations, allowing the determination of the pressure drop and the proper variation of the thermophysical properties. For the comparison between the fluids to be fair, the same temperatures and mass flow rates of the hot and cold source fluids were used for both working fluids (about 100 °C for hot source). Noteworthy is the

fact that a recuperator was not used since it does not influence the objective function (e.g. it would improve the 1st Law efficiency). The total available length for both heat exchangers was specified and its distribution among them was one of the optimization parameters. In order to take into account the variation of the fluid properties within the heat exchangers, each one was discretized in thirty sections with equal length. The LMTD scheme was used to determine the global conductance of each section and widely known correlations were used to calculate the overall heat exchange coefficient and pressure drop. The inlet turbine temperature and pressure were also taken as optimization parameters. For the given operational conditions, the net work produced obtained using R125 was 14% higher than the obtained using CO_2 due to the greater compression work required for the CO_2. Also, the thermodynamic state of the fluid at the turbine outlet was observed to be fairly close to saturation for R125 (a farther one would be safer to the turbine) and the characteristics of the heat exchange and the pressure drop of CO_2 were better. In summary, R125 showed a higher capacity to produce work than CO_2 for the parameters used.

Tuo [57] analyzed the effect of one re-heating stage on a CO_2 transcritical Rankine power cycle taking a basic cycle as reference (without a re-heating stage). Water at 100 °C (idealized as industrial reject) and water at 10 °C were used as hot and cold sources, respectively. The analysis was made with reference to net power produced and to 1st Law efficiency. Results show the existence of two different optimal re-heating pressures corresponding to maximal power produced and maximal 1st Law efficiency. The effect achieved with re-heating was more significant to the power produced than to the 1st Law efficiency indicating that re-heating is a useful strategy when the power produced is to be maximized.

Chen [32] evaluated the potential of CO_2 cycles using low temperature heat sources through computer simulations. The study analyzed the influence of several parameters on the performance of these cycles along with some applications and performance simulations. Also, a discussion regarding the temperature profiles of the fluids within the

heat exchangers, as well as about the variation of c_P (and specifically its importance to CO_2 cycles), and a comparison of a the typical CO_2 power cycle and competing organic power cycles were reported. A 2nd Law analysis dealing with the exergy destruction (or entropy generation) of CO_2 cycles and their components was discussed.

Chennouf et al. [58] studied the use of a CO_2 power cycle to generate electricity from a low enthalpy geothermal source in southern Algeria. The heat source was modeled as an underground porous tank geothermally heated. The parameters analyzed were the geothermal gradient, the permeability of the tank, the diameter and the depth of the pipes connecting the surface to the underground tank, the mass flow rate of the working fluid. The cycle operated between pressures of 7.2 MPa to 40.7 MPa and temperatures of 22.9 °C to 230.1 °C, obtaining a maximal power production of approximately 10.5 MW with a 1st Law efficiency of 17.5% for the optimal mass flow rate of the working fluid.

2.4.2 High temperature sources

Dostal et al. [10] presented an extensive and complete work on advanced CO_2 Brayton cycles for nuclear reactors. The objective was to select the cycle that was best suited to the demands keeping in mind its global optimization, component design, economic analysis, control scheme, in other words not a purely thermodynamic analysis in steady state conditions. A historical and technical contextualization of supercritical CO_2 power cycles was made and the models used for computer simulation were presented (for cycles and for their components). Thermodynamic analyses of some advanced supercritical power cycles were presented and followed by economic analysis and then by the project and components selection. A reference layout of a power plant was presented along with its operational parameters and components as well as its performance analysis. There was also a discussion about control design of cycles (e.g. temperature and pressure) and a comparison of the cycles presented with other advanced power cycles.

Utamura and Tamaura [59] discussed about the indispensability

of the use of recuperators in supercritical CO_2 power cycles in order to achieve greater 1st efficiency values than steam power cycles and about the use of microchannel heat exchangers with high effectiveness. Utamura [60] continued the latter work by taking into account the behavior of CO_2 in the pseudocritical region and its consequences. More specifically, Utamura focused on the possible heat exchange limitation in the recuperator due to the possible existence of pinch point problems. The author proposed the use of a second compressor in a typical Brayton cycle turning it into a cycle with partitioned flow in order to avoid pinch point problems within the recuperator. The minimum pressure was selected as 7.55 MPa to reduce the compressor work – taking advantage of the decreasing compressibility factor of CO_2 in the vicinity of the critical point. The pressure and temperature limits admitted were 20 MPa and 800 K, respectively, in accordance to limitations of materials used in such applications. The cycle was parametrically optimized achieving a maximal 1st Law efficiency of 45% for the optimal parameters – which is considerably higher than the 1st Law efficiency achieved by a typical Brayton cycle, which tops at roughly 39%. It was emphasized that, for the proposed cycle, the 1st Law efficiency is strongly affected by the pressure drop across the heat exchanger (hence the possible importance of microchannel heat exchangers).

Kulhanek and Dostál [55] analyzed the use of CO_2 in a typical Brayton power cycle and in more five different Brayton configurations proposed by Angelino [13]: with pre-compression, with re-compression, split-expansion, with partial cooling and an improved partial cooling with regeneration. The authors discussed about pinch point-problems within the recuperators and showed that through the division of fluid flow those problems could be prevented in all cycles except in the pre-compression cycle in which an additional compressor is needed. Results showed that the operation in the vicinity of the critical point did not improve significantly the 1st Law efficiency of the simple Brayton cycle – only with the high pressure ($\sim$ 25 MPa) was noticed a significant improvement. Also, the results clearly confirmed that there is not a global ideal setting or configuration for the cycles, but ideal ones for

different objective functions. For example, the highest 1st Law efficiency is achieved with the partial cooling cycle with the outlet pressure of the compressor in the range of 10 MPa to 15 MPa. The authors also listed some other aspects that could be investigated in future studies as the dynamic behavior of cycles, economic analyzes, usage of different materials for equipment.

2.4.3 Summary

Table 1 summarizes the selected works presented in Sub-sections 2.4.1 and 2.4.2.

Table 1 – Summary of the selected works about CO_2 power cycles

Low Temperature	High Temperature	Topics
• Yamaguchi et al. (2006) • Zhang et al. (2007) • Cayer et al. (2009) • Wang et al. (2010) • Cayer et al. (2010) • Baik et al. (2011) • Tuo (2011) • Chen (2011) • Chennouf et al. (2013)	• Dostal et al. (2004) • Utamura and Tamura (2007) • Utamura (2010) • Kulhanek and Dostal (2011)	• Transcritical Rankine and supercritical Brayton cycle • Several heat sources: solar, geothermal, waste heat, nuclear • Several configurations • Recuperators, recompression, re-heating • Pinch point analysis • Parametric optimization of parameters • Comparison between CO_2 and competing fluids

3 MODELING OF CO_2 TRANSCRITICAL RANKINE CYCLES

This chapter is dedicated to the modeling developed for the analysis of Rankine cycles. The concept of the analysis is discussed, then the modeling is extensively presented and the validation performed is discussed.

3.1 CONCEPT OF THE ANALYSIS

Among the numerous advantages obtained with the use of CO_2 in power cycles, the compactness of the plant, which can be understood, for example, as power produced per unit of volume or area of the plant, can undoubtedly be listed as a key aspect. Therefore, it is plausible to realize that, while determining the total area of a power plant one needs to take into account all its components, which include turbines, pumps, heat exchangers, fluid lines, etc – for instance, heat exchangers are responsible for a significant share of the footprint of the plant. Additionally, in order to further emphasize the compactness of such power plants, it would be desirable to determine the effect of the power plant size on key main performance parameters, such as the net power produced, 1st and 2nd Law efficiencies.

With that in mind, a key parameter commonly related to the size of heat exchange devices is the global conductance (UA) [46, 61]. Therefore, it becomes obvious that, for a given temperature of a heat source (T_{HSo}), the higher the (UA) parameter, the higher the temperature of the working fluid within the cycle (i.e., $T_{CO2,High} \rightarrow T_{HSo}$), which ultimately increases its performance (e.g., $\dot{W}_{Net}$,η_I). Notice, however, that the inverse behavior is presented by the ratio $\dot{W}_{Net}/(UA)$, since $(UA) \rightarrow \infty$ when $(T_{HSo}\text{-}T_{CO2,High}) \rightarrow 0$. Conversely, in the limit of small (UA) values, $\dot{W}_{Net}$ decreases due to the fact that the difference between the temperature of the heat source and the CO_2 immediately after the heater also increases. Therefore, in this limit, the $\dot{W}_{Net}/(UA)$ ra-

tio also decreases since the drop of $\dot{W}_{Net}$ is stronger than the drop of (UA). Thus, based on the above, its plausible that optimal $\dot{W}_{Net}/(UA)$ combinations might be determinable – details regarding this optimum defining methodology can be found in [62]. Furthermore, the parameter $(UA)_{Total}$ can also include the effect of the condenser and other heat exchangers present in the cycle. This analysis may be extended to other figures of merit.

3.2 MODELING

To further study the performance of CO_2 power plants per unit of global conductance, the thermodynamic model implemented considers four types of CO_2 transcritical Rankine cycles. Three of these are commonly reported in the literature: (i) a basic Rankine cycle (i.e., Reference), (ii) a Rankine cycle with a recuperator (i.e., Recuperative) and (iii) a re-heating Rankine cycle – these are shown in Figure 9a-c. The fourth cycle is a hybrid Rankine cycle, since it combines a recuperator and a re-heating process, as shown in Figure 9d. Furthermore, notice that, in the latter configuration, the number of re-heating stages can be as high as three, which are respectively entitled as Combined A (N=1), Combined B (N=2) and Combined C (N=3). Also, it is important to state that while the basic Rankine cycle is not often used, since variations of this basic configuration can achieve higher performances, the reason for studying an unmodified Rankine, case (i) above, is that its performance can be used as a reference for the other configurations tested.

Each of the power cycles considered was modeled using the formulation presented in Subsection 2.2.6 and involves specific control volumes around each component of the cycle, while enforcing the conservation of mass and energy, and the 2nd Law. Additionally, all heat exchangers within the cycle were considered to have a counter flow of the heating and cooling fluids and were sliced in 1000 sections to properly account for the strong dependence of the thermophysical properties of the CO_2 on the temperature around the critical point, which allowed

Figure 9 – Schematic of the Rankine power cycles simulated: (a) Reference cycle, (b) Recuperative cycle, (c) Re-heating cycle, (d) Combined A (i.e., combined cycle with one re-heating stage)

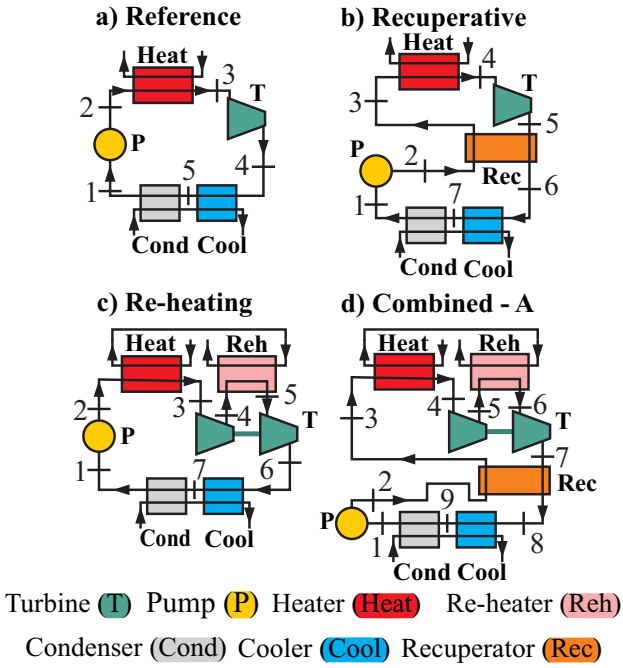

a nearly local bulk evaluation of the properties needed as presented in subsection 2.2.5. The slicing procedure allows the verification of 2nd Law violations in n+1 points. Furthermore, in all models, hydrodynamic and heat losses were disregarded in all components of the cycles considered.

The simulations performed involved a series of steps, which were implemented in numerical routines in MATLAB [63]. To account for fluids properties, the freeware library CoolProp [8, 9] was used, which is based on the equation of state reported in Reference [64]. The thermodynamic routine depended on the cycle being simulated and the heat source used (i.e., sensible or latent). For the latent heating simulations (i.e., Figures 11-18), regardless of the cycle or the operational conditions, the following parameters were held constant: pump inlet

and outlet pressures, CO_2 quality at the pump inlet (x=0) and between the two cooling heat exchangers (x=1), all turbines and pumps have isentropic efficiencies of $\eta_T = \eta_P$ =0.8, effectiveness of the recuperator $\epsilon_{Rec} = 0.85$ and mass flow rate of CO_2 ($\dot{m}_{CO2}$) of 1 kg/s — notice that the given value for ϵ_{Rec}, which is defined as the ratio between the actual thermal power transferred within the recuperator ($\dot{Q}_{Rec}$) and maximal thermal power that could be transferred ($\dot{Q}_{Rec,Max}$), will be discussed later along with Figure 18. As for the heat source, water vapor or a mixture of vapor and liquid water was used and assumed always within the saturation and at 100 °C. Therefore, $T_{CO2,High}$ could get close to 100 °C, while the vapor condensates inside the heat exchanger. As for the cooling fluid, liquid water at atmospheric pressure was used. It is relevant to mention that the flow rate of the cooling fluid ($\dot{m}_{HSi}$) was calculated such that CO_2 is brought to the thermodynamic conditions discussed above, while subjected to inlet and outlet temperatures of $T_{HSi,In}$=10 °C and $T_{HSi,Out}$=15 °C, respectively [47]. Note that the inlet pressure of the pump was set at 6.5 MPa, which represents a saturation temperature of approximately 25 °C, granting a pinch point temperature difference of at least 10 °C between the CO_2 and the cooling fluid – again, similar values for the pressure and temperature of the cooling fluid were adopted in Reference [47]. Also, the pump outlet pressure was set at 11 MPa, which returned a CO_2 post-turbine temperature higher than the after pump temperature enabling the use of a recuperator. Note that only in Figure 18 the effectiveness of the recuperator was varied.

Since there are four types of configurations considered in the present study, it would be cumbersome to fully describe the calculation procedure developed of each configuration. Therefore, for sake of illustration, an itemized description of the calculation process for the Combined A cycle, which can be considered one of the most complex configurations simulated, is shown below – other calculation routines can be seen in the Appendix A. The calculation procedure of Combined A cycle can be seen in the flowchart represented by Figure 10. Therefore, following Figure 10 from top to bottom along with the thermodynamic

Figure 10 – Flowchart indicating the calculation procedure for Rankine Combined A cycle configuration

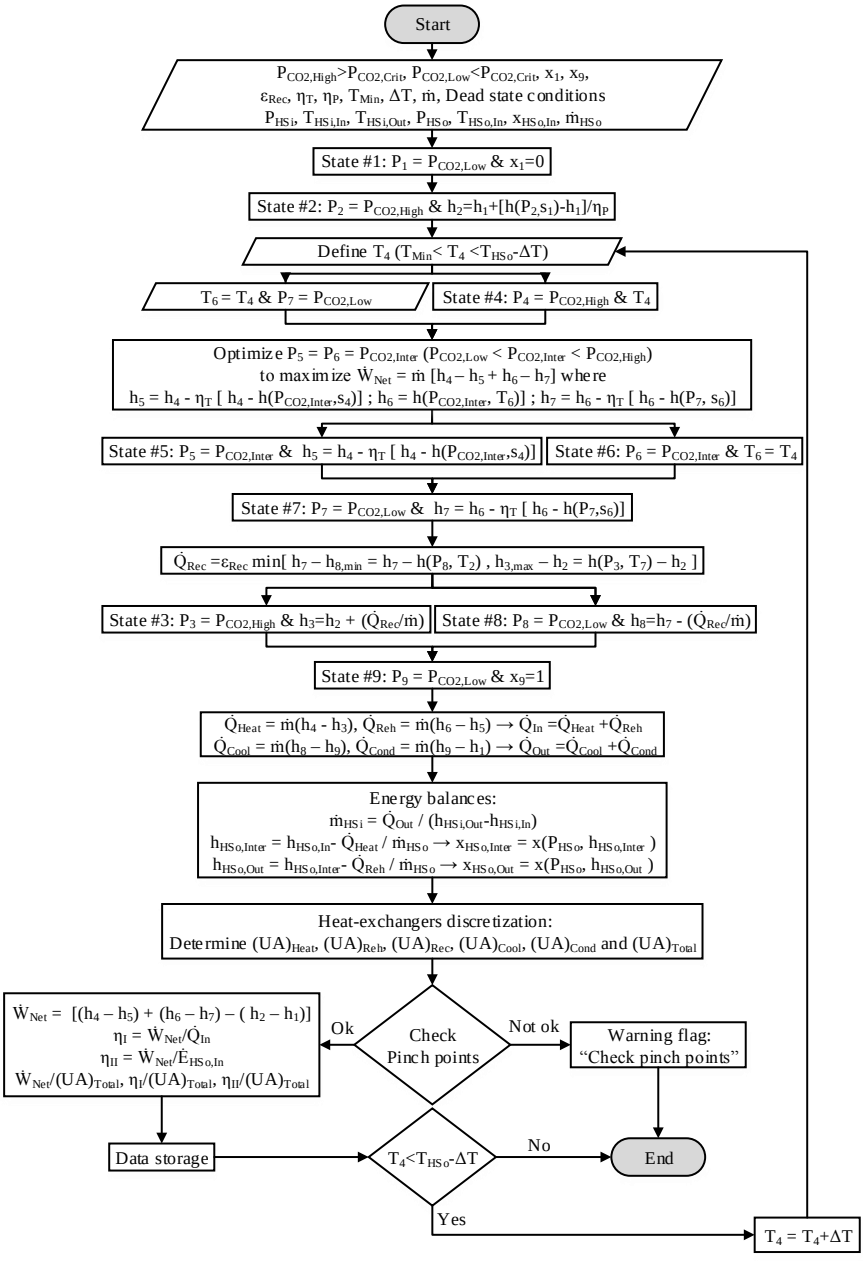

indexing described in Figure 9d, one starts by setting P_1=6.5 MPa and specifying a value for P_2, which are referred to in the study as $P_{CO2,Low}$ and $P_{CO2,High}$, respectively – notice that $P_{CO2,High}$ must be higher than the critical pressure of CO_2, while $P_{CO2,Low}$ must be lower, such that they characterize a transcritical power cycle. As previously described, the routine also sets the thermodynamic state of CO_2 after the cooler as saturated vapor (i.e., x_9=1) and saturated liquid after the condenser (i.e., x_1=0). Also, the values of ϵ_{Rec}, η_T, η_P, $\dot{m}$, the minimum inlet temperature of the turbine (T_{Min}) and its the increment (ΔT) are also provided to the routine and kept constant throughout the simulations. Furthermore, the inlet and outlet thermodynamic states of the fluid working as heat sink is defined by P_{HSi} = 101.325 kPa $T_{HSi,In}$ = 10 °C, $T_{HSi,Out}$ = 15 °C. Similarly, the inlet thermodynamic state of the heating fluid is considered saturated vapor ($x_{HSo,In}$=1) at P_{HSo}=101.325 kPa (T_{HSo}=100 °C), with mass flow rate ($\dot{m}_{HSo}$) of 1 kg/s. Next, having P_2 and the pump efficiency, one can determine h_2. Following, the optimization process of T_4 is initiated by selecting a T_4 while respecting its upper and lower bonds (i.e., T_{Min} and T_{HSo}). Then, T_6 is equated to T_4, $P_7 = P_{CO2,Low}$ and P_4=$P_{CO2,High}$. Next the intermediate pressure ($P_{CO2,Inter}$) is optimized, such that power produced by both turbines is maximized for the previously selected T_4 – note that $P_{CO2,Inter} = P_5$ and P_6. The determination of P_5 allows the calculation of h_5 and, since $P_7 = P_{CO2,Low}$ and state "6" is fully defined through (T_6 and P_6), h_7 can be calculated while relying on the isentropic efficiency of the turbine – see "State #7" in the flowchart. Next, the amount of thermal power exchanged in the recuperator is calculated – see Figure 10 for specific equations. After calculating $\dot{Q}_{Rec}$, one can fully characterize states "3" and "8", also allowing the calculation of the thermal power transferred in the condenser, cooler, heater, re-heater, as well as the total thermal power gained ($\dot{Q}_{In}$) and released ($\dot{Q}_{Out}$). The complete set of thermodynamic states for the CO_2, allows the determination of the intermediate and outlet enthalpies of the heat source ($h_{HSo,Inter}$ and $h_{HSo,Outr}$, respectively). The mass flows rate of the cooling fluid is calculated through a energy balance within the cooler and the condenser.

Finally, all heat exchangers are discretized and their global conductances (UA) are determined while checking for the existence of pinch points problems, which allows the calculation of the absolute and $(UA)_{Total}$ normalized values of $\dot{W}_{Net}$, η_I and η_{II}. Next, T_4 is updated by a ΔT, and the simulation is re-run, which allows the determination of the curves shown in Figures 11-15. Recall that these curves were obtained for a given $P_{CO2,High}$ and that the routine needs to be rerun for different $P_{CO2,High}$, different configurations, etc.

Furthermore, for the sensible heating calculations, the solution process followed a similar routine, however, in this case, two independent variables were considered, i.e., $P_{CO2,High}$ and T_{HSo}. In order to simulate cycles operating at higher temperatures, the phase change heating fluid considered was replaced with a sensible heating gas, more specifically, dry air with a mass flow rate of 15 kg/s – note that the scale of the mass flow rate of the heat source was intentionally selected such that it would allow a noticeable temperature drop as it released heat to CO_2, in accordance to Equation 3.1. In this case, the heat source temperature was not necessarily limited by the saturation temperature of the water and higher values for T_{HSo} and for the operational pressure of the cycle ($P_{CO2,High}$) could be considered. Consequentially, several combinations of T_{HSo} and $P_{CO2,High}$ were tested in order to study the optimal sizing trends for the transcritical cycles considered herein.

$$\dot{Q} = \dot{m}\Delta h \approx \dot{m}\bar{c}_P\Delta T \tag{3.1}$$

More information regarding the calculation procedure for the other configurations is available in Appendix A.

3.3 VALIDATION

The thermodynamic simulations were validated against two sets of independent results presented in the literature, i.e., References [47] and [17], which are also obtained from thermodynamic simulations (experimental results were unavailable). The comparisons were implemented by simply enforcing the operational parameters employed in

these References directly in our code – note that the operational parameters used considered T_{HSo} = 100 °C, $\eta_T = \eta_P$ =0.8, $T_{HSi,In}$=10 °C and $T_{HSi,Out}$=20 °C – further information can be found directly in each Reference. Tables 2 and 3 below display the results obtained for the power produced and 1st Law efficiency and the percentage deviation between the present work and the References, which is defined by Equation 3.2.

$$\text{Deviation}=100 \cdot \frac{|\text{Present work-Reference}|}{\text{Present work}} \tag{3.2}$$

Table 2 – Validation #1 of CO_2 transcritical Rankine cycles

Validation against Reference [47]			
	Present work	Reference [47]	Deviation [%]
w_{Net} [kJ/kg]	18.801	18.8	<0.1
η_I [%]	8.61	8.6	0.11

Table 3 – Validation #2 of CO_2 transcritical Rankine cycles

Validation against Reference [17]			
	Present work	Reference [17]	Deviation [%]
$\dot{W}_{Net}$ [W]	289.5	289.8	<0.1
η_I [-]	0.0564	0.056	0.71

As expected, the agreement is very good, indicating the correctness of the thermodynamic model tested. Furthermore, it is also relevant to mention that several other consistency tests were implemented along the study, even though these are not explicitly reported. For instance, verification studies considering the correctness of energy and $\dot{W}_{Net}$-$\dot{I}_{Total}$ balances, pinch points, etc, were often enforced.

4 RESULTS OF CO_2 TRANSCRITICAL RANKINE CYCLES

This Chapter discussed the results obtained with the analysis of Rankine cycles. There are three main Sections in this Chapter: results for latent heat sources (Section 4.1), results for sensible heat sources (Section 4.2) and normalized 2nd Law optimization (Section 4.3).

4.1 LATENT HEAT SOURCE

The proposed analysis starts by highlighting the effect of the total global conductance $(UA)_{Total}$, which is shown on the x-axis of Figures 11, 12 and 13, respectively, the total net power produced, the 1st and 2nd Law efficiencies – notice that $(UA)_{Total}$ is calculated by selecting the temperature downstream the heater (i.e., T_3 in Figure 9a).

From Figure 11, $\dot{W}_{Net}$ tends to increase as the temperature difference between the condensing fluid of the heat source, which is maintained at 100 °C, and the working fluid (i.e., CO_2) is minimized (i.e., as $(UA)_{Total}$ increases). Additionally, the results shown in Figure 11 indicate that the Reference cycle is capable of generating the same net power output as the Recuperative cycle – the maximal net power produced by both cycles levels off approximately between 12 and 13 kW. The main difference is that the Reference cycle is able to produce that with a significantly smaller total global conductance. Obviously, this difference is mostly due to the additional area needed by the recuperator. From the same figure, it can also be observed that the Combined cycles are the ones that present the highest net power output while requiring overall $(UA)_{Total}$ values comparable to that of a Recuperative cycle – notice also the existence of a diminishing return as the number of re-heating stages increases. However, while the trends displayed by the Combined cycle configurations are somewhat encouraging, it is important to keep in mind that, ideally, the most sought region in Figures 11 and 12 is its upper left corner, since it represents the highest

net power output with the smallest total global conductance. Therefore, the cycle with re-heating is arguably the best performing cycle given its combination of relatively high performance and reduced $(\mathrm{UA})_{\mathrm{Total}}$.

Figure 11 – Effect of $(\mathrm{UA})_{\mathrm{Total}}$ on $\dot{\mathrm{W}}_{\mathrm{Net}}$ for all Rankine cycles simulated considering a latent heat source

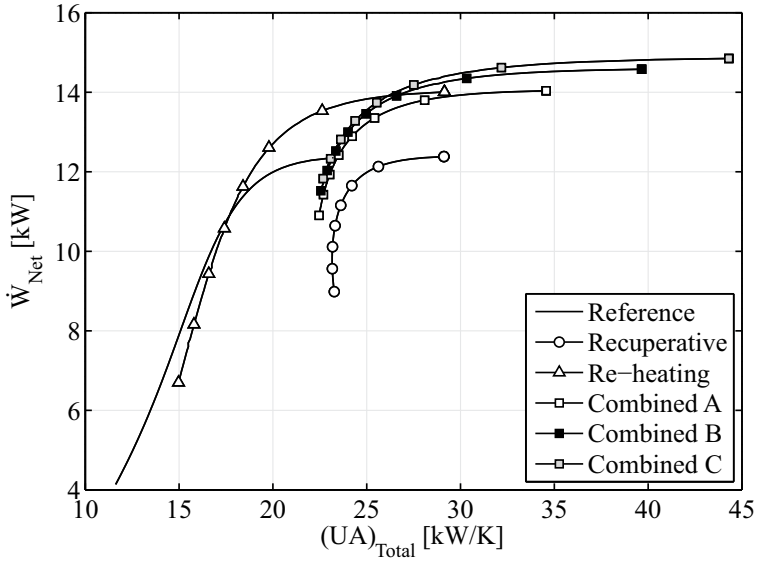

Figure 12 shows the effect of $(\mathrm{UA})_{\mathrm{Total}}$ on η_{I}. As can be seen, the general trends obtained for the 1st Law are very similar to the ones obtained for the net power produced (Figure 11). However, the absolute value of the efficiencies changes more significantly when comparing configurations with and without a recuperator. For instance, the Reference and the Re-heating cycles continue to present the lowest values of $(\mathrm{UA})_{\mathrm{Total}}$ when η_{I} is maximal – the efficiency for both of these configurations is between 0.055 and 0.06. Differently, when a recuperator is added to the cycle, a certain amount of thermal energy, which is lost in the Reference and the Re-heating cycles, is recovered through the recuperator and reutilized, hence, minimizing the amount of thermal energy that needs to be supplied by the heat source. Consequently, by definition, η_{I} tends to increase as shown by the curves representing

Figure 12 – Effect of $(UA)_{Total}$ on η_I for all Rankine cycles simulated considering a latent heat source

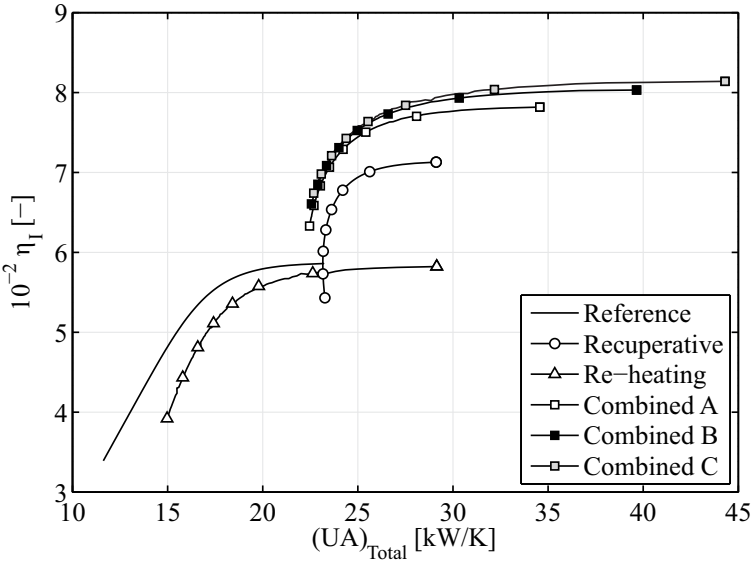

Figure 13 – Effect of $(UA)_{Total}$ on η_{II} for all Rankine cycles simulated considering a latent heat source

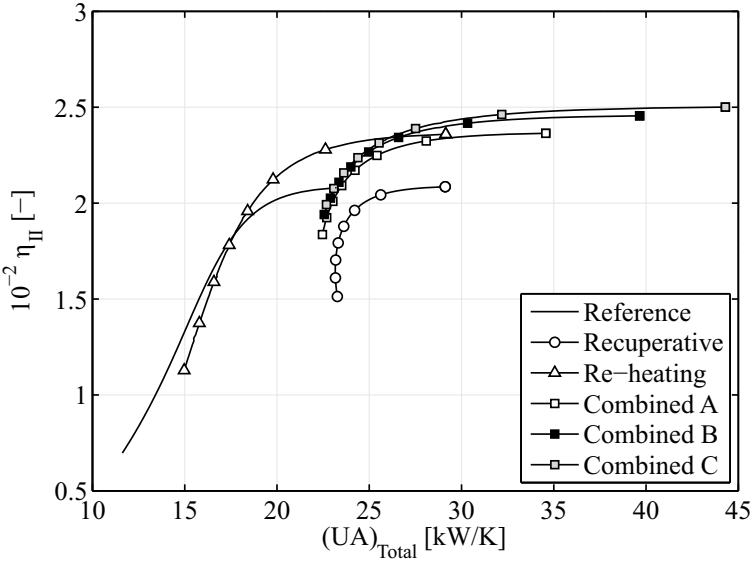

the cycles with a recuperator (i.e., Recuperative and Combined). Furthermore, Combined cycles present even higher efficiencies than the Recuperative cycle. This is due to the fact that during the re-heating processes, more heat is added to the cycle, which increases the power output and the thermal energy recovered within the recuperator, since the CO_2 temperature downstream turbine tends to increase while having the same low exit pressure.

Figure 13 shows the effect of $(UA)_{Total}$ on η_{II}. With the definition of η_{II} in mind (Equation 2.3) and knowing that the exergy transfer rate provided by the heat source ($\dot{E}_{HSo,In}$) is constant – P_{HSo}, T_{HSo} and $\dot{m}_{HSo}$ are constant – the curves presented are a simple rescaling of the those in Figure 11.

As previously discussed in Section 3.1, one of the main goals of this study is to determine the optimal scale of CO_2 transcritical Rankine power plants. Therefore, Figures 14, 15 and 16 show the effect of $(UA)_{Total}$ on $\dot{W}_{Net}$, η_I and η_{II} per unit of $(UA)_{Total}$, respectively. In Figure 14, it becomes clear that a well-established optimum exists for each configuration, with the Re-heating cycle displaying the highest ratio followed by the Reference cycle. The existence of a peak for each of the curves is obviously associated with competing slopes caused by the effect of $T_{CO2,High}$ on $\dot{W}_{Net}$ and the respective $(UA)_{Total}$ needed. For instance, for low $(UA)_{Total}$ values, $\dot{W}_{Net}$ decreases drastically as $T_{CO2,High}$ also decreases – recall that the value of $\dot{W}_{Net}$ is associated with the CO_2 temperature after the heater. Consequently, the drop in $\dot{W}_{Net}/(UA)_{Total}$ as $(UA)_{Total}$ decreases indicates that the ratio is dominated by the reduction of $\dot{W}_{Net}$ rather than the increase of the ratio caused by the inverse of $(UA)_{Total}$. In the limit of large $(UA)_{Total}$ values, $\dot{W}_{Net}$ tends to stabilize (see Figures 11 and 12) as the maximal temperature of CO_2 within the cycle approaches the heat source temperature with increasing values of $(UA)_{Total}$, causing the inevitable drop in the $\dot{W}_{Net}/(UA)_{Total}$ ratio. Also interesting is to observe that, while the Combined configurations offered the highest $\dot{W}_{Net}$ values according to Figure 11, these present maximal $\dot{W}_{Net}/(UA)_{Total}$ performances that are roughly between 15-20 % lower than the peak performance of the

Re-heating cycle. The reasoning for this behavior is mostly due to the fact that the peak performance for these curves are located in far right side of the respective peaks for the Re-heating and Reference cycles, which have configurations with much smaller $(\mathrm{UA})_{\mathrm{Total}}$ values.

Figure 14 – Effect of $(\mathrm{UA})_{\mathrm{Total}}$ on $\dot{\mathrm{W}}_{\mathrm{Net}}/(\mathrm{UA})_{\mathrm{Total}}$ for all Rankine cycles simulated considering a latent heat source

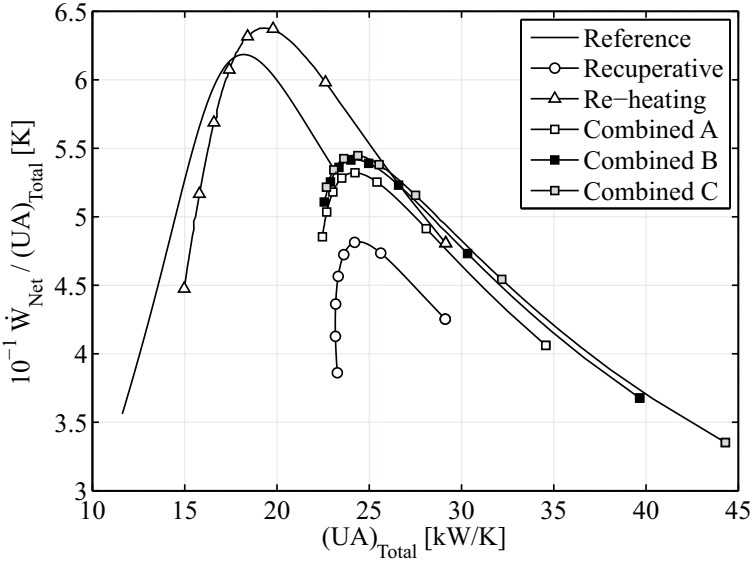

Similarly, the curves for $\eta_{\mathrm{I}}/(\mathrm{UA})_{\mathrm{Total}}$ shown in Figure 15 present a similar behavior as the ones shown in Figure 14. One of the key differences is that the Reference cycle displays the highest ratio among all configurations simulated, even when compared to the Recuperative cycle. This is related to the fact that the Recuperative cycle needs a larger (UA) value due to the presence of the recuperator, which leads to a $\eta_{\mathrm{I}}/(\mathrm{UA})_{\mathrm{Total}}$ ratio that is lower than the ratio of the Reference cycle.

Figure 16 presents the $(\mathrm{UA})_{\mathrm{Total}}$ normalized 2$^{\mathrm{nd}}$ Law efficiency. Similarly to Figures 11 and 13, Figure 16 is a rescaling of the curves presented in Figure 14 since the overall incoming exergy us fixed. The same considerations made to Figure 13 with respect to Figure 11 are applied to Figure 16 with respect to Figure 14, i.e., the curves are a

Figure 15 – Effect of $(UA)_{Total}$ on $\eta_I/(UA)_{Total}$ for all Rankine cycles simulated considering a latent heat source

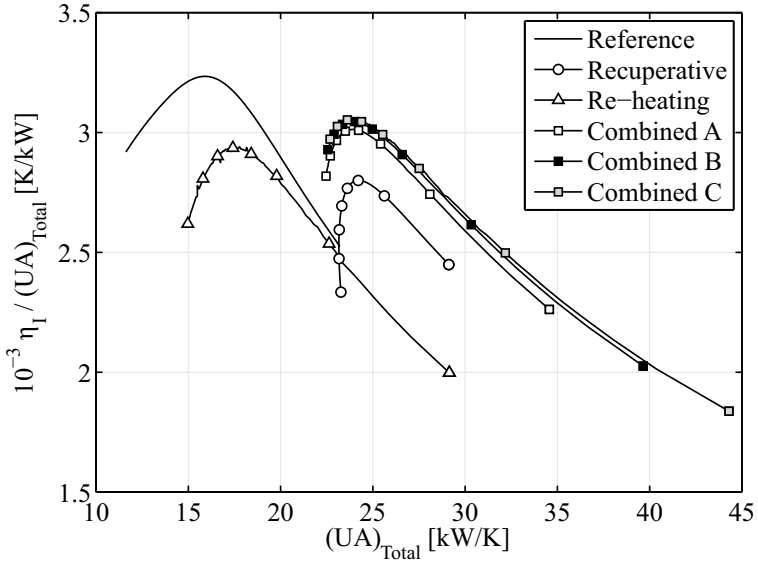

Figure 16 – Effect of $(UA)_{Total}$ on $\eta_{II}/(UA)_{Total}$ for all Rankine cycles simulated considering a latent heat source

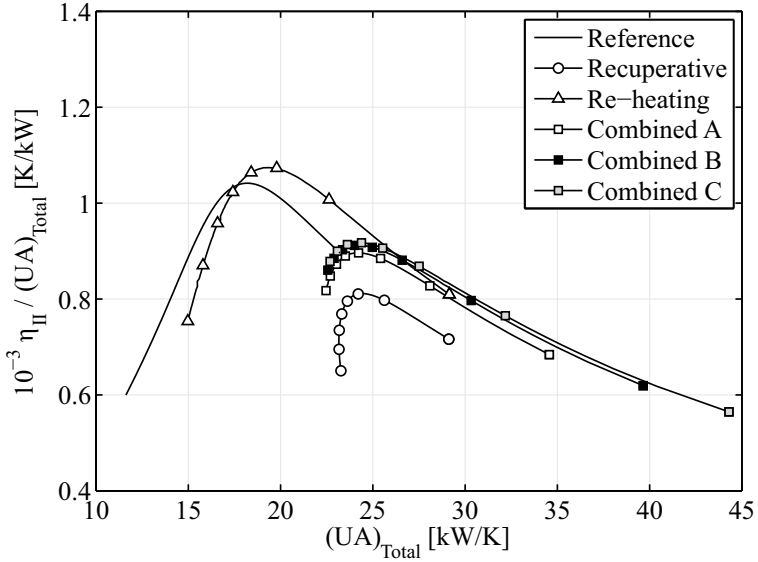

simple rescaling.

To complement the results shown in Figure 14, one can also indicate how $(UA)_{Total}$ is distributed among all heat exchangers within the cycle and the direct relation between $(UA)_{Total}$ and the maximal CO_2 temperature within the cycle ($T_{CO2,High}$). Therefore, Figure 17 shows the effect of $T_{CO2,High}$ (x-axis) on $(UA)_{Total}$ (left y-axis) and its distribution per heat exchanger present in the cycle (right y-axis). While these results can be shown for all configurations considered, the above-mentioned distribution will be detailed only for the Recuperative cycle. As expected, the behavior shown in Figure 17 reveals a steep increase of $(UA)_{Total}$ as the temperature of CO_2 tends to the temperature of the heat source. Obviously, this is associated with the reduction of the temperature difference between both streams, which leads to higher values of $(UA)_{Total}$. Also interesting is that, while the (UA) spent in the heater increases with $T_{CO2,High}$, the (UA) used in the condenser remains basically constant, even when $T_{CO2,High} \rightarrow 100\,°C$. Differently, the (UA) spent in the cooler, which represents the sensible heat transfer part of the heat rejection system, presents a minor, almost unnoticeable, increase. This is associated with the fact that the thermodynamic state at the turbine outlet moves away from the saturated vapor condition as $T_{CO2,High} \rightarrow 100\,°C$, which increases the amount of thermal energy that needs to be exchanged. Finally, it is also worth mentioning that the (UA) factor for the recuperator presents a drop of roughly 20% as $T_{CO2,High}$ increases. At first, this behavior might be considered counterintuitive, however, a closer look indicates that the reduction is associated with the fact that the amount thermal power transferred within the recuperator is less influenced by $T_{CO2,High}$ than the average temperature circulating the in recuperator, which results in the drop of (UA).

Also, the effectiveness (ϵ) of the heat exchangers used in the cycles can have a significant effect on their performances. For sake of conciseness, the influence of the effectiveness on the performance of the cycles is shown for the Combined A cycle (i.e., Figure 9d) only in terms of $(UA)_{Total}$ (x-axis) and $\eta_I/(UA)_{Total}$ (y-axis), and refers to the effectiveness of the recuperator (ϵ_{Rec}). The results shown in Figure 18

Figure 17 – Effect of $T_{CO2,High}$ (x-axis) on $(UA)_{Total}$ (left y-axis) and on $(UA)_{Total}$ distribution (right y-axis) for the Rankine Recuperative cycle

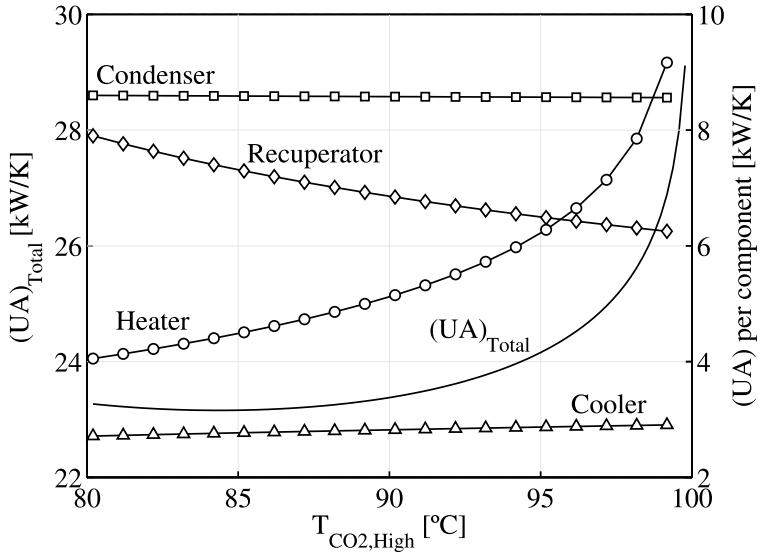

indicate that the figure of merit $\eta_I/(UA)_{Total}$ can drop to almost a third of its maximal value by varying ϵ_{Rec} between 0.30 and 0.999. This behavior is expected because η_I increases asymptotically and $(UA)_{Total}$ exponentially with ϵ_{Rec}, i.e., η_I tends to stabilize with $\epsilon_{Rec} \rightarrow 1$, but $(UA) \rightarrow \infty$, which certainly decrease the ratio $\eta_I/(UA)_{Total}$.

Potentially more interesting is that, for $\epsilon_{Rec} > 0.90$ or so, there are two possible solutions (i.e., two values for $\eta_I/(UA)_{Total}$) for some $(UA)_{Total}$ – notice that the transition between the single and the dual solution regions depends on several parameters and the estimate presented (i.e., ~ 0.9) should not be considered an absolute transition value. This dual solution can be associated to the fact that, for a given $(UA)_{Total}$, and aside from the fraction utilized for the cooler and the condenser (which are almost constant), the remaining $(UA)_{Total}$ can be unequally divided between the heater and the recuperator. Consequently, two plausible solutions can be obtained for a single $(UA)_{Total}$. Additionally, the results reported present the existence of a maximal

value of $\eta_I/(UA)_{Total}$ for a given ϵ_{Rec}. These maximal values, which are indicated by the open circles, are related to the tradeoff between η_I and $(UA)_{Total}$ as discussed in Figures 14 and 15. Finally, it is also worth mentioning that, according to Figure 18, there is an optimal effectiveness value ($\epsilon_{Rec,Opt}$ ~0.6), which offers an overall maximum for $\eta_I/(UA)_{Total}$ – this occurs for $(UA)_{Total}$~20 kW/K. While the drop of $\eta_I/(UA)_{Total}$ for $\epsilon_{Rec} > \epsilon_{Rec,Opt}$ can be understood as discussed above, its reduction for $\epsilon_{Rec} < \epsilon_{Rec,Opt}$ is less obvious. This reduction is in fact associated with the substantial reduction of η_I as $(UA)_{Total}$ decreases. Therefore, based on the results displayed in Figure 18, it can be observed that $\epsilon_{Rec} = 0.85$ allows for a reasonably high performance of the recuperator without disregarding practical aspects associated with even higher values of ϵ_{Rec}; hence, this is the effectiveness value considered for all recuperators used in the Rankine study. Furthermore, similar sets of the curves as the ones shown in Figure 18 can be obtained for other figures of merit (i.e.,$\dot{W}_{Net}/(UA)_{Total}$ and $\eta_{II}/(UA)_{Total}$). While these are not shown, the general trend is similar to the one depicted in Figure 18.

Finally, it is important to comment on the fact that the values displayed up to now (e.g., Figures 14, 15 and 16) are not necessarily independent of the inlet temperature of the water used to cool down the cycle. For instance, simulations performed showed that the absolute and relative values determined of the figures of merit considered could change quite significantly with the cooling water temperature. For example, if the cooling water inlet temperature is set at 15 °C, only 5 °C more than the value used to determine the values presented so far, the Combined cycles display a higher normalized 1st Law efficiency (i.e., $\eta_I/(UA)_{Total}$) than the Reference cycle, which is the opposite of the tend observed in Figures 14 and 15.

Figure 18 – Effect of (ϵ_{Rec}) on $\eta_{II}/(UA)_{Total}$ for the Rankine Combined A cycle considering a latent heat source

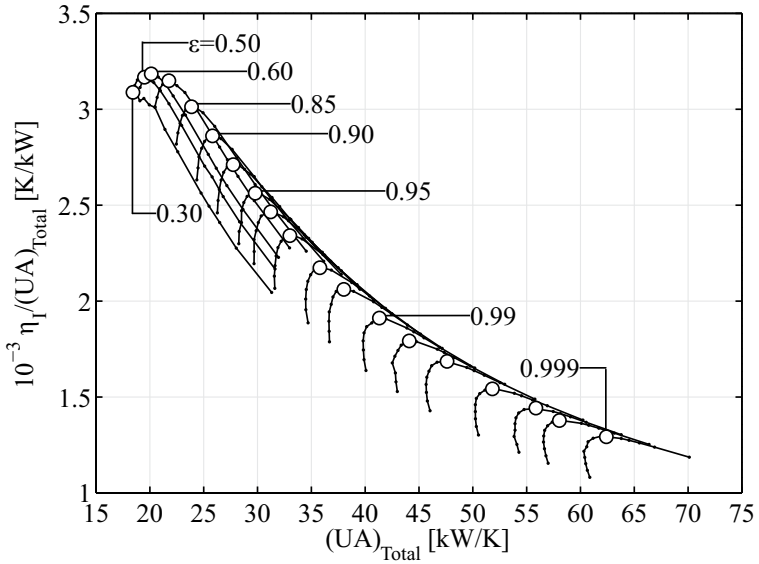

4.2 SENSIBLE HEAT SOURCE

Figures 19, 20 and 21 detail the behavior of $\dot{W}_{Net}$, η_I, and η_{II}, respectively, considering that the cycle operates at $P_{CO2,High}$=20 MPa and the heat source operates at T_{HSo}=200 °C and $\dot{m}_{HSo}$=15 kg/s. When analyzing these Figures, several points needed to be discussed. The first is the trend displaying the strong dependence of the absolute figures of merit with $(UA)_{Total}$ (e.g., $(UA)_{Total}$<20 in the Reference cycle). Again, this trend is related to the fact that the CO_2 temperature increases with $(UA)_{Total}$ since it is directly related to the conductance of the heater. The second point of interest is the fact that some curves are truncated, as they apparently do not reach the far right side of the figure. More specifically, this becomes evident for the $\dot{W}_{Net}$ curves of the Re-heating and the Combined A cycles (i.e., Figure 19), where its occurrence is associated with the appearance of pinch point problems within the re-heaters – recall that this could have been eliminated by increasing

the $\dot{m}_{HSo}$, however, in the limit where the air flow rate is extremely high, the sensible heat source approaches the latent heating condition. Furthermore, due to the existence of pinch point problems and the need for higher values of (UA) for the re-heaters, the expected convergence of the $\dot{W}_{Net}$ and η_{II} curves of the Re-heating and the Combined A cycles, as seen on Figures 11 and 13, is not observed. The same can be said about the η_{I} curves for the Reference and Re-heating cycles on Figure 20 with respect to Figure 12. Furthermore, the results of Figure 20 are, trend wise, closer to the results of the preceding section, where the recuperator, present in the Recuperative and Combined A cycles, is responsible for the significant difference between the 1st Law efficiencies when compared to the Reference and Re-heating cycles.

Figure 19 – Effect of $(UA)_{Total}$ on $\dot{W}_{Net}$ for all Rankine cycles simulated considering a sensible heat source

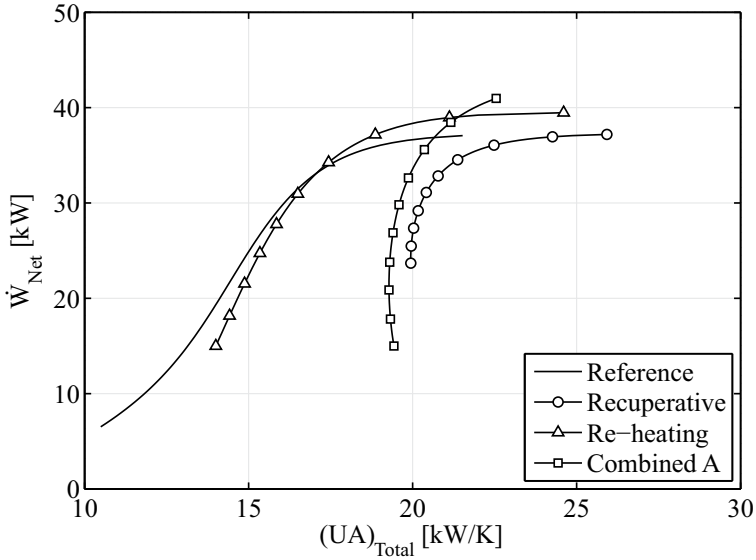

Figures 22, 23 and 24 show that the normalized figures of merit also display the parabolic behavior, clearly indicating the existence of well defined optimized solutions. According to Figures 22 and 24, the best overall configuration with respect to $\dot{W}_{Net}/(UA)_{Total}$ and $\eta_{II}/(UA)_{Total}$,

Figure 20 – Effect of $(UA)_{Total}$ on η_I for all Rankine cycles simulated considering a sensible heat source

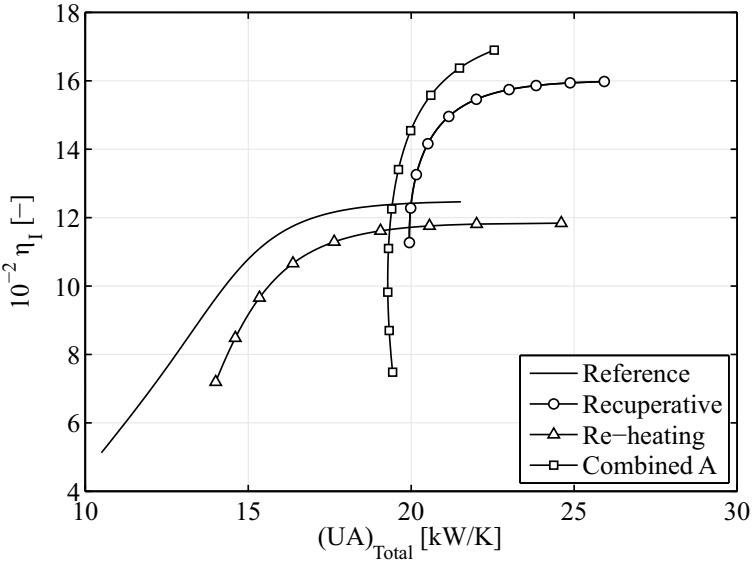

Figure 21 – Effect of $(UA)_{Total}$ on η_{II} for all Rankine cycles simulated considering a sensible heat source

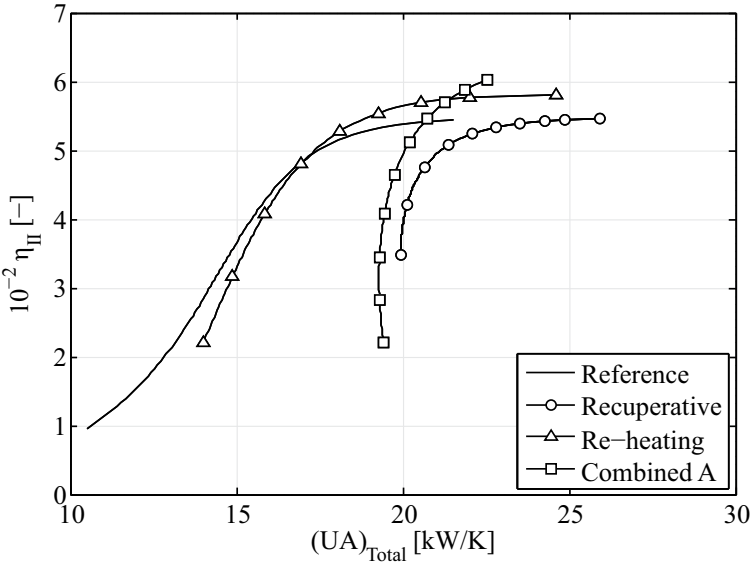

respectively, is the Re-heating cycle, which presents the highest ordinate values along with a comparatively low abscissa, while the Combined cycle has the highest $\eta_I/(UA)_{Total}$, as shown in Figure 23. As previously mentioned, other values of $P_{CO2,High}$ and T_{HSo} were tested and similar results were achieved. For instance, simulations for the same $P_{CO2,High}$ values used in Figures 19-24 (i.e., 20 MPa) and a considerably higher T_{HSo} (i.e., 500 °C), which are not explicitly shown, indicate a closer overall normalized behavior between the different cycles. Also, the results reporting the absolute values of the figures of merit indicate that the curves for the Reference and the Re-Heating cycles display much closer values among themselves to the extent where an overlap can be observed – the same can be said about the Recuperative and the Combined A cycles. This behavior is associated with the minor effect caused by the re-heating process for high T_{HSo} values, which can be easily explained through a T-s diagram for the CO_2 since, in the limit of high T_{HSo} values, the isenthalpic curves tend to become nearly horizontal lines. In other words, the recuperator causes the most significant performance change for cycles operating with sensible heating.

Next, Figure 25 displays a summary of the relation between $P_{CO2,High}$ and $\dot{W}_{Net}/(UA)_{Total}$ for the Combined A cycle, and four values of T_{HSo} (i.e., 200 °C, 300 °C, 400 °C and 500 °C) – one should note that each of the $[\dot{W}/(UA)_{Total}]_{Max}$ points shown in Figure 25 is obtained from an individual optimization process where $(UA)_{Total}$ is taken as an independent variable, leading to $(UA)_{Total,Opt}$. As expected, $[\dot{W}/(UA)_{Total}]_{Max}$ increases with $P_{CO2,High}$ and T_{HSo}. Furthermore, the optimal $T_{CO2,High}$ ($T_{CO2,High,Opt}$) can be determined by associating the color scale located on the right hand side of the frame with the inner color of each symbol. As can be observed, for each of the four T_{HSo} curves, $T_{CO2,High,Opt}$ is basically unaffected by $P_{CO2,High}$; i.e., note that the filling color of all symbols for a given T_{HSo} curve are very similar. While not shown, the equivalent version of Figure 25 was also developed for the Reference, Recuperative and Re-heating cycles. The results obtained display an overall similar behavior to the results presented for the Combined A cycle.

Figure 22 – Effect of $(UA)_{Total}$ on $\dot{W}_{Net}/(UA)_{Total}$ for all Rankine cycles simulated considering a sensible heat source

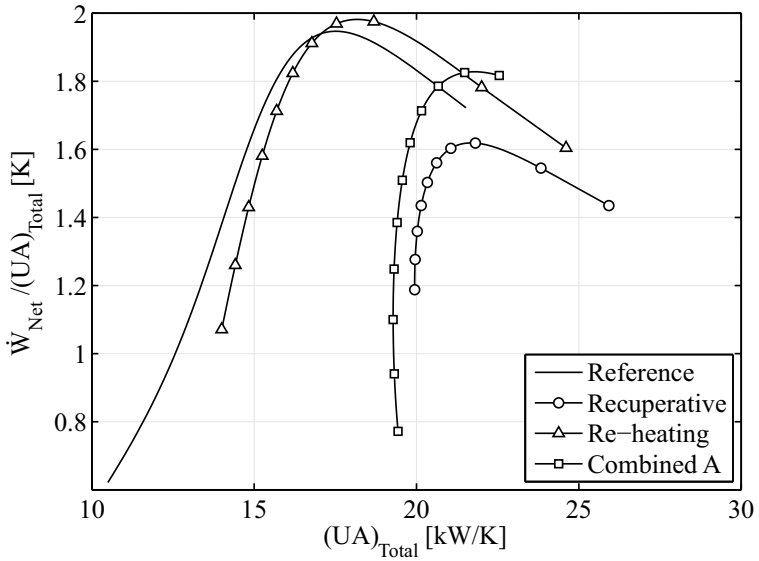

Figure 23 – Effect of $(UA)_{Total}$ on $\eta_I/(UA)_{Total}$ for all Rankine cycles simulated considering a sensible heat source

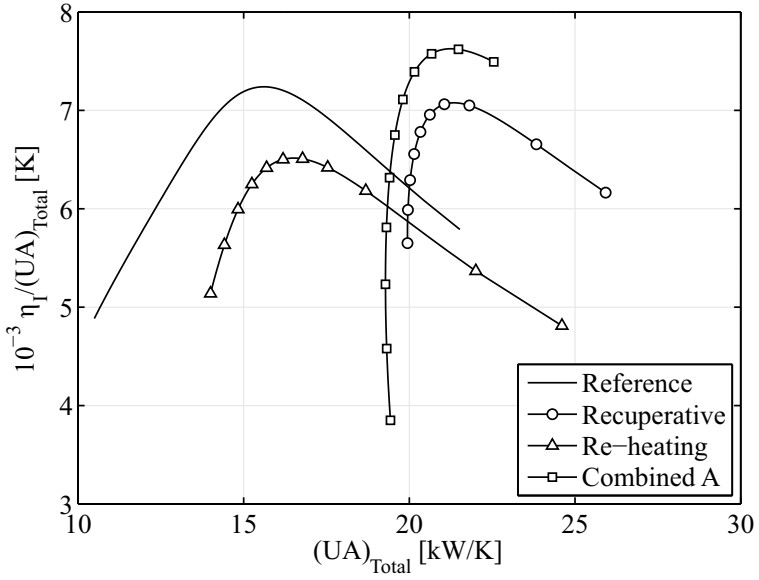

Figure 24 – Effect of $(UA)_{Total}$ on $\eta_{II}/(UA)_{Total}$ for all Rankine cycles simulated considering a sensible heat source

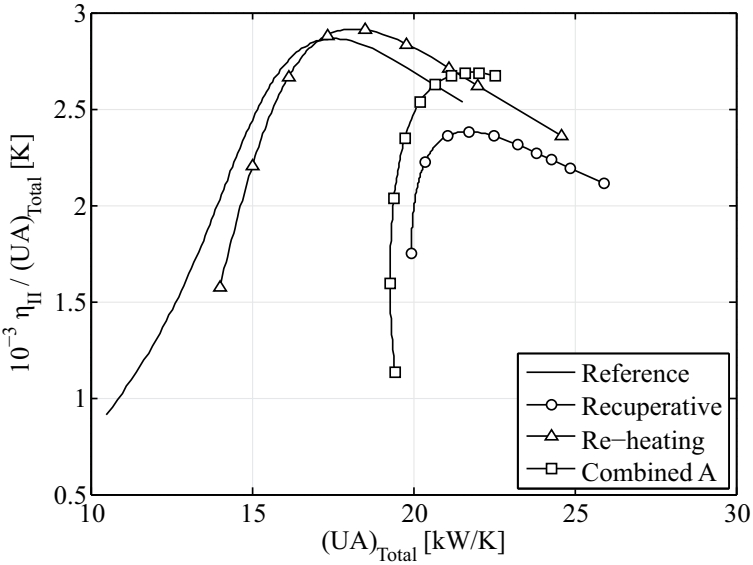

Figure 25 – Effect of $P_{CO2,High}$ on $[\dot{W}/(UA)_{Total}]_{Max}$ for the Rankine Combined A cycle for sensible heat sources with different T_{HSo}

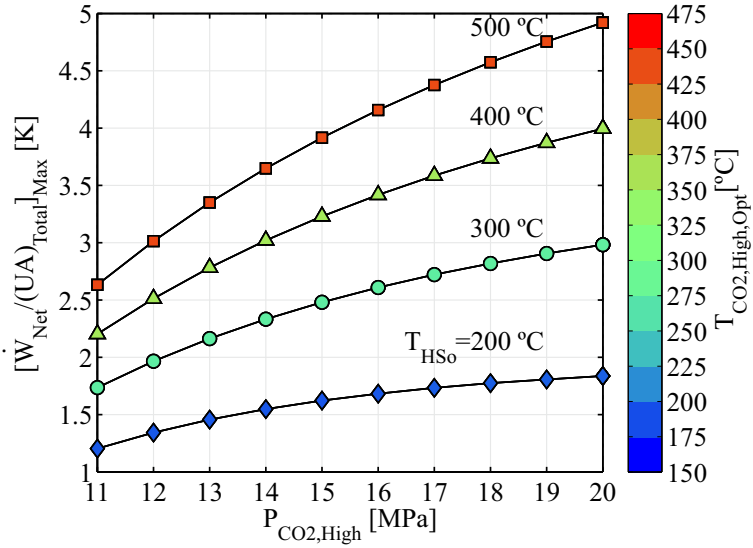

Similarly, Figure 26 shows that, for the Combined A cycle, the ratio $[\eta_I/(UA)_{Total}]_{Max}$ is also highly affected by $P_{CO2,High}$. However, the magnitude of the impact of T_{HSo} depends on the cycle being considered. For instance, as can be observed, the normalized 1st Law efficiency for the Combined A cycle increases by roughly 150% when T_{HSo} varies from 200 °C to 500 °C within the pressure range considered – similar values where obtained for the Recuperative cycle, even though these are not shown. Differently, for the Reference and Re-heating cycles, the same normalized parameter increases by roughly 50% if considering the same ranges of $P_{CO2,High}$ and T_{HSo}. This dependence on the type of cycle can be related to the presence of a recuperator (i.e., Figures 9b and 9d). More importantly, perhaps, is that the Reference and Re-Heating cycles require significantly lower $T_{CO2,High}$ (i.e., ~ 300-350 °C) to reach maximal values of $[\eta_I/(UA)_{Total}]_{Max}$.

A summary of the relation between $P_{CO2,High}$ and $\eta_{II}/(UA)_{Total}$ is not show because, as already discussed, it would only present a rescaling of the curves in Figure 25.

Figure 26 – Effect of $P_{CO2,High}$ on $[\eta_I/(UA)_{Total}]_{Max}$ for the Rankine Combined A cycle for sensible heat sources with different T_{HSo}

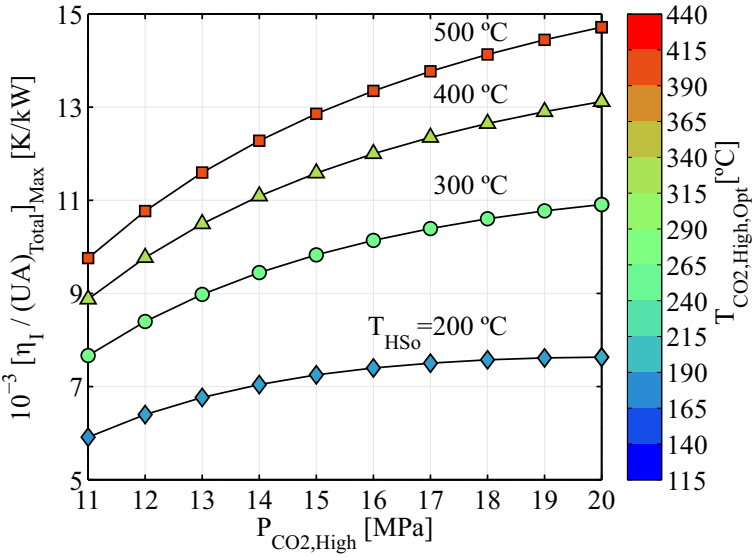

4.3 NORMALIZED 2nd LAW OPTIMIZATION

This section focuses exclusively on the absolute and normalized study of η_{II} for CO_2 transcritical Rankine cycles with a sensible heat source. The cycles considered were slightly modified from those of Figure 9 to allow greater values of $\eta_{II}/(UA)_{Total}$ and, consequently, greater values of η_{II} as well. The modifications implemented, which are shown in Figure 27, allow $\dot{m}_{HSo}$ and $\dot{m}_{HSi}$ to be divided in two independent fractions, Φ and λ, respectively – note that the splitting of the $\dot{m}_{HSo}$ of the fluid of the heat source (Figure 27a) is only applicable to Re-heating and Combined A cycles, while the splitting of the $\dot{m}_{HSi}$ of the cooling fluid is applied to all configurations.

Figure 27 – Schematic of the flow rate division implemented within the heating and the cooling heat exchangers

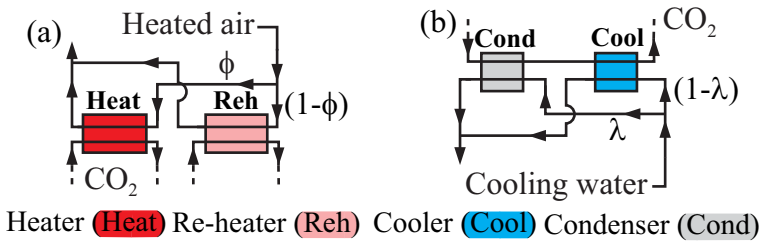

With the splitting of the flow of the heat source, a better independent thermal matching between heat source and CO_2 in heaters and re-heaters may be achieved, decreasing the required total mass flow rate and, therefore, the overall incoming exergy flow. Even more, the better fitting temperature profiles in heaters and re-heaters also decrease $(UA)_{Heat}$ and $(UA)_{Reh}$. A similar analysis is valid to the splitting of the cooling fluid, i.e., lower mass flow rate and reduction of $(UA)_{Cool}$ and $(UA)_{Cold}$ are achieved. Analyzing Equation 2.3, the possible improvements become obvious, i.e., increasing of η_{II} and, even strongly, of $\eta_{II}/(UA)_{Total}$.

An optimization routine was implemented aiming to maximize $\eta_{II}/(UA)_{Total}$, which considers the equivalent parameters utilized to ob-

tain Figures 19-24 and will be exemplified by considering the Combined A cycle (Figure 9d) with the modifications presented in 27. Initially, it should be established that $P_{CO2,High}$=20 MPa, T_{HSo}=200 °C and $\dot{m}_{CO2}$= 1 kg/s. Additionally, as described in Section 3.2, in the present routine T_4=T_6<T_{HSo}, while T_3 and T_8 are a function of T_2, T_7 and ϵ_{Rec}. Additionally, T_5 is determined such that the total combined power output of both turbines is maximized from the optimization of P_5 and consequently P_6, while an isentropic efficiency of 0.8 for both turbines is imposed (same value assumed to the isentropic efficiency of the pump). For the cooling fluid, P_{HSi}=101.325 kPa, $T_{HSi,In}$=10 °C, $T_{HSi,Out}$=15 °C and, $\dot{m}_{HSi}$ and λ are variable and determined through energy balances. Again, P_0 and T_0 were set equal to the cooling fluid inlet conditions. Therefore, based on such assumptions, it can be realized that there are four unknowns left in the problem: the two outlet temperatures of the heat source leaving the heater and the re-heater ($T_{HSo,Out,Heat}$ and $T_{HSo,Out,Reh}$, respectively), the total mass flow rate of the heat source ($\dot{m}_{HSo}$) and its splitting fraction (Φ). However, there are only two constitutive equations applicable to the problem, i.e., the 1st Law, enforced within the heater and within the re-heater as presented in Equation 4.1.

$$\begin{cases} \Phi\,\dot{m}_{HSo}\,(h_{HSo,In} - h_{HSo,Out,Heat}) = \dot{m}_{CO2}\,(h_4 - h_3) \\ (1-\Phi)\,\dot{m}_{HSo}\,(h_{HSo,In} - h_{HSo,Out,Reh}) = \dot{m}_{CO2}\,(h_6 - h_5) \end{cases} \tag{4.1}$$

Consequently, in order to determine the set of parameters that maximizes $\eta_{II}/(UA)_{Total}$, the $T_{HSo,Out,Heat}$ and $T_{HSo,Out,Reh}$ parameters were selected as inputs of the optimization routine. Recalling that T_3 and T_5 are known, the temperature difference between the heat source fluid that leaves the heater ($T_{HSo,Out,Heat}$) and the CO_2 that enters it (T_3), which will be referred to as $(\Delta T)_{Heat}$ and, similarly, the temperature difference between the heat source fluid that leaves the re-heater ($T_{HSo,Out,Reh}$) and the CO_2 that enters the it (T_5), which will

be referred as $(\Delta T)_{Reh}$. Equation 4.2 presents the above definition.

$$\begin{cases} (\Delta T)_{Heat} = T_{HSo,Out,Heat} - T_3 \\ (\Delta T)_{Reh} = T_{HSo,Out,Reh} - T_5 \end{cases} \tag{4.2}$$

Therefore, recalling that P_{HSo}=101.325 kPa and assisted by guessed values of $(\Delta T)_{Heat}$ and $(\Delta T)_{Reh}$, the specific outlet enthalpies of the heat source fluid at the heater and the re-heater (i.e., $h_{HSo,Out,Heat}$ and $h_{HSo,Out,Reh}$, respectively) may be calculated as functions of pressure and temperature, as show in Equation 4.3.

$$\begin{cases} h_{HSo,Out,Heat} = h_{HSo}\left(P_{HSo}, T_3 + (\Delta T)_{Heat}\right) \\ h_{HSo,Out,Reh} = h_{HSo}\left(P_{HSo}, T_5 + (\Delta T)_{Reh}\right) \end{cases} \tag{4.3}$$

Then, Equation 4.1 may be rearranged and rewritten in terms of Equation 4.3 as shown in Equations 4.4 and 4.5.

$$\Phi = \left[1 + \frac{(h_6 - h_5)\,(h_{HSo,In} - h_{HSo,Out,Heat})}{(h_4 - h_3)\,(h_{HSo,In} - h_{HSo,Out,Reh})}\right]^{-1} \tag{4.4}$$

$$\dot{m}_{HSo} = \dot{m}_{CO2}\left[\frac{(h_4 - h_3)}{(h_{HSo,In} - h_{HSo,Out,Heat})} + \frac{(h_6 - h_5)}{(h_{HSo,In} - h_{HSo,Out,Reh})}\right] \tag{4.5}$$

Therefore, by guessing $(\Delta T)_{Heat}$ and $(\Delta T)_{Reh}$ for a given $T_{CO2,High}$, Equations 4.4 and 4.2 are utilized to determine Φ and $\dot{m}_{HSo}$, which then allows the determination of $\eta_{II}/(UA)_{Total}$. Next, new values for $(\Delta T)_{Heat}$ and $(\Delta T)_{Reh}$ are used, and $\dot{m}_{HSo}$ and Φ are recalculated, allowing $\eta_{II}/(UA)_{Total}$ to be reevaluated. This process is repeated until the figure of merit $\eta_{II}/(UA)_{Total}$ reaches a maximum. Finally, $T_{CO2,High}$ (T_{Min}<$T_{CO2,High}$<T_{HSo}) is varied and, then, the other configurations of cycle are considered.

Figure 28 shows schematically the temperature profiles of the heat source and of the working fluid in the heater and in the re-heater, according to Figure 27, for the Re-heating or the Combined A cycles.

The effect of both $(\Delta T)_{Heat}$ and $(\Delta T)_{Reh}$ on the temperature profiles of the heat source and of the working fluid and, therefore, on the performance of the cycles may be better understood by analyzing the two possible extreme conditions, i.e., high and low values of $(\Delta T)_{Heat}$ and $(\Delta T)_{Reh}$.

For given fixed values of the thermal energy to be exchanged by both heat exchangers – due to the fact that these values depend only on the internal points of the cycles –, high values of $(\Delta T)_{Heat}$ and $(\Delta T)_{Reh}$ increase the temperature difference between the heat source and the working fluid. As only small temperature variations between the inlet and outlet temperatures of the heat source are allowed, according to Equation 3.1, their required mass flow rates – $\Phi\,\dot{m}_{HSo}$ for the heater and $(1\text{-}\Phi)\dot{m}_{HSo}$ for the re-heater – increase, and, therefore, the 2nd Law efficiency, in accordance to Equation 2.3, decreases. At the same time, as the heat exchangers become less efficient with high values of $(\Delta T)_{Heat}$ and $(\Delta T)_{Reh}$, $(\Delta T)_{LM}$ values increase along the heat exchanger, therefore, the required (UA) for both heat exchangers decrease, in accordance to Equation 2.5. The opposite effect occur to low values of $(\Delta T)_{Heat}$ and $(\Delta T)_{Reh}$.

With respect to the cooling fluid, recalling that P_{HSi}=101.325 kPa, $T_{HSi,In}$=10 °C and $T_{HSi,Out,Cool}$=$T_{HSi,Out,Cond}$=$T_{HSi,Out}$=15 °C, λ and $\dot{m}_{HSi}$ are well defined by the energy balances of the cooler and de condenser as shown if Equation 4.6.

$$\begin{cases} (1-\lambda)\,\dot{m}_{HSi}\,(h_{HSi,Out,Cool}-h_{HSi,In}) = \dot{m}_{CO2}\,(h_8-h_9) \\ \lambda\,\dot{m}_{HSi}\,(h_{HSi,Out,Cond}-h_{HSi,In}) = \dot{m}_{CO2}\,(h_9-h_1) \end{cases} \tag{4.6}$$

With a simple algebraic rearrangement of Equation 4.6, λ and $\dot{m}_{HSi}$ may be directly calculated as show in Equations 4.7 and 4.8.

$$\lambda = \left[1+\frac{(h_8-h_9)\,(h_{HSi,Out,Cond}-h_{HSi,In})}{(h_9-h_1)\,(h_{HSi,Out,Cool}-h_{HSi,In})}\right]^{-1} \tag{4.7}$$

Figure 28 – Temperature profiles of the heat source and of the working fluid in the heater and in the re-heater according to Figure 27

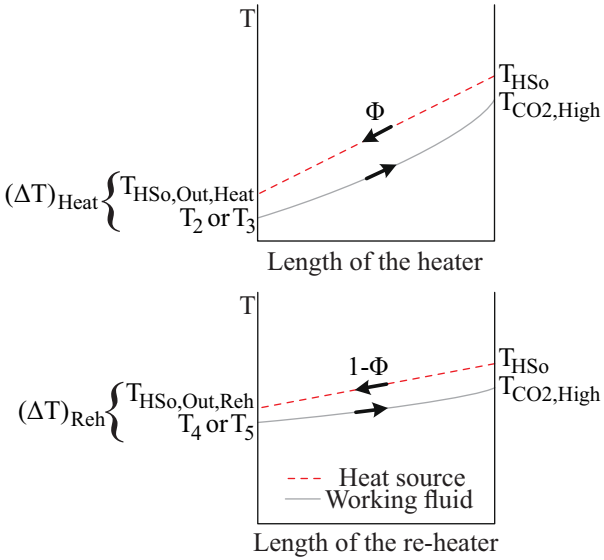

$$\dot{m}_{HSi} = \dot{m}_{CO2}\left[\frac{(h_8 - h_9)}{(h_{HSi,Out,Cool} - h_{HSi,in})} + \frac{(h_9 - h_1)}{(h_{HSi,Out,Cond} - h_{HSi,In})}\right] \quad (4.8)$$

Figure 28 shows schematically the temperature profiles of the heat sink fluid and of the working fluid in the condenser and in the cooler according to Figure 27. A similar analysis done in Figure 28 could be performed to Figure 29, however, as the inlet and outlet temperatures of the heat sink are fixed, this is not presented.

Figure 30 shows the results from this optimization process, indicating the existence of clear optimal values for $\eta_{II}/(UA)_{Total}$ as function of $(UA)_{Total}$. More specifically, for the operational conditions employed (i.e., that $P_{CO2,High}$=20 MPa, $T_{HSo,High}$=200 °C), the Reference cycle along with the Recuperative configuration present the highest performance, followed by the Re-heating and Combined cycles. Also, the

Figure 29 – Temperature profiles of the heat sink and of the working fluid in the condenser and in the cooler according to Figure 27

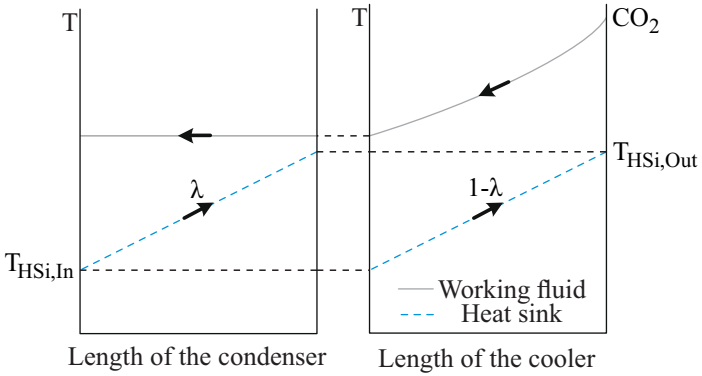

appearance of maximal values for $\eta_{II}/(UA)_{Total}$ can be linked to the abrupt drop of $\dot{W}_{Net}$ as $(UA)_{Total}$ tends to zero, and to the overwhelming increase of $(UA)_{Total}$ over $\dot{W}_{Net}$ as $(UA)_{Total}$ increases. From the optimal solutions obtained for $\eta_{II}/(UA)_{Total}$, the absolute values of η_{II} can be easily obtained as shown in Figure 31. Differently from the results observed in Figure 30, η_{II} curves displayed in Figure 31 generally are less affected by $(UA)_{Total}$. Also, there is a clear performance difference between the curves for the Recuperative and the Reference when compared with the Combined A and the Re-heating configurations. Recalling Equation 2.3, it can be concluded that this difference in behavior is related to the re-heating process, which requires larger values of $\dot{m}_{HSo}$, increasing the inflow of exergy. Potentially more relevant is the fact that, by splitting $\dot{m}_{HSo}$ as shown in Figure 27, the magnitude of $\dot{m}_{HSo}$ is lowered if compared with the same cycles operating with an in-series heater and re-heater (i.e., Figure 9 c and d). As a result, η_{II} increased approximately between 5 and 7 times when comparing the results presented in Figures 21 and 31, and $\eta_{II}/(UA)_{Total}$ increased approximately between 4 and 5 times when comparing the results presented in Figures 24 and 30.

Figure 32 shows the ratio between the optimized and non-optimized

Figure 30 – Effect of $(\mathrm{UA})_{\mathrm{Total}}$ on $(\eta_{\mathrm{II}}/(\mathrm{UA})_{\mathrm{Total}})$ for all Rankine cycles simulated considering a sensible heat source with optimized hot and cold sources

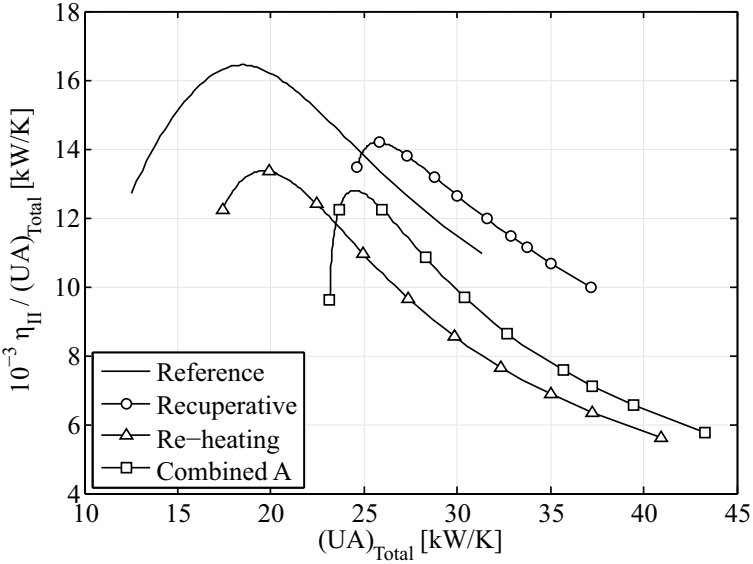

Figure 31 – Effect of $(\mathrm{UA})_{\mathrm{Total}}$ on η_{II} for all Rankine cycles simulated considering a sensible heat source with optimized hot and cold sources

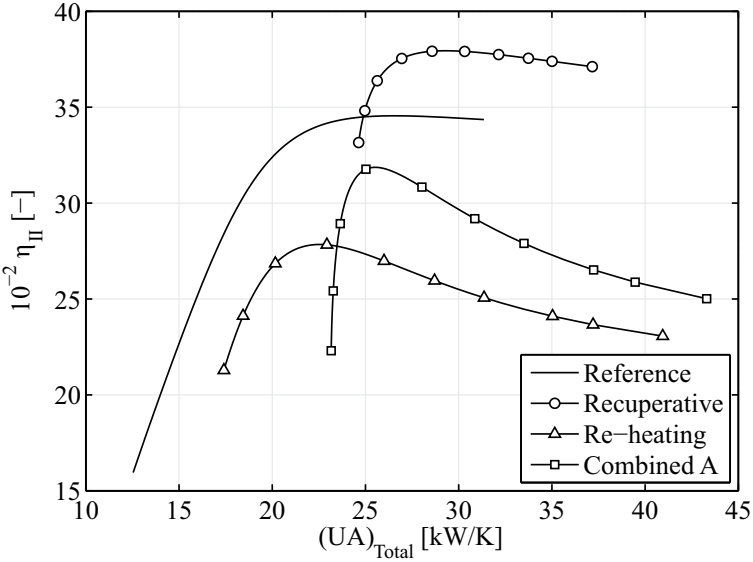

mass flow rates of the heat source fluid indicating a minimal reduction of roughly 70% by splitting the flow. The strong reduction of $\dot{m}_{HSo}$ observed for the Reference and Recuperative cycles, even though their heat sources flow streams were not divided – the mass flow rate was simply calculated through energy balances –, indicates that the $\dot{m}_{HSo}$=15 kg/s adopted in Section 4.2 was oversized. Therefore, with the $\dot{m}_{HSo}$ required in Section 4.2, one could increase the number of power plants supplied and/or increase $\dot{m}_{CO2}$, leading to a higher total $\dot{W}_{Net}$.

Nevertheless, as more heat needs to be transferred between both fluids, $(UA)_{Total}$ increases. However, as the optimization is performed in the heat source and sink only, $\dot{W}_{Net}$ and η_I, which exclusively depend on the internal points of the cycle, remain unchanged. Therefore, even though $\eta_{II}/(UA)_{Total}$ is maximized, $\dot{W}_{Net}/(UA)_{Total}$ and $\eta_I/(UA)_{Total}$ decrease with the optimization procedure proposed.

Figure 32 – Effect of $(UA)_{Total}$ on $\dot{m}_{HSo,Opt}/\dot{m}_{HSo,Non\text{-}opt}$ for all Rankine cycles simulated considering a sensible heat source with optimized hot and cold sources

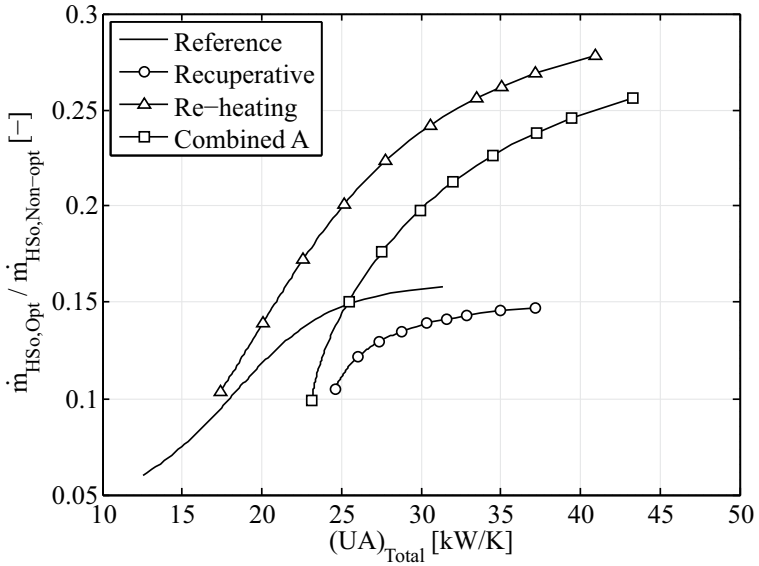

5 MODELING OF CO_2 SUPERCRITICAL BRAYTON CYCLES

Instead of simply repeating the previously performed Rankine analyzes described in Chapters 3 and 4, a more complex investigation was proposed for the Brayton cycle. More specifically, a multivariable analysis and optimization of a CO_2 supercritical Brayton cycle was performed, while enforcing a fixed minimum temperature of CO_2 within the cycle just above its critical temperature to further analyze the effect of property change on the performance of power cycles in absolute terms and per unit of total global conductance.

The Brayton cycle considered is equivalent to the Rankine Combined A cycle with an optimized heat source (i.e. the cycle shown in Figure 9d with the heat source modification shown in Figure 27a), but, for the present simulations, the operational pressures and temperatures are always above the critical point. A schematic of the thermodynamic model implemented in the present Chapter is shown in Figure 33. Because of the significant number of optimization variables considered (i.e., six), only one cycle configuration was chosen. As it was done in section 4.3, the normalized 2^{nd} Law efficiency was chosen as objective function to the optimization process.

The same formulation, considerations and simplifications used in Chapter 3 with respect to equations, discretization, hypotheses imposed to the Rankine cycles were used in the Brayton modeling. Again, the simulations performed involved a series of steps, which were implemented in numerical routines in MATLAB [63], along with the thermophysical property library CoolProp [8, 9]. Since latent heat sources are strongly limited to low temperatures and the goal was to allow Brayton cycles to explore higher temperature levels, differently from the Rankine analyzes presented, only sensible heat sources were considered. The heat source was again chosen as dry air with a variable mass flow rate.

The following parameters were held constant throughout all sim-

Figure 33 – Schematic of the Combined Brayton cycle simulated: cycle with recuperator, divided expansion with one re-heating stage and optimized heat source

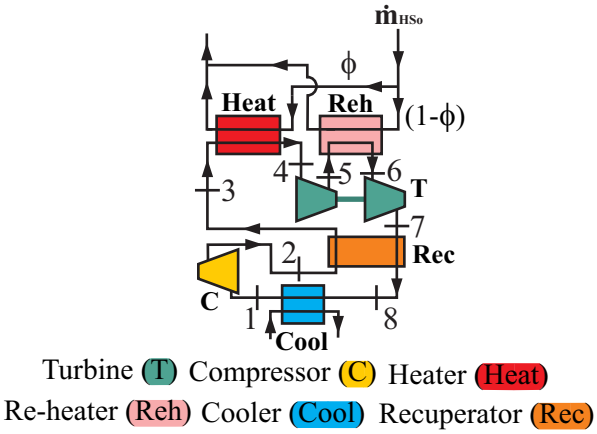

ulations: CO_2 minimum temperature within the cycle ($T_{CO2,Min}$) of 32 °C (just above the critical temperature), isentropic efficiencies of turbines and compressor of $\eta_T = \eta_C$ =0.8, effectiveness of the recuperator (ϵ_{Rec} = 0.8) and CO_2 mass flow rate ($\dot{m}_{CO2}$) of 1 kg/s – the definition of the effectiveness of the recuperator will be further discussed later in the text. As the cooling fluid, liquid water at atmospheric pressure was used again and its mass flow rate ($\dot{m}_{HSi}$) was also calculated such that CO_2 was brought to $T_{CO2,Min}$, while subjected to inlet and outlet temperatures of $T_{HSi,In}$=20 °C and $T_{HSi,Out}$=25 °C, respectively – both temperatures were chosen 10 °C higher than the values used for the Rankine calculations, since the higher value of $T_{CO2,Min}$ allows for a wider range of cooling conditions.

Once again, it is worth mentioning that pinch point analyzes were performed in such way that the 2nd Law was never violated. The same formulation adopted in the optimization procedure from Section 4.3, was adapted for the Brayton cycle and utilized in this section – i.e., $(\Delta T)_{Heat}$ and $(\Delta T)_{Reh}$ definitions of Equation 4.2, Φ and $\dot{m}_{HSo}$ expressions of Equations 4.7 and 4.8.

The optimization procedure adopted considered six independent

parameters and five optimization layers. The innermost layer (IML) was dedicated to the simultaneous optimization of $(\Delta T)_{Heat}$ and $(\Delta T)_{Reh}$, the next layers were dedicated to $P_{CO2,High}$, $T_{CO2,High}$, $P_{CO2,Low}$ and the outermost to T_{HSo}. A schematic of these optimization layers is shown in Figure 34.

Figure 34 – Schematic of the adopted optimization layers

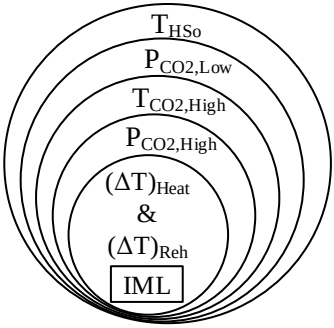

The calculation and optimization of the model developed relied on a "layer into layer" scheme, being the flowchart shown in Figure 35, the innermost layer. This scheme was elaborated so the effect of each parameter on the objective function could be analyzed having the parameters in the inner layers already optimized. Also, despite the fact that the proposed study relies on a multivariable analysis, the optimization algorithm utilized throughout the simulations is a gradient based routine, which was not conceived to global optimization of multiple parameters (i.e., each variable was optimize individually, except the two of the innermost layer).

The calculation routine presented in Figure 35 is very similar to the one already presented in the flowchart of Section 3.2. Therefore, the entire itemized description is not presented, but only key particularities will be pointed out. In terms of components, the only changes made to cycle were the replacement of the pump for a compressor, and the elimination of the condenser – there is no latent heat in the cooling phase. In terms of parameters definitions, the major changes were that

Figure 35 – Flowchart indicating the procedure of the innermost layer of optimization for the Brayton Combined cycle

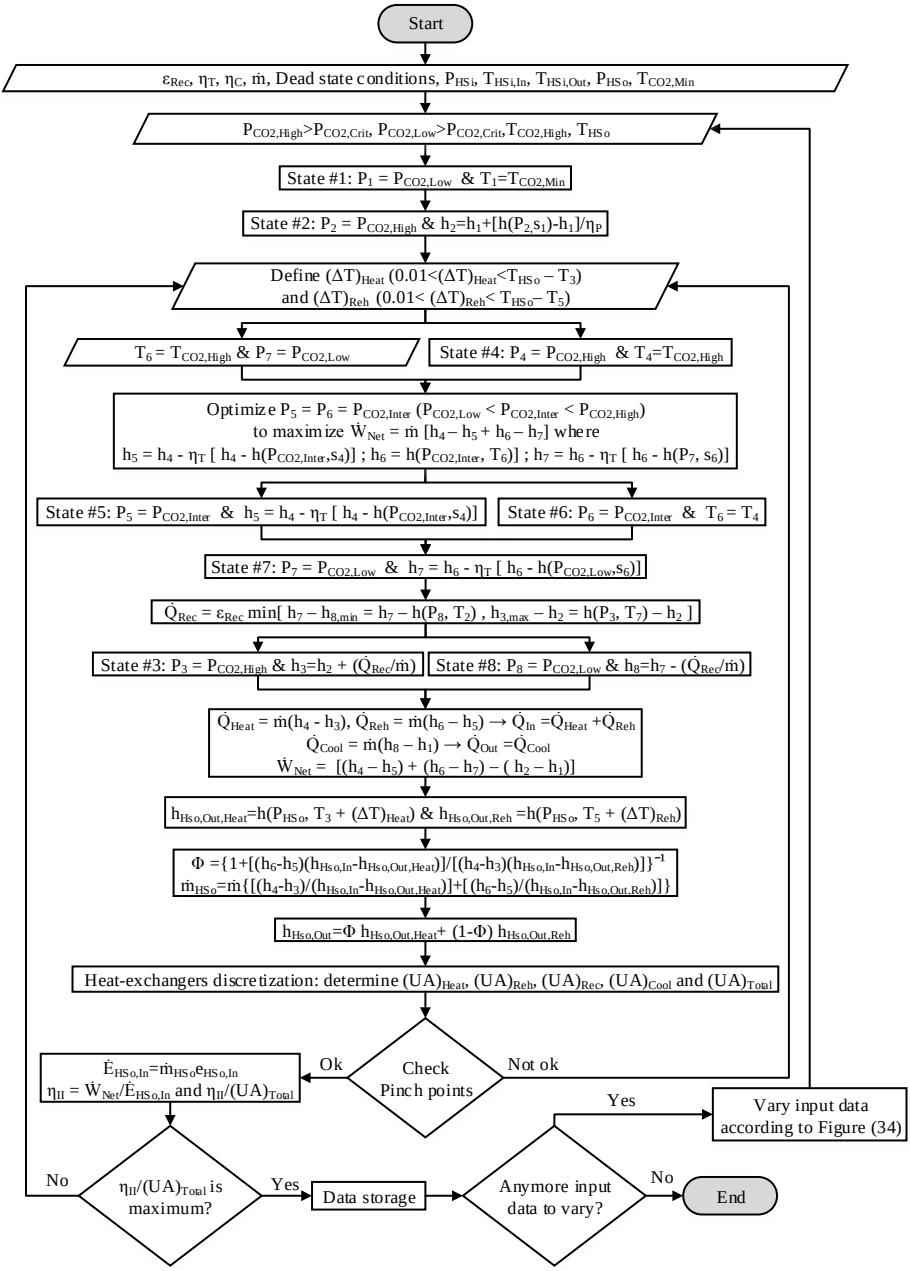

both $P_{CO2,High}$ and $P_{CO2,Low}$ are always set higher than $P_{CO2,Crit}$, and $T_{CO2,Min}$ is also fixed just above $T_{CO2,Crit}$, in such way that the working fluid is always in supercritical state. As assumed in the Rankine model, the dead state conditions were set as the pressure and temperature of the inlet cooling water, i.e. P_0=101.325 kPa and T_0=20 °C, so this state has the lowest exergy level within the entire system.

One of the main limitations of the Rankine cycles reported in Chapters 3 and 4 was related to the effectiveness of the heat exchangers due to the existence of pinch point problems, i.e., recall that some curves appeared to be truncated for the Re-heating and the Combined A cycles of Figures 19-24. Usually, the effectiveness ϵ, which varies $0<\epsilon<1$, is defined as the ratio between the actual thermal power transferred within the heat exchanger ($\dot{Q}$) and the maximal thermal power that could be transferred ($\dot{Q}_{Max}$) in terms of the 1st Law. This definition was not found sufficiently good when applied to fluids which experience considerable variations of thermophysical properties such as the CO_2 near to the critical point. Therefore, along the study, simulations found that, depending on the parameters set, a given ϵ value, which is valid in terms of the 1st Law, could violate the 2nd Law. Recall that in Chapters 3 and 4 the solution to pinch point problems was to simply stop the simulation and present a warning flag (see the bottom of Figure 10). Differently, in this Chapter $\dot{Q}_{Max}$ is iteratively determined, such that neither the 1st nor the 2nd Law is violated. Therefore, for a given set of parameters, $\dot{Q}_{Max}$ is calculated and then it is verified if a maximal effectiveness ϵ =0.999 violates the 2nd Law throughout the heat exchanger discretization procedure presented in Subsection 2.2.5. If a violation is detected, $\dot{Q}_{Max}$ is gradually reduced until the highest $\dot{Q}_{Max}$ which does not violate the 2nd Law is found (this value is denoted by $\dot{Q}_{Max,II}$). Then $\dot{Q}_{Max,II}$ is used to calculate $\dot{Q}$ according to Equation 5.1 guaranteeing $0<\epsilon<1$ and respecting both the 1st and 2nd Laws.

$$\dot{Q} = \epsilon \, \dot{Q}_{Max,II} \tag{5.1}$$

5.1 VALIDATION

The thermodynamic simulations were validated against independent results presented in the literature, i.e., results for a Brayton cycle with a recuperator presented in Reference [55], which considered η_T =0.9, η_P =0.89, ϵ_{Rec} =0.95, $T_{CO2,Min}$=32 °C and $T_{CO2,High}$=550 °C (further information can be found directly in the Reference [55]).

Tables 4 and 5 display the values of the 1st Law efficiency from the simulations performed and the ones interpreted from graphs present in Reference [55] as well as the deviation between them, which was already defined in Equation 3.2, as functions of the pressure ratio (PR), which is defined by Equation 5.2, for $P_{CO2,High}$ = 10 MPa and $P_{CO2,High}$=25 MPa, respectively.

$$PR = \frac{P_{CO2,High}}{P_{CO2,Low}} \tag{5.2}$$

As expected, the agreement is very good and, as mentioned in section 3.3, several other consistency tests were implemented throughout the study.

Table 4 – Validation #1 for CO_2 Brayton cycle

$P_{CO2,High}$=10 MPa			
PR [-]	η_I (Present work) [%]	η_I (Reference [55]) [%]	Deviation [10^{-3} %]
2.0	37.15	37.16	26.82
2.2	37.87	37.87	03.42
2.4	38.25	38.23	38.01
2.6	38.40	38.40	04.11
2.8	38.40	38.40	11.97
3.0	38.31	38.32	11.71
3.2	38.15	38.15	03.80
3.4	37.94	37.96	53.73
3.6	37.69	37.70	36.60
3.8	37.42	37.43	29.13
4.0	37.13	37.14	12.15

Table 5 – Validation #2 for CO_2 Brayton cycle

$P_{CO2,High}$=25 MPa			
PR [-]	η_I (Present work) [%]	η_I (Reference [55]) [%]	Deviation [10^{-3} %]
2.4	42.25	42.25	02.37
2.6	39.59	39.58	04.84
2.8	38.81	38.79	33.93
3.0	38.77	38.75	34.46
3.2	39.07	39.06	15.56
3.4	39.30	39.28	71.47
3.6	38.99	38.99	19.70
3.8	38.69	38.68	40.53
4.0	38.38	38.37	36.75

6 RESULTS OF CO_2 SUPERCRITICAL BRAYTON CYCLES

This Chapter presents and discusses the results obtained with the proposed investigation of the selected Brayton cycle. The influence of each optimization parameter on the selected objective function, i.e., $\eta_{II}/(UA)_{Total}$, is individually analyzed and the obtained results are presented. The discussion starts from the innermost to the outermost layer, shown in Figure 34, aiming to present and understand the effect of each parameter on the performance of the cycle.

Due to the large amount of data obtained with the optimization process performed, a qualitative set of parameters was selected and reported for each layer shown in Figure 34. The parameters chosen are: T_{HSo}=400 °C, $P_{CO2,Low}$=9 MPa, $T_{CO2,High}$=237.5 °C and $P_{CO2,High} \sim$ 27.1 MPa – so the inlet specific exergy of the heat source is fixed. Also, a single local optimum was selected and presented in Figures 36- 40 aiming to facilitate the understanding and transition between optimization layers.

6.1 THE EFFECT OF EACH OPTIMIZATION VARIABLE

For the first layer, Figure 36 shows the effect of $(\Delta T)_{Heat}$ and $(\Delta T)_{Reh}$, which were simultaneously optimized, on $\eta_{II}/(UA)_{Total}$. The results are shown through a concave surface, which was obtained by varying 0 °C<$(\Delta T)_{Heat}$<40 °C and 0 °C<$(\Delta T)_{Reh}$<30 °C, while keeping the other parameters fixed. The discussion starts by indicating that the analysis presented in the discussion of Figure 28 is needed to explain the existence of the maximum shown in Figure 36. Therefore, it is important to mention that at each point simulated and reported in Figure 36, the value of heat to be exchanged by the heater and the re-heater, as well as the net power produced, are fixed (they are fixed at each point, but not the same among all of them). Thus, high $(\Delta T)_{Heat}$ and $(\Delta T)_{Reh}$ values impose a large temperature difference between the heat

source and the working fluid. Consequently, under such conditions, small temperature variations between the inlet and outlet temperatures of the heat source are allowed, which according to Equation 3.1, increases its mass flow rate and the incoming exergy flow, lowering the 2nd Law efficiency. At the same time, as the heat exchangers become less efficient with high values of $(\Delta T)_{Heat}$ and $(\Delta T)_{Reh}$, $(\Delta T)_{LM}$ values increase along the heat exchanger, decreasing the required (UA) for both heat exchangers. The opposite effect occurs when low values of $(\Delta T)_{Heat}$ and $(\Delta T)_{Reh}$ are considered. Even though both η_{II} and $(UA)_{Total}$ are inversely proportional to $(\Delta T)_{Heat}$ and $(\Delta T)_{Reh}$, their rates of change are not identical. For instance, for low values of $(\Delta T)_{Heat}$ and $(\Delta T)_{Reh}$, the drop in $\eta_{II}/(UA)_{Total}$ is dictated by the exponential growth of $(UA)_{Total}$.

Figure 36 – Effect of $(\Delta T)_{Heat}$ and $(\Delta T)_{Reh}$ on $\eta_{II}/(UA)_{Total}$: first optimization layer

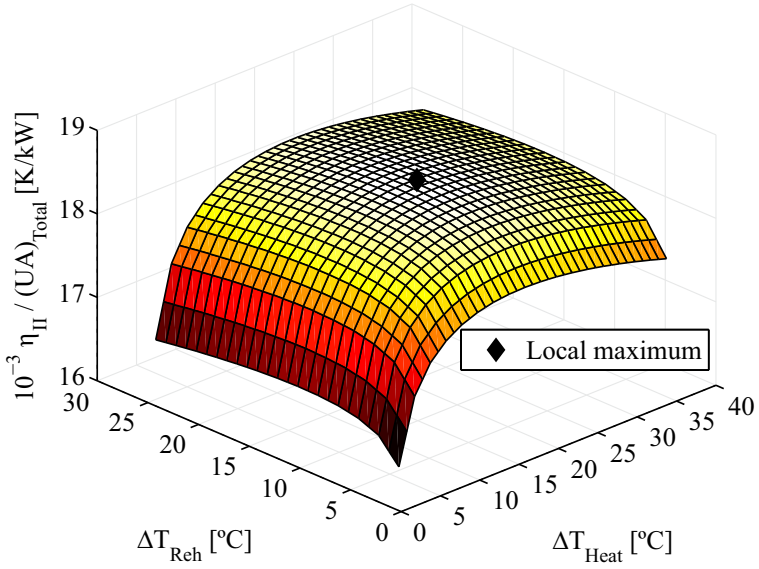

Figure 37 shows the effect of $P_{CO2,High}$ on $\eta_{II}/(UA)_{Total}$, which represents the second optimization layer on Figure 34. Three curves are shown, representing three different $T_{CO2,High}$ values. Each curve is

obtained by optimizing $(\Delta T)_{Heat}$ and $(\Delta T)_{Reh}$ for different $P_{CO2,High}$ values ranging from 15 MPa to 45 MPa, while keeping the remaining parameters fixed. In the limit of low $P_{CO2,High}$, the behavior of the ratio $\eta_{II}/(UA)_{Total}$ is easily understood as it is dominated by the drop of η_{II} caused by the drop of $\dot{W}_{Net}$ – for a fixed $T_{CO2,High}$, as $P_{CO2,High}$ decreases, the enthalpy difference between the upstream and downstream states of the turbines decreases. In the limit of high $P_{CO2,High}$ values, again, for a fixed $T_{CO2,High}$, as $P_{CO2,High}$ increases, $\dot{W}_{Net}$ also decreases (it presents a maximum) as the effect of $P_{CO2,High}$ on the power produced diminishes, but the power spent with the compressor continuously increases. On the other hand, the total thermal power supplied to the working fluid by the heat source increases implying in higher $\dot{m}_{HSo}$ and $(UA)_{Total}$ values. The thermal power supplied to the heater slightly decreases as its inlet temperature increases and as the difference between its inlet and the outlet specific enthalpies decreases. The thermal power supplied to the re-heater strongly increases as its inlet temperature decreases. So, the ratio $\eta_{II}/(UA)_{Total}$, in the limit of high $P_{CO2,High}$, decreases due to increasing $\dot{m}_{HSo}$ and $(UA)_{Total}$ values and decreasing $\dot{W}_{Net}$ values.

Figure 38 shows the effect of $T_{CO2,High}$ on $\eta_{II}/(UA)_{Total}$, representing the third optimization layer. Similarly to Figure 37, three $P_{CO2,Low}$ curves are shown while $T_{CO2,High}$ is set as a dependent variable. Each of the three curves are obtained by optimizing $(\Delta T)_{Heat}$, $(\Delta T)_{Reh}$ and $P_{CO2,High}$ while varying $150\,°C < T_{CO2,High} < T_{HSo}$ and keeping the remaining parameters constrained. In the limit of low $T_{CO2,High}$, the ratio $\eta_{II}/(UA)_{Total}$ is dominated by the drop of η_{II} caused by the drop of $\dot{W}_{Net}$. In the limit of high $T_{CO2,High}$, the heat supplied to the working fluid by the heat source increases, which also requires higher $\dot{m}_{HSo}$ and $(UA)_{Total}$ values. Therefore, for high $T_{CO2,High}$, the figure of merit decreases as $\dot{m}_{HSo}$ and $(UA)_{Total}$ increase, despite the fact that $\dot{W}_{Net}$ also increases.

Figure 39 shows the effect of $P_{CO2,Low}$ on $\eta_{II}/(UA)_{Total}$, i.e., the fourth optimization layer. Each point shown on the curves is calculated by optimizing $(\Delta T)_{Heat}$, $(\Delta T)_{Reh}$, $P_{CO2,High}$ and $T_{CO2,High}$ while vary-

Figure 37 – Effect of $P_{CO2,High}$ on $\eta_{II}/(UA)_{Total}$: second optimization layer

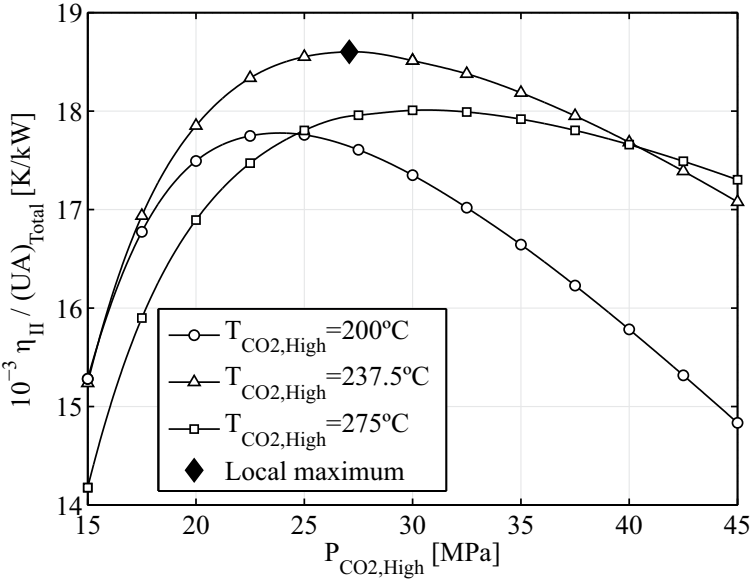

Figure 38 – Effect of $T_{CO2,High}$ on $\eta_{II}/(UA)_{Total}$: third optimization layer

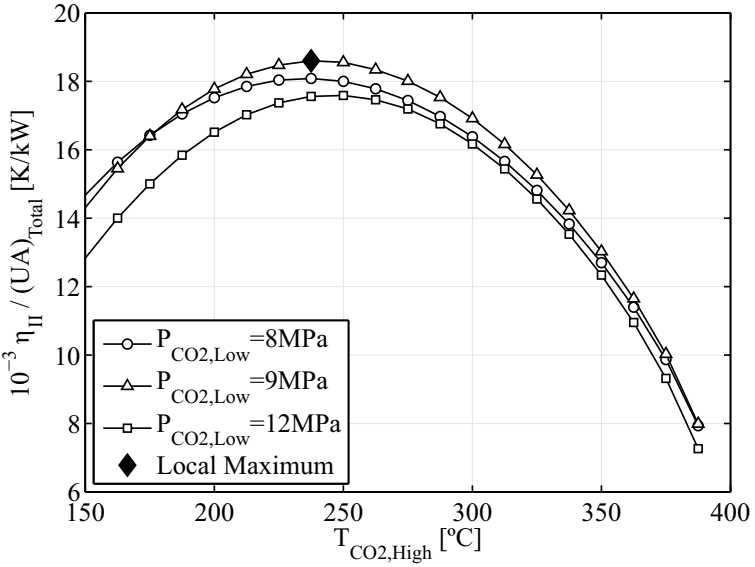

ing 7.4 MPa<$P_{CO2,Low}$<12 MPa and keeping T_{HSo} fixed. While these curves still present a turning point, a less trivial behavior is observed as $P_{CO2,Low}$ approaches $P_{CO2,Crit}$. Focusing first on the concave sections of these curves, it can be observed that, for high values of $P_{CO2,Low}$, the ratio $\eta_{II}/(UA)_{Total}$ is also ruled by the drop of η_{II}, which is associated with the drop of $\dot{W}_{Net}$. In the limit of low $P_{CO2,Low}$, while still considering $P_{CO2,Low}$>8 MPa[1], as $P_{CO2,Low}$ decreases, the ratio $\eta_{II}/(UA)_{Total}$ is influenced by the increase of η_{II} and $(UA)_{Total}$. η_{II} increases mainly due to the increase of $\dot{W}_{Net}$ as just explained for the high $P_{CO2,Low}$ values. $(UA)_{Total}$, on the other hand, increases due to the strong influence of the thermophysical properties near to the critical point on the temperature profile of CO_2 – one must remember that $T_{CO2,Min}$=32 °C is maintained fixed, which is just above $T_{CO2,Crit}$, therefore, for all $P_{CO2,Low}$, the inlet state of the compressor is located always over the 32 °C isothermal – which implies that $\left.\frac{\partial T}{\partial s}\right|_P \rightarrow 0$. Therefore, there is a significant drop of $(\Delta T)_{LM}$ along the cooler leading to a large increment for the $(UA)_{Cool}$, and $(UA)_{Total}$ consequently. Even though both η_{II} and $(UA)_{Total}$ increase as $P_{CO2,Low}$ decreases, their slopes are not the same, in fact $(UA)_{Cool}$ increases faster than η_{II}, which is the reason for the drop of $\eta_{II}/(UA)_{Total}$.

Next, by allowing $P_{CO2,Low}$ to approach $P_{CO2,Crit}$, $\eta_{II}/(UA)_{Total}$ presents a sharp and unexpected growth. As $T_{CO2,Min}$ is maintained fixed near to $T_{CO2,Crit}$, the decrease of $P_{CO2,Low}$ moves the outlet of the cooler away from the critical region, i.e., to the right side of the saturation curve in a T-s diagram. As consequence, the amounts of heat supplied to the cycle and rejected by it decrease – a larger share of the cooler becomes located in regions where the variations of thermophysical properties are weaker –, which implies in lower $(UA)_{Total}$. Another effect observed as $P_{CO2,Low}$ approaches $P_{CO2,Crit}$ is the reduction of $\dot{W}_{Net}$ – note that in this limit, while the total power produced by the turbines increases slightly, the power required by the compressor increases strongly as the specific volume of the working fluid increases.

[1] This value is not fixed as it may vary with $T_{CO2,Min}$.

Therefore, the $\eta_{II}/(UA)_{Total}$ ratio increases because the decrease of $(UA)_{Total}$ is considerably larger than the decrease observed for $\dot{W}_{Net}$. Noteworthy is the fact that the $P_{CO2,Low}$ value at which the loop occurs depends on $T_{CO2,Min}$, i.e., as $T_{CO2,Min}$ moves away from $T_{CO2,Crit}$, the sharp growth seen is diminished because of the lower influence of the critical region on the heat exchanger performance.

Figure 39 – Effect of $P_{CO2,Low}$ on $\eta_{II}/(UA)_{Total}$: fourth optimization layer

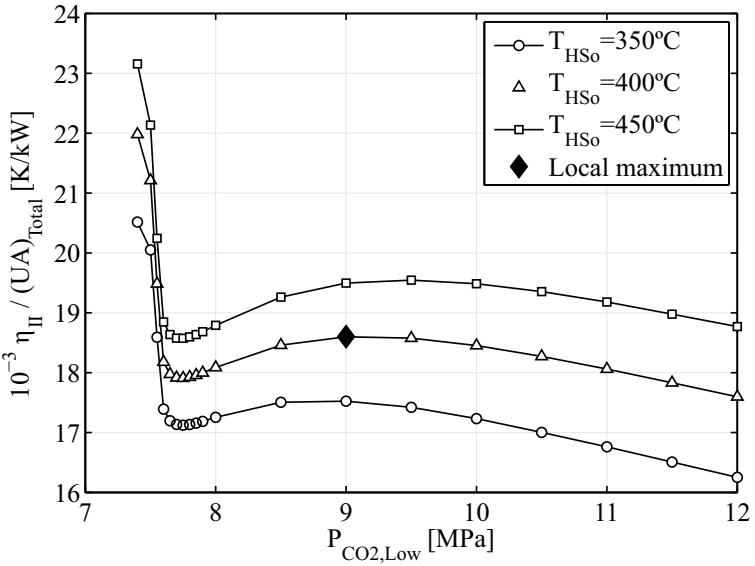

A summary of the optimization results is presented in Figure 40 for various T_{HSo} – the value of T_{HSo} is determined by the inner color of the symbols within the curves according to the color scale at the right hand side of the Figure – as a function of $(UA)_{Total}$. By analyzing Figure 40, one of the first comments to be made is the existence of a loop for each curve. The existence of such loops is due to the sharp growth of $\eta_{II}/(UA)_{Total}$ with the decrease of $(UA)_{Total}$, which was discussed in the previous Figure. The second comment is relative to the existence of a well defined local maximum for each T_{HSo} curve. Even more, by analyzing the maxima, the absence of an optimal T_{HSo} becomes evident as $[\eta_{II}/(UA)_{Total}]_{Max}$ directly increases with T_{HSo} in the range of

T_{HSo} simulated. Thus, differently from the other parameters considered (i.e., $(\Delta T)_{Heat}$, $(\Delta T)_{Reh}$ $P_{CO2,High}$, $T_{CO2,High}$ and $P_{CO2,Low}$), and in accordance to results presented by Figures 25 and 26, the outermost optimization layer simply could not find a optimal T_{HSo}.

Figure 40 – Effect of $(UA)_{Total}$ on $\eta_{II}/(UA)_{Total}$ for different T_{HSo}

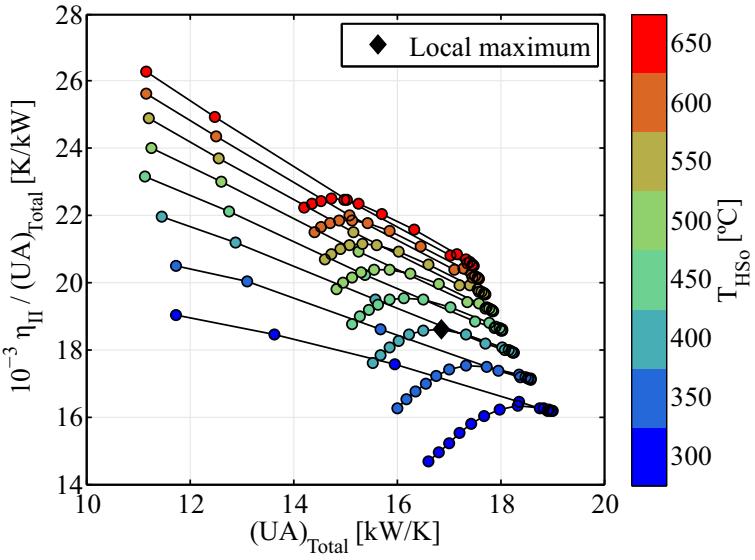

A summary of the non-normalized performance of the Brayton cycle is presented by Figures 41 and 42. Note that all values presented in these figures were obtained through the optimization process discussed in the previous Section. Also, similarly to the format previously used, the value of T_{HSo} is determined by the inner color of the symbols within the curves according to the color scale at the right hand side of each Figure, which presents the curves for $\dot{W}_{Net}$ and η_I, respectively. As expected, both non-normalized figures of merit continuously increase with $(UA)_{Total}$ for $P_{CO2,Low}$ far from $P_{CO2,Crit}$. Also, as $P_{CO2,Low}$ approaches $P_{CO2,Crit}$, the curves present the loops with a significant drop of $\dot{W}_{Net}$ and a slightly drop of η_I, which indicate a decrease in the performance of the cycles.

After analyzing the results, the local maxima are taken as a

compromise solution between the objective function of the optimization (i.e., the ratio $\eta_{II}/(UA)_{Total}$) and the largely used figures of merit $\dot{W}_{Net}$ and η_I. The optimal parameters for the local maxima presented in Figure 40 are summarized in Table 6 and graphically presented in Figure 43 as function of T_{HSo}. The optimal parameters clearly increase, almost linearly, with T_{HSo}, but with different slopes for each one.

Noteworthy is the fact that the (UA)-based analysis may not be the best approach when near to the critical point as it is not evident what are the variations of U and A, separately – e.g., a large value of (UA) may be result of large U, large A or a combination of both. As stated by Reference [4], at the same given conditions, CO_2 may present higher values of (UA) when compared to other working fluids, but it is mainly due to the increase of U (caused by variations of thermophysical properties) and, therefore, it presents a smaller area of heat exchanger and power plant size, consequently.

Figure 41 – Effect of $(UA)_{Total}$ on $\dot{W}_{Net}$ for different T_{HSo}

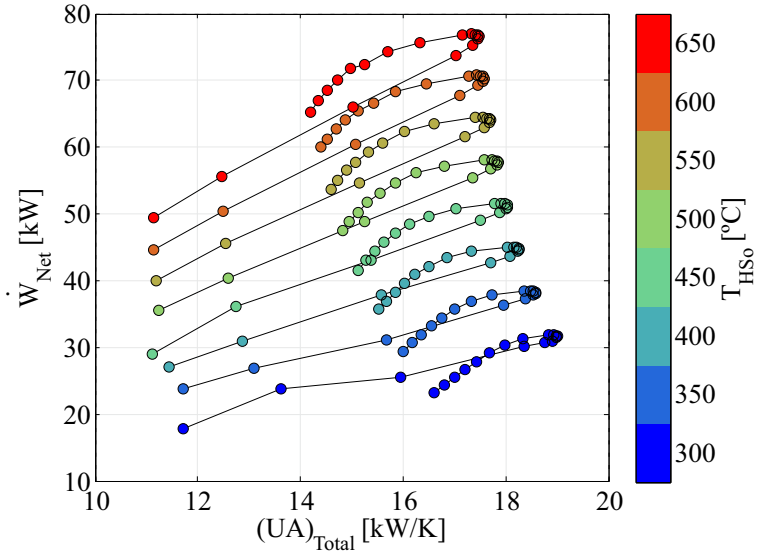

Figure 42 – Effect of $(UA)_{Total}$ on η_I for different T_{HSo}

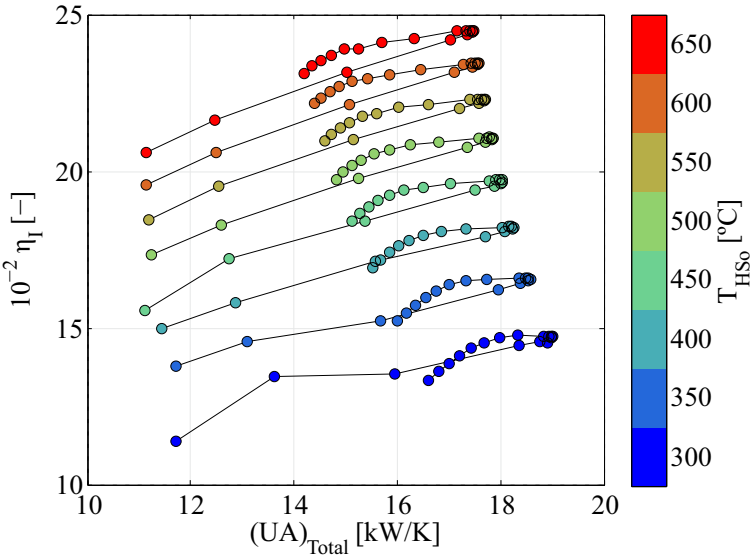

Table 6 – Optimal parameters for the $\eta_{II}/(UA)_{Total}$ curves presented in Figure 40 for different T_{HSo}

Parameters of the optima on $\eta_{II}/(UA)_{Total}$					
T_{HSo} [°C]	$P_{CO2,Low}$ [MPa]	$T_{CO2,High}$ [°C]	$P_{CO2,High}$ [MPa]	$(\Delta T)_{Heat}$ [°C]	$(\Delta T)_{Reh}$ [°C]
300	∼8.45	192.47	∼21.83	14.91	9.97
350	∼8.83	218.35	∼24.71	16.63	11.18
400	∼9.17	240.97	∼27.57	18.05	12.45
450	∼9.46	262.87	∼30.38	19.46	13.49
500	∼9.73	283.23	∼32.90	20.62	14.54
550	∼9.97	304.64	∼35.50	21.95	15.60
600	∼10.19	325.14	∼38.56	23.20	16.70
650	∼10.38	342.96	∼40.86	24.26	17.65

Figure 43 – Graphical representation of the optimal parameters for the curves of $\eta_{II}/(UA)_{Total}$ presented in Figure 40 as functions of T_{HSo}

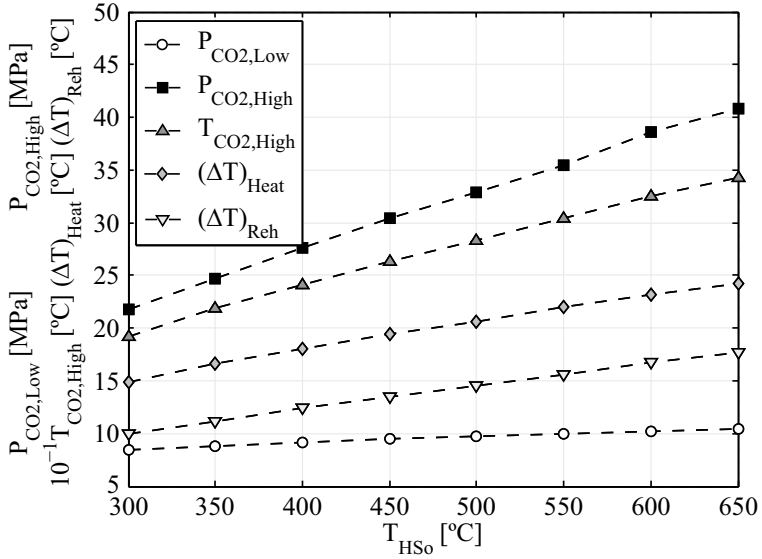

7 CONCLUSIONS

This thesis proposed a new optimization methodology of the performance of CO_2 transcritical Rankine and supercritical Brayton cycles, through normalizing their three main figures of merit (i.e., net power produced, 1st and 2nd Law efficiencies) per unit of total global conductance of the cycle – i.e., the (UA) value needed for operating the cycle. As extensively discussed in the thesis, while low $(UA)_{Total}$ values tend to reduce the thermal energy transferred in the heater, leading to low values of all three normalized figures of merit considered, high $(UA)_{Total}$ values also tend to reduce such normalized figures as the temperature difference between the two fluids exchanging heat approaches zero. Therefore, maximal values for all three normalized figures were obtained.

Considering the CO_2 transcritical Rankine cycles with latent heat source, the calculations clearly indicated that the normalized figures of merit do present maximal values suggesting the existence of an optimal scale for such power plants. Also interesting is that, while more complex cycles (e.g., Combined A) might present an absolute power production higher than simpler cycles (e.g., Reference), these can have a lower normalized power production as shown in Figures 11-15. Similar conclusions can also be generally obtained with respect to the 1st Law efficiency. Nevertheless, these should not be taken as an absolute statement since other parameters (e.g., T_{HSi}) interfere on the relative performance of these cycles.

In the study of CO_2 transcritical Rankine cycles with sensible heat source, the general trends displayed are somewhat similar to the ones revealed for the latent heating case. Certainly, the main observation is that, given the appropriated mass flow rate of the heat source, the normalized figures of merit also displayed clearly visible optimal values. On the other hand, if the mass flow rate of the heat source is such that the temperature of the heating fluid and CO_2 coincide for

a $(UA)_{Total}$ value that is less than $(UA)_{Total,Opt}$, a turning point will not be reached. Furthermore, the calculations also showed that there is a direct relationship between the operational pressure ($P_{CO2,High}$) and the optimal value of $T_{CO2,High}$, for all configurations tested. The calculations also indicate that the 2nd Law efficiency can be drastically improved by optimally splitting the flow rates of the heat source and sink.

In the analysis of the selected CO_2 supercritical Brayton cycle, the multivariable optimization of $\eta_{II}/(UA)_{Total}$ was considered. An extensive discussion on the effect of each of the six optimization parameters on the objective function was presented along with a summary of the results. The general trends shown agree with the results presented for the Rankine cycles as expected. Well defined maxima were found when considering all optimization parameters except T_{HSo}, which showed a direct relationship to the objective function. Furthermore, all the five parameters linearly vary with T_{HSo}. The effect of the properties variations in the vicinity of the critical point became evident particularly when analyzing the effect of $P_{CO2,Low}$ on the objective function. The curve of each $(UA)_{Total}$-normalized figure of merit presented a loop when plotted as function of $(UA)_{Total}$, due to large variations of $(UA)_{Total}$.

As optima were found for all configurations, set of parameters and figures of merit, the determination of the best or the most suitable combination of these is not possible as the analysis itself depends on several points, such as the desired output of the cycle or the available heat source. Even more, it must be clear the fact that each maximum found was different from each other, which indicates the impossibility to simultaneously optimize all normalized figures of merit or the necessity of compromise solutions.

Furthermore, while the results presented clearly suggest the importance of the global conductance on the performance of the cycles, it is fundamental to try narrowing the gap between the present study and its potential practical applications. In that regard, the present study calls attention for a new type of figure of merit, the normalized performance of thermal cycles, which is a very prolific field of study

in related areas. Take for instance the development of thermal devices such as heat exchanger with maximal heat transfer density (i.e., the ratio between the amount of thermal power transferred per volume of fluid needed), e.g., [62, 65]. As often discussed in these studies, the maximization of volumetric performance indicates the ideal scale of the devices being optimized. Obviously, if the device under consideration is a heat exchanger, the optimal scale does not ensure that the absolute amount of thermal energy that is required to be exchanged will be transferred between the hot and cold fluids, as that needs to be matched by changing the size of the device, while respecting the optimal volumetric ratio determined. Therefore, the same can be said about the present analysis as the scales obtained for the cycles serve as an indicator of the maximal value of that can be produced, assuming that this is the variable of interest, per unit of $(\mathrm{UA})_{\mathrm{Total}}$. Similarly, if more power is needed for a certain application, the overall size of the plant should be increased. This information is especially relevant when dealing with CO_2 as the working fluid, since it is known for allowing the development of power plants with high compactness levels.

Finally, it is worth mentioning that while the results presented unquestionably suggest the relevance of the normalized parameters when designing such cycles in a competitive manner, further research is obviously needed to mitigate some of the simplifications adopted along the simulations. One obvious demand is to better define the footprint of the plant, which should include other components since the $(\mathrm{UA})_{\mathrm{Total}}$ factor is only related to the heat exchangers. Also, a more detailed modeling of the heat exchanger should be considered. In fact, the need for this information can lead to other research lines since many of these components are still in early developmental stages. Nevertheless, the trends displayed here are still valid in terms of reassuring the relevance of the $(\mathrm{UA})_{\mathrm{Total}}$ factor on the performance of plants; however, these basically need to be further refined to close the gap between fundamental research and product commercialization.

7.1 SUGGESTIONS FOR FUTURE WORKS

Some suggestions for future works are listed below:

- Analyze more configurations of cycles
- Better define the footprint of the plant taking other of its components into account
- Introduce detailed heat exchanger models for supercritical CO_2
- Analyze correlations for Nusselt number and for friction factor developed for supercritical CO_2
- Simulate and analyze the effect of pressure drop in heat exchangers with supercritical CO_2
- Decouple the global conductance (UA) in global heat transfer coefficient (U) and heat transfer area (A) through the calculation of convective heat transfer coefficients to allow the analysis of heat transfer area-normalized figures of merit, e.g., $\dot{W}_{Net}/A_{Total}$, η_I/A_{Total} and η_{II}/A_{Total}

REFERENCES

[1] IEA. *Key World Energy Statistics 2014*. [S.l.]: OECD Publishing, 2014. (Key World Energy Statistics).

[2] ZHANG, X. et al. Theoretical analysis of a thermodynamic cycle for power and heat production using supercritical carbon dioxide. *Energy*, v. 32, n. 4, p. 591 – 599, 2007.

[3] DOSTAL, V.; HEJZLAR, P.; DRISCOLL, M. The supercritical carbon dioxide power cycle: Comparison to other advanced power cycles. *Nuclear Technology*, 2006.

[4] CAYER, E.; GALANIS, N.; NESREDDINE, H. Parametric study and optimization of a transcritical power cycle using a low temperature source. *Applied Energy*, v. 87, n. 4, p. 1349 – 1357, 2010.

[5] SARKAR, J. Second law analysis of supercritical CO_2 recompression brayton cycle. *Energy*, v. 34, n. 9, p. 1172 – 1178, 2009.

[6] NIU, X.-D. et al. Experimental study of heat transfer characteristics of supercritical CO_2 fluid in collectors of solar rankine cycle system. *Applied Thermal Engineering*, v. 31, n. 6–7, p. 1279 – 1285, 2011.

[7] LIPA, J.; EDWARDS, C.; BUCKINGHAM, M. Specific heat of CO_2 near the critical point. *Physical Review A*, 1977.

[8] BELL, I. et al. Pure and pseudo-pure fluid thermophysical property evaluation and the open-source thermophysical property library coolprop. *Industrial & Engineering Chemistry Research*, 2014.

[9] BELL, I. *Coolprop website*. Available at: <http://coolprop.org>. Latest access date: December 13th, 2014.

[10] DOSTAL, V.; DRISCOLL, M.; HEJZLAR, P. A supercritical carbon dioxide cycle for next generation nuclear reactors. *MIT-ANP-TR-100*, 2004. Available at: <http://hdl.handle.net/1721.1/17746>.

[11] YAMAGUCHI, H. et al. Solar energy powered rankine cycle using supercritical CO_2. *Applied Thermal Engineering*, v. 26, n. 17–18, p. 2345 – 2354, 2006.

[12] LUDINGTON, A. *Tools for supercritical carbon dioxide cycle analysis and the cycle's applicability to fast reactors*. Thesis (Master) — MIT, 2009.

[13] ANGELINO, G. Carbon dioxide condensation cycles for power production. *Journal of Engineering for Gas Turbines and Power*, American Society of Mechanical Engineers, v. 90, n. 3, p. 287–295, 1968.

[14] ANGELINO, G. Real gas effects in carbon dioxide cycles. ASME Paper No. 69-GT-103, v. 91, n. 7, p. 68, 1969.

[15] FEHER, E. G. The supercritical thermodynamic power cycle. *Energy conversion*, Pergamon, v. 8, n. 2, p. 85–90, 1968.

[16] SARKAR, J.; BHATTACHARYYA, S. Optimization of recompression S-CO_2 power cycle with reheating. *Energy Conversion and Management*, v. 50, n. 8, p. 1939 – 1945, 2009.

[17] BAIK, Y.-J. et al. Power-based performance comparison between carbon dioxide and R125 transcritical cycles for a low-grade heat source. *Applied Energy*, v. 88, n. 3, p. 892 – 898, 2011.

[18] AKBARI, A. D.; MAHMOUDI, S. M. Thermoeconomic analysis & optimization of the combined supercritical CO_2 (carbon dioxide) recompression brayton/organic rankine cycle. *Energy*, v. 78, n. 0, p. 501 – 512, 2014.

[19] WANG, J. et al. Parametric optimization design for supercritical CO_2 power cycle using genetic algorithm and artificial neural network. *Applied Energy*, v. 87, n. 4, p. 1317 – 1324, 2010.

[20] SCHUSTER, A.; KARELLAS, S.; AUMANN, R. Efficiency optimization potential in supercritical organic rankine cycles. *Energy*, v. 35, n. 2, p. 1033 – 1039, 2010.

[21] SARKAR, J. Thermodynamic analyses and optimization of a recompression N_2O brayton power cycle. *Energy*, v. 35, n. 8, p. 3422 – 3428, 2010.

[22] DINCER, I.; AL-MUSLIM, H. Thermodynamic analysis of reheat cycle steam power plants. *International Journal of Energy Research*, 2001.

[23] BROWN, J. S.; YANA-MOTTA, S. F.; DOMANSKI, P. A. Comparitive analysis of an automotive air conditioning systems operating with CO_2 and R134a. *International Journal of Refrigeration*, v. 25, n. 1, p. 19 – 32, 2002.

[24] AHAMED, J.; SAIDUR, R.; MASJUKI, H. A review on exergy analysis of vapor compression refrigeration system. *Renewable and Sustainable Energy Reviews*, v. 15, n. 3, p. 1593 – 1600, 2011.

[25] TOFFOLO, A. A synthesis/design optimization algorithm for rankine cycle based energy systems. *Energy*, v. 66, n. 0, p. 115 – 127, 2014.

[26] CAVALLINI, A. et al. Two-stage transcritical carbon dioxide cycle optimisation: A theoretical and experimental analysis. *International Journal of Refrigeration*, v. 28, n. 8, p. 1274 – 1283, 2005.

[27] PEARSON, A. Carbon dioxide – new uses for an old refrigerant. *International Journal of Refrigeration*, v. 28, n. 8, p. 1140 – 1148, 2005.

[28] KIM, M.-H.; PETTERSEN, J.; BULLARD, C. W. Fundamental process and system design issues in CO_2 vapor compression systems. *Progress in Energy and Combustion Science*, v. 30, n. 2, p. 119 – 174, 2004.

[29] MONTAGNER, G. *Um estudo da aplicação de ciclos transcríticos de CO_2 em sistemas comerciais de refrigeração*. Dissertation (Ph.D.) — Universidade Federal de Santa Catarina, 2013.

[30] LORENTZEN, G. Revival of carbon dioxide as a refrigerant. *International Journal of Refrigeration*, v. 17, n. 5, p. 292 – 301, 1994.

[31] HEJZLAR, P. et al. Assessment of gas cooled fast reactor with indirect supercritical co2 cycle. *Nuclear Engineering and and Technology*, v. 38, n. 2, p. 109–118, 2006.

[32] CHEN, Y. *Thermodynamic Cycles using Carbon Dioxide as Working Fluid: CO_2 transcritical power cycle study*. Dissertation (Ph.D.) — KTH Royal Institute of Technology, 2011.

[33] DE LA TOUR, C. C. Exposée de quelques résultats obtenu par l'action combinée de la chaleur et de la compression sur certains liquides, tels que l'eau, l'alcool, l'éther sulfurique et l′essence de pétrole rectifiée. *Annales de Chimie et de Physique*, v. 21, n. 178-182, p. 127–132, 1822.

[34] DE LA TOUR, C. C. Nouvelle note sur les effets qu'on obtient par l'application simultané de la chaleur et de la compression a certains liquides. *Annales de Chimie et de Physique*, v. 22, p. 410–415, 1823.

[35] BERCHE, B.; HENKEL, M.; KENNA, R. Fenômenos críticos: 150 anos desde Cagniard de la Tour. *Revista Brasileira de Ensino de Física*, v. 31, n. 2, p. 2602.1–2602.4, jun. 2009.

[36] ANDREWS, T. Bakerian lecture: On the continuity of the gaseous and liquid states of matter. *Proceedings of the Royal Society of London*, The Royal Society, v. 18, n. 114-122, p. 42–45, 1869.

[37] STANLEY, H. E. *Introduction to phase transitions and critical phenomena*. Oxford: Oxford University Press, 1971.

[38] HALL, W.; JACKSON, J. Heat transfer near the critical point. *Advances in Heat Transfer*, Academia Press, v. 7, n. 1, p. 86, 1971.

[39] BOLMATOV, D.; BRAZHKIN, V.; TRACHENKO, K. Thermodynamic behaviour of supercritical matter. *Nature communications*, Nature Publishing Group, v. 4, 2013.

[40] ÇENGEL, Y. A.; BOLES, M. A.; KANOĞLU, M. *Thermodynamics: an engineering approach*. New York: McGraw-Hill, 2011.

[41] TURCHI, C. S. et al. Thermodynamic study of advanced supercritical carbon dioxide power cycles for high performance concentrating solar power systems. *International Conference on Energy Sustainability - ASME*, p. 375–383, 2012.

[42] QUOILIN, S. An introduction to thermodynamics applied to organic rankine cycles. Massachussetts Institute of Technology, 2008. Available at: <http://orbi.ulg.ac.be/handle/2268/138797>.

[43] INCROPERA, F. P. et al. *Fundamentals of heat and mass transfer*. 7th ed. ed. Hoboken, NJ: John Wiley & Sonns, 2011.

[44] SHAH, R. K.; SEKULIC, D. P. *Fundamentals of heat exchanger design*. [S.l.]: John Wiley & Sons, 2003.

[45] NELLIS, G.; KLEIN, S. *Heat Transfer*. New York: Cambridge University Press, 2009.

[46] BEJAN, A. *Advanced Engineering Thermodynamics*. 3rd. ed. New York: John Wiley & Sons, Inc, 2006.

[47] CAYER, E. et al. Analysis of a carbon dioxide transcritical power cycle using a low temperature source. *Applied Energy*, v. 86, n. 7–8, p. 1055 – 1063, 2009.

[48] CHEN, Y.; LUNDQVIST, P. Analysis of supercritical carbon dioxide heat exchangers in cooling process. *International Refrigeration and Air Conditioning Conference at Purdue*, 2006.

[49] PETUKHOV, B. S. Heat transfer and friction in turbulent pipe flow with variable physical properties. *Advances in heat transfer*, Academic Press, New York, v. 6, n. 503, p. i565, 1970.

[50] KURGANOV, V. A.; KAPTILNYI, A. G. Flow structure and turbulent transport of a supercritical pressure fluid in a vertical heated tube under the conditions of mixed convection. experimental

data. *International journal of heat and mass transfer*, v. 36, n. 13, p. 3383–3392, 1993.

[51] KRASNOSHCHEKOV, E.; KURAEVA, I.; PROTOPOPOV, V. Local heat transfer of carbon dioxide at supercritical pressure under cooling conditions. *High Temperature (translated from Teplofizika Vysokikh Temperatur)*, v. 7, n. 5, p. 856–862, 1970.

[52] PITLA, S. S.; GROLL, E. A.; RAMADHYANI, S. New correlation to predict the heat transfer coefficient during in-tube cooling of turbulent supercritical CO_2. *International Journal of Refrigeration*, v. 25, n. 7, p. 887 – 895, 2002.

[53] YOON, S. H. et al. Heat transfer and pressure drop characteristics during the in-tube cooling process of carbon dioxide in the supercritical region. *International Journal of Refrigeration*, v. 26, n. 8, p. 857 – 864, 2003.

[54] CHENG, L.; RIBATSKI, G.; THOME, J. R. Analysis of supercritical CO_2 cooling in macro- and micro-channels. *International Journal of Refrigeration*, v. 31, n. 8, p. 1301 – 1316, 2008.

[55] KULHANEK, M.; DOSTAL, V. Supercritical carbon dioxide cycles thermodynamic analysis and comparison. *Supercritical CO_2 Power Cycle Symposium*, p. 24–25, 2011.

[56] ZHANG, X. et al. Analysis of a novel solar energy-powered rankine cycle for combined power and heat generation using supercritical carbon dioxide. *Renewable Energy*, v. 31, n. 12, p. 1839 – 1854, 2006.

[57] TUO, H. Analysis of a reheat carbon dioxide transcritical power cycle using a low temperature heat source. ASME, p. 219–225, 2011.

[58] CHENNOUF, N. et al. Valuation and estimation of geothermal electricity production using carbon dioxide as working fluid in the south of algeria. *Energy Procedia*, v. 36, n. 0, p. 967 – 976, 2013.

[59] UTAMURA, M. Thermal-hydraulic characteristics of microchannel heat exchanger and its application to solar gas turbines. American Society of Mechanical Engineers, p. 287–294, 2007.

[60] UTAMURA, M. Thermodynamic analysis of part-flow cycle supercritical CO_2 gas turbines. *Journal of Engineering for Gas Turbines and Power*, v. 132, n. 11, p. 111701, 2010.

[61] BEJAN, A. *Shape and Structure, from Engineering to Nature*. Cambridge: Cambridge University Press, 2000.

[62] BEJAN, A. *Convection Heat Transfer*. 3rd. ed. New York: John Wiley & Sons, Inc, 2004.

[63] MATHWORKS. *MathWorks website*. Available at: <http://mathworks.com>. Latest access date: December 13th, 2014.

[64] SPAN, R.; WAGNER, W. A new equation of state for carbon dioxide covering the fluid region from the triple-point temperature to 1100 K at pressures up to 800 MPa. *Journal of Physical and Chemical Reference Data*, 1996.

[65] DA SILVA, A. K.; GOSSELIN, L. Volumetric maximization of coolant usage in closed self-driven circuits. *International Journal of Heat and Mass Transfer*, v. 53, n. 19–20, p. 3969 – 3976, 2010.

APPENDIX A – FLOWCHARTS

In this appendix, additional flowcharts are presented to illustrate the calculation procedure used to determine the optimized parameters of the configurations of the Rankine cycles shown in Figures 9 and 27. The description starts by showing the flowchart for the Reference (Figure 44), Recuperative (Figure 45) and re-heating (Figure 46) cycles, all with a latent heat source. Next, the flowchart for the Combined A cycle with sensible heat source with the modifications displayed in Figure 27 (Figures 47 and 48) is shown.

Figure 44 – Flowchart for the Reference Rankine cycle with latent heat source

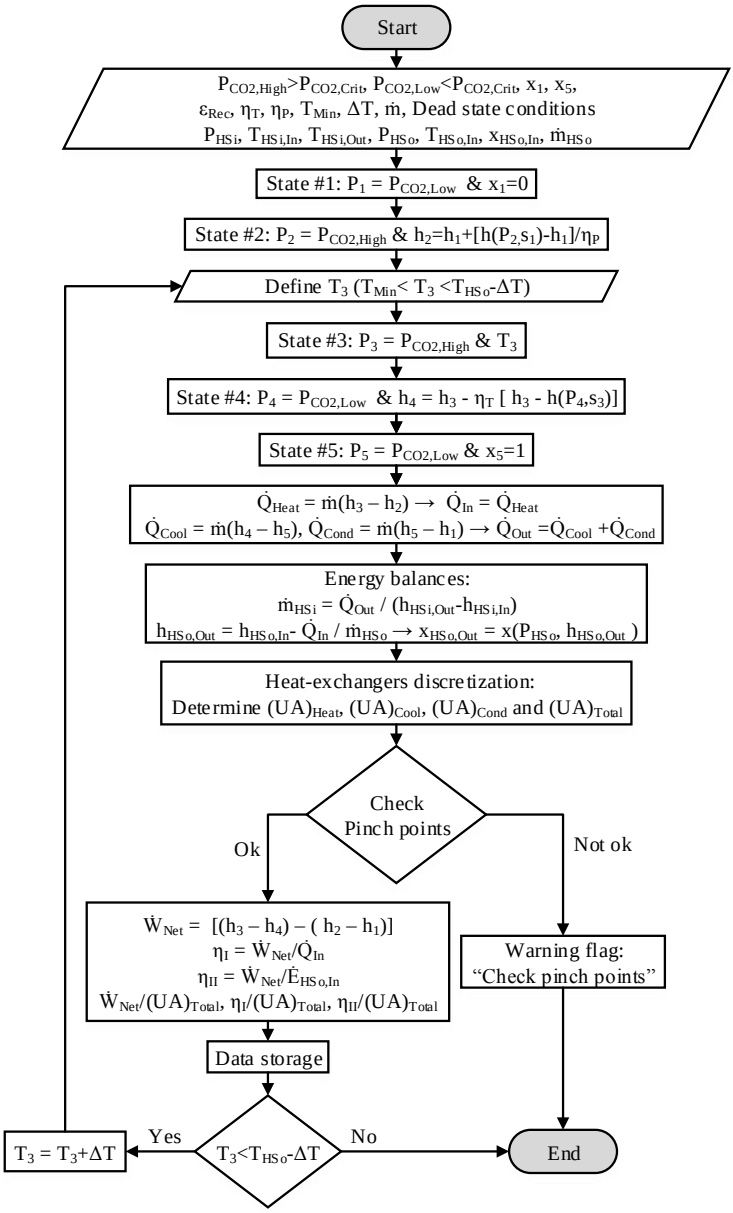

Figure 45 – Flowchart for the Recuperative Rankine cycle with latent heat source

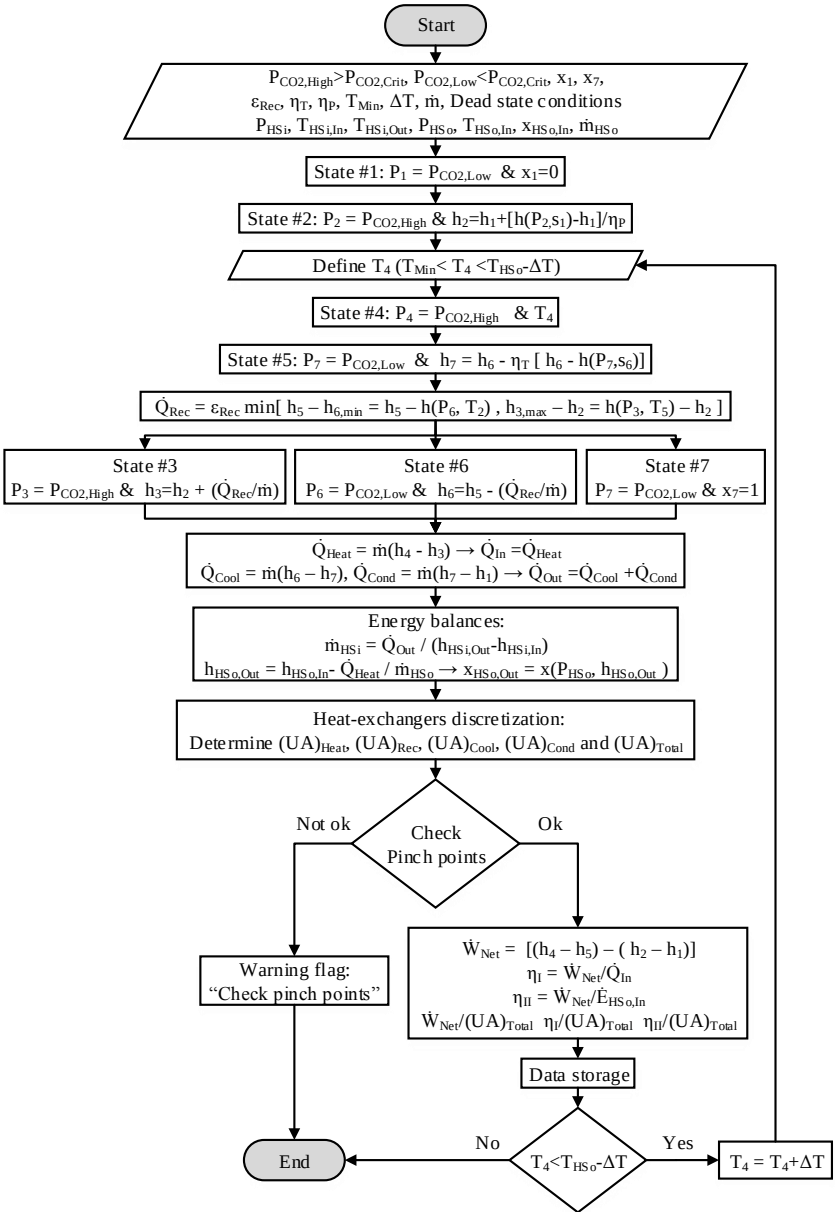

Figure 46 – Flowchart for the Re-heating Rankine cycle with latent heat source

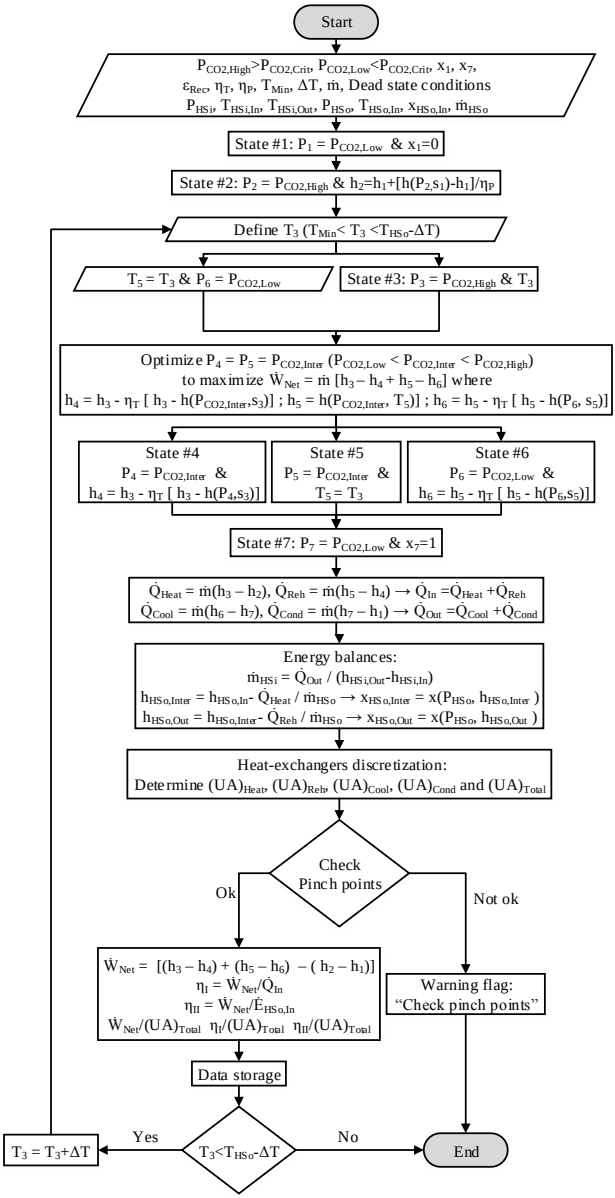

Figure 47 – Flowchart for the Combined A Rankine cycle with sensible heat source and with the modifications displayed in FIgure 27

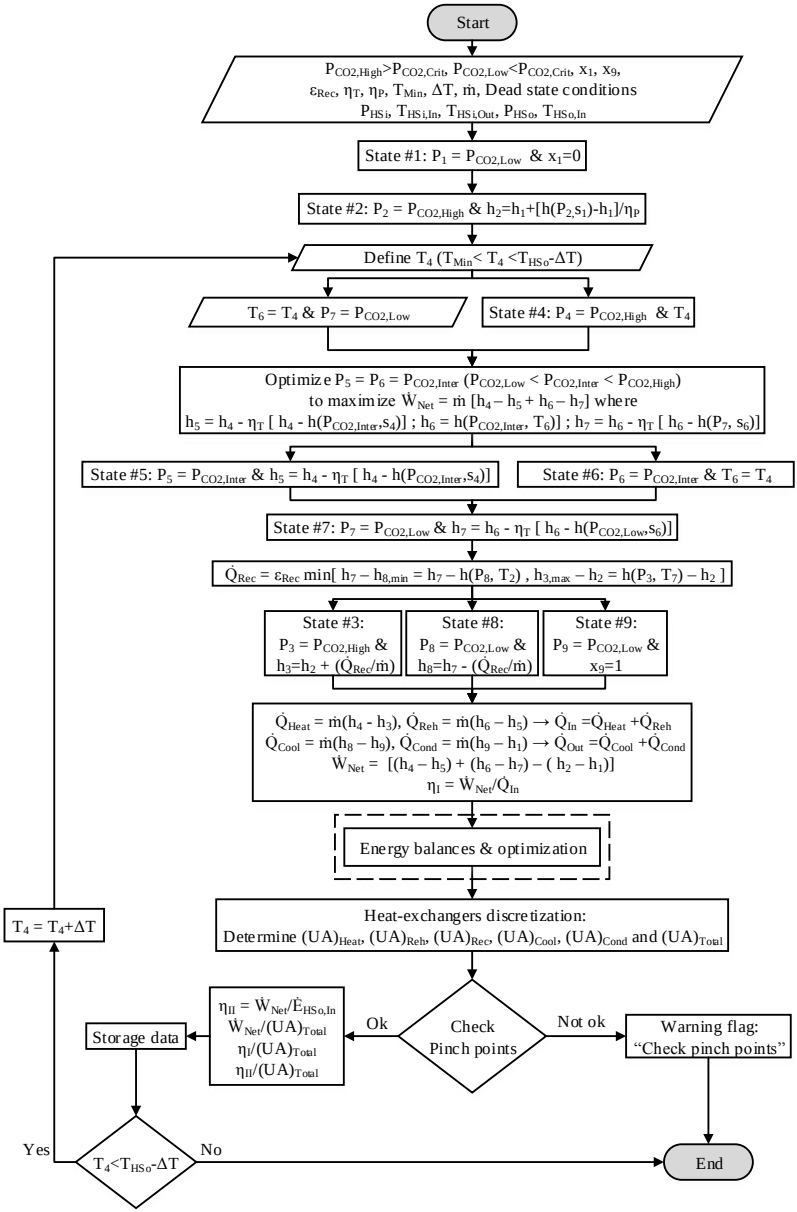

Figure 48 – “Energy balances and Optimization” detailed step of Figure 47

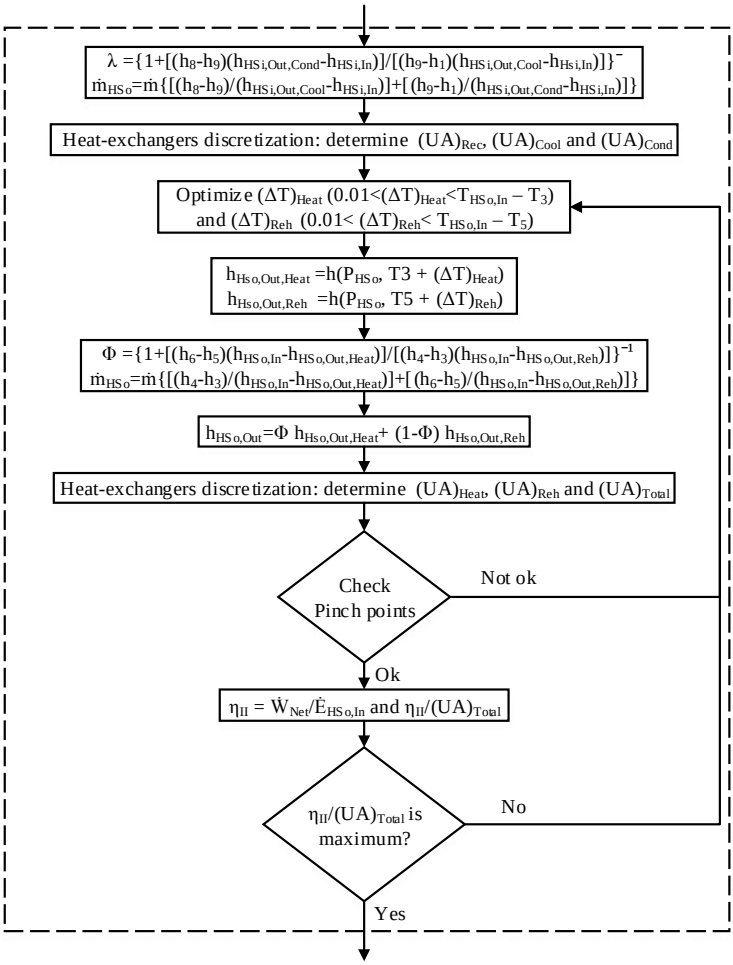

APPENDIX B – REPRESENTATIVE SAMPLE CALCULATION

The main objective of this appendix is to extend the analysis shown in Section 3.2, which provides a step-by-step walkthrough of the flowchart representing Combined A cycle with a latent heat source. Therefore, the description below aims to enhance the understanding of the flowcharting methodology employed in this study by adding a representative sample calculation. To illustrate the calculation process, the maximal value of $\dot{W}_{Net}/(UA)_{Total}$ shown in Figure 14 for the Reference cycle, i.e., the cycle represented in Figure 9a is obtained. The calculation process starts by selecting the configuration and heating method used:

- Configuration: reference cycle with latent heat source

Next, the variables below are specified:

- $P_{CO2,High}$ = 11 MPa, $P_{CO2,Low}$=6.5 MPa, x_1 = 0, x_1 = 1, ϵ_{Rec} = 0.85, η_T= η_P = 0.8, $\dot{m}$ = 1 kg/s, $T_{HSi,In}$ = 10 °C, $T_{HSi,Out}$ = 15 °C, P_{HSi} = 101.325 kPa, P_{HSo} = 101.325 kPa, $T_{HSo,In}$ = 100 °C, $x_{HSo,In}$ = 1, $\dot{m}_{HSo}$ = 1 kg/s. Note that the dead state conditions are P_0 = 101.325 kPa and T_0 = 10 °C

Having the information above, it is possible to completely define the thermodynamic states #1 and #2 as shown below:

- State #1: P_1 = 6.5 MPa & x_1 = 0 → h_1 = 276.7237 kJ/kg, s_1 = 1.2547 kJ/(kg °C), e_1 = 190.8745 kJ/kg and T_1 = 25.4425 °C

- State #2: P_2 = 11 MPa & h_2 = h(P_1,x_1)+[h(P_2,s_1)-h(P_1,x_1)]/η_P = 284.4564 kJ1kg → s_2 = 1.2597 kJ/(kg °C), e_2 = 197.1857 kJ/kg and T_2 = 35.1508 °C

Next, it is relevant to mention that T_3 needs to be selected, which will indeed impact the cycle performance, in this case $\dot{W}_{Net}/(UA)_{Total}$. Therefore, the maximal value of $\dot{W}_{Net}/(UA)_{Total}$ as shown in Figure 14 for the Reference cycle is obtained when $T_3 = 92.7835\,°C$ which will be the value employed in these calculations. Consequently, by specifying T_3, state #3 is completely defined. Similarly, states #4 and #5 can also be defined.

- State #3: $P_3 = 11\,MPa$ & $T_3 = 92.7835\,°C \rightarrow h_3 = 483.7377\,kJ/kg$, $s_3 = 1.8619\,kJ/(kg\,°C)$, $e_3 = 225.9576\,kJ/kg$

- State #4: $P_4 = 11\,MPa$ & $h_4 = h(P_3,T_3) - \eta_T\,[h(P_3,T_3)\text{-}h(P_4,s_3)] = 464.7488\,kJ/kg \rightarrow s_4 = 1.8766\,kJ/(kg\,°C)$, $e_4 = 202.8151\,kJ/kg$ and $T_4 = 51.8701\,°C$

- State #5: $P_5 = 6.5\,MPa$ & $x_5 = 1 \rightarrow h_5 = 392.8470\,kJ/kg$, $s_5 = 1.6436\,kJ/(kg\,°C)$, $e_5 = 196.8801\,kJ/kg$ and $T_5 = 25.4425\,°C$

Having all thermodynamic states defined, one can defined all the thermal power transferred.

- $\dot{Q}_{Heat} = \dot{m}(h_3\text{-}h_2) = 199.2816\,kW \rightarrow \dot{Q}_{In} = 199.2816\,kW$

- $\dot{Q}_{Cool} = \dot{m}(h_4\text{-}h_5) = 71.9018\,kW$ & $\dot{Q}_{Cond} = \dot{m}(h_5\text{-}h_1) = 116.1233\,kW \rightarrow \dot{Q}_{Out} = 188.0525\,kW$

Next, the mass flow rate of the heat sink, and the thermodynamic exiting state of the heat source can be determined:

- $\dot{m}_{HSi} = \dot{Q}_{Out}/(h_{HSi,Out}\text{-}h_{HSi,In}) = 8.9715\,kilogram/s$

- $h_{HSo,Out} = h_{HSo,In} - \dot{Q}_{In}/\dot{m}_{HSo} = 2476.2496\,kJ/kg \rightarrow x_{HSo,Out} = x(P_{HSo,Out},h_{HSo,Out}) = 0.91$

Furthermore, using the procedure described in the text, it is possible to determine (UA) for each of the heat exchangers present in the cycle.

- $(UA)_{Heat} = 6.1008\,kW/K$, $(UA)_{Cool} = 3.7104\,kW/K$, $(UA)_{Cond} = 8.3894\,kW/K$ and $(UA)_{Total} = 18.2006\,kW/K$

Next, the existence of pinch point problems is checked, allowing for the calculation of the net power produced, and the 1st and 2nd Law efficiencies.

- $\dot{W}_{Net} = (h_3\text{-}h_4)\text{ - }(h_2\text{-}h_1) = 11.2562\,kW$
- $\dot{W}_{Net}/\dot{Q}_{In} = 0.056484$
- $\dot{W}_{Net}/(\dot{m}_{HSo}\,e_{HSo,In}) = 0.018957$

As well as the normalized values,

- $\dot{W}_{Net}/(UA)_{Total} = 0.618\,45\,K$
- $\eta_I = \dot{W}_{Net}/\dot{Q}_{In} = 0.003\,103\,4\,K/kW$
- $\eta_{II} = \dot{W}_{Net}/(\dot{m}_{HSo}\,e_{HSo,In}) = 0.001\,041\,6\,K/kW$

One should notice that, as expected, the values obtained above for $(UA)_{Total}$ and $\dot{W}_{Net}/(UA)_{Total}$ agree with the results displayed in Figure 14. Finally, the calculation process is concluded with the storage of the data.